CORRELATING SURFACE AND BURIED INTERFACIAL STRUCTURES TO POLYMER ADHESION

by

Anne V. Vázquez

A dissertation submitted in partial fulfillment
of the requirements for the degree of
Doctor of Philosophy
(Chemistry)
in The University of Michigan
2010

Doctoral Committee:

Professor Zhan Chen, Chair
Professor Raoul Kopelman
Professor Roseanne J. Sension
Associate Professor Lingjie J. Guo

To Frank, Mom and Dad

ACKNOLWEDGEMENTS

The research in this dissertation would not have been possible without the guidance of Professor Zhan Chen, my research advisor. I truly appreciate the opportunity to work in his lab and conduct such interesting research. Professor Chen is an excellent advisor who taught me a great deal not only about conducting research but also about many of the other activities in academia.

I would also like to thank Professor Kopelman, Professor Sension and Professor Guo for serving on my thesis committee and for providing valuable feedback and suggestions for my work. I would like to also thank Professor Sension for allowing me to work in her lab during my REU experience as an undergraduate.

I would like to acknowledge Dr. Nick Shephard, Dr. Susan Rhodes and Dr. Shaun Ahn from Dow Corning Corporation for their collaboration on many of our projects. I have truly appreciated our discussions and the feedback they have given us on the research.

Many of the past and present members of the Chen lab have contributed to my ability to complete the work in this thesis. I would especially like to thank Dr. Cheryl Steinecker, whose research laid the foundation for the work studying adhesion promoters. I would also like to acknowledge Bernardo Orvañanos and Brad Holden who worked with me as undergraduates and did excellent research. I appreciate the support and

friendship from everyone in the lab. They brought a lot of laughter and fun to this experience.

I would like to thank Professor Brian Coppola for giving me the amazing opportunity to conduct curriculum development research in addition to my work in the Chen lab. Professor Coppola has been an inspiring mentor and a great source of support during my graduate career. I would also like to thank Professor Joseph Krajcik from the School of Education for his support, and everyone at the IDEA Institute for their support and for funding our curriculum development work.

The curriculum development work designing an honors studio for Chemistry 260 was done with Professor Samuel Pazicni while he was a postdoctoral fellow at the University of Michigan. I learned so much about teaching from Sam, and our project was one of the highlights of my graduate career. This project would not have been possible without a wonderful team of undergraduates who worked with us: Kaitlin McLoughlin, Melanie Sabbagh, Jeff Simon, Adam Runkle, Alex Sapick and Eric Chen.

I would like to thank the members of the Chemistry Department at Muhlenberg College for their support and encouragement during my undergraduate career. Special thanks go to Professor Bruce Anderson for being an excellent research advisor and to Professor Don Shive for giving me my first teaching opportunity as a learning assistant in the general chemistry class.

Financial support from the Graduate Assistanceship in Areas of National Need is acknowledged. Also, Rackham Travel Grants and Vaughn Symposium Poster and Speaker Awards allowed me to travel to present my research at conferences. The

research presented was supported by an NSF CAREER award, Dow Corning Corporation and the Semiconductor Research Council.

I would not have made it through this experience without the support of my family. Thank you to my parents, Jane and Joe DeSimone, for their love and encouragement. I wouldn't be where I am without them. Thank you to my husband, Frank Vázquez, for his unconditional love and amazing support through the many ups and downs of the last five years. I could not have gotten through this experience if I didn't have him by my side.

Section 1.3.1 was adapted from work published by the American Chemical Society (*Langmuir*, **2004**, *20*, 5467-5473) who holds the copyright thereto. Section 1.3.2 was adapted from work published by the American Chemical Society (*J. Phys. Chem. B.*, **2006**, *110*, 914-918) who holds the copyright thereto. Section 1.3.3 was adapted from work published by Elsevier (*J. Colloid Interface Sci.*, **2007**, *308* 170-175) who holds the copyright thereto. Chapter 2 was adapted from work published by Elsevier (*J. Colloid Interface. Sci.*, **2009**, *331*, 408-416) who holds the copyright thereto. Chapter 3 was adapted from work published by the American Chemical Society (*ACS Applied. Mater. Interf.*, **2010**, *2*, 96-103) who holds the copyright thereto.

TABLE OF CONTENTS

LIST OF FIGURES

LIST OF TABLES

LIST OF ABBREVIATIONS

AC	amorphous cell
AFM	atomic force microscopy
ATMS	3-aminopropyltrimethoxysilane
ATR-FTIR	attenuated total reflection-Fourier transform infrared spectroscopy
BADGE	bisphenol A diglycidyl ether
BDDGE	1,4-butanediol diglycidyl ether
BTMS	n-butyltrimethoxysilane
COMPASS	Condensed-phase Optimized Molecular Potentials for Atomic Simulation Studies
DFG	difference frequency generation
d_4-PET	poly(ethylene terephthalate) with deuterated ethylene glycol subunits
d-PS	deuterated polystyrene
EDA	ethylene diamine
γ-GPS	(3-glycidoxypropyl)trimethoxysilane
MD	molecular dynamics
MVS	methylvinylsiloxanol
PBT	poly(butylene terephthalate)
PDMS	poly(dimethylsiloxane)
PET	poly(ethylene terephthalate)

PMMA	poly(methyl methacrylate)
PS	polystyrene
OPG/OPA/DFG	optical parametric generation/amplification and difference frequency generation system
OTMS	*n*-octadecyltrimethoxysilane
RMS	root mean squared
SFG	sum frequency generation
TDFTMS	(tridecafluoro-1,1,2,2-tetrahydrooctyl)trimethoxysilane
XPS	X-ray photoelectron spectroscopy

CHAPTER 1

INTRODUCTION

1.1 Background

Robust adhesion of polymers is needed for a variety of applications in the automotive, aviation and aerospace, medical, construction and electronics fields.[1-4] In many applications, replacing mechanical fasteners with polymer adhesives can significantly reduce fuel consumption, which conserves energy and operation cost.

Although polymer adhesion is important in many applications, it is also complex and poorly understood. There are a variety of different mechanisms that can contribute to adhesion, such as wetting of the adhesive onto the adherend, mechanical interlocking and formation of an interpenetrating network, electrostatic interactions, the formation of hydrogen bonds and the formation of covalent chemical bonds. Often, more than one of these adhesion mechanisms can affect the formation of an adhesive bond.[4-8]

There are multiple classes of polymer adhesives that are used in different applications. Silicone elastomers are one such class that are extensively used in the electronics industry for their thermal stability, flexibility, and unique rheological properties.[1-3, 9] Specifically, addition-cured silicone elastomers offer advantages because of their simple, controllable cure chemistry. However, these polymers lack intrinsic polar

functional groups that can easily react to form covalent adhesive bonds to other polymeric materials. For some applications, such as those in microfluidics, oxidative surface treatments are used to add polar groups to the silicone surface to improve adhesion.[10-13] However, in other applications it is advantageous to design self-priming silicone adhesives that do not require surface pretreatments. In these applications, adhesion-promoters can be incorporated into the silicone elastomer prior to application to substrate to render the silicone elastomer self-adherent.

Silane adhesion promoters are commonly used to enhance the adhesion of silicone elastomers to a variety of substrates including metals, inorganic substrates and polymers. Generally, a small amount of silane adhesion promoter is either mixed into the silicone elastomer prior to application to the substrate, or the silane adhesion promoter is used as an interlayer between the substrate and the silicone elastomer. Specifically, alkoxysilane-based adhesion promoters have been shown to be effective for improving the adhesion between silicone elastomer and some engineering thermoplastics.[14-17]

Another important class of polymer adhesives is epoxy resins. Epoxy resins are used extensively in the electronics industry as electronically-insulating underfill adhesives in flip-chip devices. While flip-chip devices have the advantages of being smaller and faster than wire-bound devices, these devices depend heavily on the adhesion of the underfills. If the underfill fails at any of its adhesive interfaces, the device can fail. Environmental conditions such as moisture can lead to underfill adhesion failure.[18-22]

It is understood that adhesive bonds are dominated by interactions at the interface between the adhesive and adherend because that is where the two materials first interact. Therefore, to design better polymer adhesives, it is important to understand the interfacial

molecular-level mechanisms leading to the formation of an adhesive bond. This can be accomplished by studying polymer adhesive surfaces as well as the interfaces between polymer adhesives and their adherends. It is important to study polymer adhesive surface structures and polymer adhesive structures at adherend interfaces, as well as the ordering and alignment of silane adhesion promoting molecules on buried interfaces. Further, studying the effect of environmental factors such as moisture on polymer adhesive surfaces and buried interfaces can improve understanding of their impact on adhesion.

Polymer surfaces and interfaces have been extensively studied by a variety of methods,[23-33] but most conventional techniques do not provide detailed molecular information about just surfaces and/or interfaces needed to understand adhesion mechanisms. X-ray photoelectron spectroscopy (XPS), an elemental technique, is one of the most surface-sensitive techniques; however, XPS requires a high vacuum environment, so studying polymer adhesives in air or in liquid environments is impossible. Vibrational techniques including attenuated total reflection Fourier transform infrared spectroscopy (ATR-FTIR) and Raman spectroscopy have both been used to study polymer adhesives.[8,34,35] However, neither of these techniques have high intrinsic surface or interfacial sensitivity and cannot easily be used to study buried interfaces formed by adhesive bonds. By definition, any material that is strongly adhered cannot be easily separated for surface analysis. Further, breaking an adhesive bond may significantly alter the interfacial structures so these mechanisms could not be studied.

Sum frequency generation (SFG) vibrational spectroscopy is a powerful analytical technique to study surfaces and buried interfaces at the molecular level *in situ.* SFG has been used to study polymer surfaces and interfaces including polymer and co-polymer

surfaces, polymer restructuring in water, polymer/silane interfaces, polymer/biomolecule interfaces and polymer/polymer interfaces.[36-62] As will be discussed in Section 1.2, SFG is inherently surface and interface sensitive due to its selection rules. This makes SFG an ideal tool for studying polymer surface and interface structures to better understand polymer adhesion. Section 1.3 reviews prior research on polymer surfaces and polymer/silane interfaces, providing the foundation for the current work presented in this dissertation.

1.2 Sum Frequency Generation Vibrational Spectroscopy

1.2.1 Brief SFG Overview

IR-visible SFG is a process in which two input laser beams at frequencies ω_1 (visible) and ω_2 (IR) overlap in a medium, generating a third output beam whose frequency is the sum of the two input frequencies ($\omega_{SF} = \omega_1 + \omega_2$).[63,64] In an SFG experiment, the IR beam (ω_2) is scanned over the vibrational region of interest. When ω_2 matches a vibrational resonance of the medium, the sum frequency beam (ω_{SF}) is resonantly enhanced and a peak is observed. Figure 1.1 shows the geometry of the SFG experiments detailed in later sections.

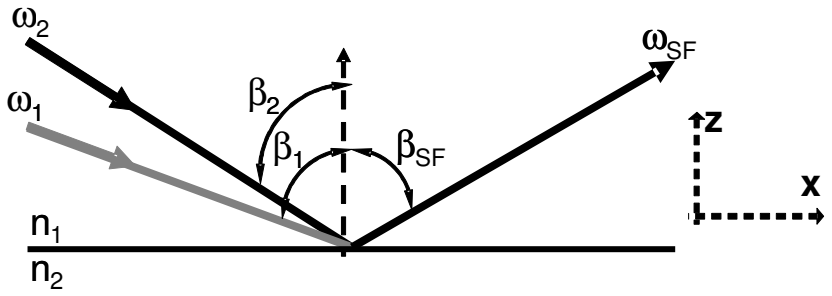

Figure 1.1 Copropagating geometry used for SFG experiments.

Because SFG is a second order nonlinear optical technique, it is forbidden in materials with inversion symmetry under the electric dipole approximation. Most bulk polymers are centrosymmetric and therefore do not exhibit SFG signal. However, at a surface or interface, the bulk inversion symmetry is broken and SFG signal is allowed.[63-67] Additionally, SFG can be used to determine the orientation and orientational distribution of surface or interfacial chemical groups by changing the polarizations of the input and output laser beams.[63-67]

1.2.2 SFG Theory

When a molecule is exposed to an electric field which is not very strong, the induced polarization, **P**, is proportional to the strength of the electric field, **E**, as described by

$$\mathbf{P} = \chi^{(1)}\mathbf{E} \tag{1.1}$$

where $\chi^{(1)}$ is the first-order linear susceptibility of the material. For the high-energy light from lasers, the linear approximation of the polarization is no longer sufficient and higher order terms must be taken into account when calculating polarization. Under the electric dipole approximation, the polarization can be described by

$$\mathbf{P} = \mathbf{P}^{(1)} + \mathbf{P}^{(2)} + \mathbf{P}^{(3)} + ... = \chi^{(1)}\mathbf{E} + \chi^{(2)} : \mathbf{EE} + \chi^{(3)} \vdots \mathbf{EEE}... \tag{1.2}$$

where $\chi^{(2)}$ is the second order nonlinear susceptibility, a third-rank tensor, and $\chi^{(3)}$ is the third order nonlinear susceptibility, a fourth-rank tensor.[66,67] When two beams of light with frequencies ω_1 and ω_2, and amplitudes E_1 and E_2, respectively, mix, the second order nonlinear polarization induced can be described as the following

$$\mathbf{P}^{(2)} = \chi^{(2)} : \mathbf{E}_1 \cos(\omega_1 t)\mathbf{E}_2 \cos(\omega_2 t). \tag{1.3}$$

This expression can be transformed using trigonometric identities to

$$\mathbf{P}^{(2)} = \frac{1}{2}\chi^{(2)} : \mathrm{E}_1\mathrm{E}_2[\cos(\omega_1 + \omega_2)t + \cos(\omega_1 - \omega_2)t], \tag{1.4}$$

showing that there are two oscillating dipoles at frequencies (ω_1+ω_2) and (ω_1-ω_2), respectively. This expression shows the origin of SFG and difference frequency generation (DFG). The (ω_1+ω_2) term is for SFG and the (ω_1-ω_2) term is for DFG. [66, 67] The intensity, *I*, of the light emitted from SFG depends on $|\mathbf{P}^{(2)}|^2$ and can be related to the following:

$$I(\omega_{SF}) \propto \left|\chi^{(2)}\right|^2 I(\omega_1) I(\omega_2) \tag{1.5}$$

where $I(\omega_1) = \left|\mathbf{E}_1\right|^2$, and $I(\omega_2) = \left|\mathbf{E}_2\right|^2$ and $\omega_{SF} = \omega_1 + \omega_2$.[66]

In an SFG experiment, the non-zero components of $\chi^{(2)}$, the second-order nonlinear susceptibility, are measured. Recall that SFG is forbidden in centrosymmetric environments. To understand why SFG is surface and interface sensitive, consider a centrosymmetric environment. For this environment, under the inversion operation,

$$\chi^{(2)}_{ijk} = \chi^{(2)}_{-i-j-k} \tag{1.6}$$

where *ijk* refers to coordinates in the laboratory frame of reference. However, because $\chi^{(2)}_{ijk}$ is a polar tensor, the following must also be true:

$$\chi^{(2)}_{ijk} = -\chi^{(2)}_{-i-j-k}. \tag{1.7}$$

Thus, in a medium with inversion symmetry, $\chi^{(2)}_{ijk}$ must be equal to zero to satisfy both equations (1.6) and (1.7), and SFG is forbidden. Most bulk materials are centrosymmetric and therefore yield no SFG signal. However, at a surface or interface, the bulk inversion symmetry is broken, $\chi^{(2)}_{ijk}$ does not have to equal zero, and SFG signal is possible.[67]

For SFG signal to be generated, the two input beams must overlap both spatially and temporally on the sample. As seen in Figure 1.1, the output SFG signal is at an angle β_{SF} to the surface normal. Applying the phase-matching condition, the following can be deduced:

$$n_{SF}\omega_{SF}\sin\beta_{SF} = n_1\omega_1\sin\beta_1 \pm n_2\omega_2\sin\beta_2 \tag{1.8}$$

or

$$n_{SF}k_{SF}\sin\beta_{SF} = n_1k_1\sin\beta_1 \pm n_2k_2\sin\beta_2 \tag{1.9}$$

where n_i is the index of refraction for medium i, ω is the frequency of the light, β is the angle of the beam with respect to the surface normal, and k is equal to ω/c, where c is the speed of light. The positive sign is used in equations (1.8) and (1.9) when the input beams are copropagating, as seen in Figure 1.1.[67]

The SFG signal is both transmitted through the sample and reflected from the sample. All experiments described in later sections use the reflected geometry, as shown in Figure 1.1. In the reflected direction, the intensity of the sum frequency signal can be written as

$$I(\omega_{SF}) = \frac{8\pi^3\omega^2\sec^2\beta_{SF}}{c^3 n_1(\omega_{SF})n_1(\omega_1)n_1(\omega_2)}\left|\chi^{(2)}_{eff}\right|^2 I_1(\omega_1)I_2(\omega_2) \tag{1.10}$$

where $n_i(\Omega)$ is the index of refraction of medium I at frequency Ω, β_{SF} is the reflection angle of the generated sum frequency beam, and $I_1(\omega_1)$ and $I_2(\omega_2)$ are the intensities of the two input fields.[68] The effective second-order nonlinear susceptibility, $\chi^{(2)}_{eff}$, of the sample can be related to the second-order nonlinear susceptibility, $\chi^{(2)}$, in the lab coordinate system by

$$\chi^{(2)}_{eff} = \left[\hat{\mathbf{e}}(\omega_{SF})\cdot\mathbf{L}(\omega_{SF})\right]\cdot\chi^{(2)}:\left[\mathbf{L}(\omega_1)\cdot\hat{\mathbf{e}}(\omega_1)\right]\left[\mathbf{L}(\omega_2)\cdot\hat{\mathbf{e}}(\omega_2)\right] \tag{1.11}$$

where $\hat{\mathbf{e}}(\Omega)$ is the unit polarization vector and $\mathbf{L}(\Omega)$ is the Fresnel factor at frequency Ω.[54] By this relation, the various tensor elements of $\chi^{(2)}$ can be deduced from different tensor elements of $\chi^{(2)}_{eff}$ measured using different polarization combinations of the laser beams. $\chi^{(2)}$ is a third-rank tensor and therefore has 27 elements, which would be many terms to deduce for each experiment. However, for azimuthally isotropic non-chiral surfaces or interfaces, there are only seven non-zero elements of $\chi^{(2)}$. The lab coordinates are chosen such that the z axis is along the surface normal of the surface or interface under study, as seen in Figure 1.1. In this case, the seven non-zero elements of $\chi^{(2)}$ are $\chi_{xxz}=\chi_{yyz}$, $\chi_{xzx}=\chi_{yzy}$, $\chi_{zxx}=\chi_{zyy}$, and χ_{zzz}. Collecting SFG spectra with different polarization combinations of the two input and output beams can allow one to deduce the seven non-zero terms of the $\chi^{(2)}$ tensor. These polarization combinations used in SFG experiments are ssp (s-polarized SFG output, s-polarized $\mathbf{E}_1$ input (visible), and p-polarized $\mathbf{E}_2$ input(IR)), sps, pss, and ppp.[67] These non-zero elements of $\chi^{(2)}$ can be written as

$$\chi^{(2)}_{eff,ssp} = L_{yy}(\omega_{SF})L_{yy}(\omega_1)L_{zz}(\omega_2)\sin\beta_2\chi_{yyz}, \tag{1.12a}$$

$$\chi^{(2)}_{eff,sps} = L_{yy}(\omega_{SF})L_{zz}(\omega_1)L_{yy}(\omega_2)\sin\beta_1\chi_{yzy}, \tag{1.12b}$$

$$\chi^{(2)}_{eff,pss} = L_{zz}(\omega_{SF})L_{yy}(\omega_1)L_{yy}(\omega_2)\sin\beta_{SF}\chi_{zyy}, \tag{1.12c}$$

$$\begin{aligned}\chi^{(2)}_{eff,ppp} = &-L_{xx}(\omega_{SF})L_{xx}(\omega_1)L_{zz}(\omega_2)\cos\beta_{SF}\cos\beta_1\sin\beta_2\chi_{xxz}\\ &-L_{xx}(\omega_{SF})L_{zz}(\omega_1)L_{xx}(\omega_2)\cos\beta_{SF}\sin\beta_1\cos\beta_2\chi_{xzx}\\ &+L_{zz}(\omega_{SF})L_{xx}(\omega_1)L_{xx}(\omega_2)\sin\beta_{SF}\cos\beta_1\cos\beta_2\chi_{zxx}\\ &+L_{zz}(\omega_{SF})L_{zz}(\omega_1)L_{zz}(\omega_2)\sin\beta_{SF}\sin\beta_1\sin\beta_2\chi_{zzz}.\end{aligned} \tag{1.12d}$$

where β_i is the incident angle of the field $\mathbf{E}_i$ and $L_{xx}(\Omega)$, $L_{yy}(\Omega)$, and $L_{zz}(\Omega)$ are the Fresnel factors for beam Ω. The Fresnel factors can be written as

$$L_{xx}(\Omega) = \frac{2n_1(\Omega)\cos\gamma}{n_1(\Omega)\cos\gamma + n_2(\Omega)\cos\beta}, \tag{1.13a}$$

$$L_{yy}(\Omega) = \frac{2n_1(\Omega)\cos\beta}{n_1(\Omega)\cos\beta + n_2(\Omega)\cos\gamma}, \tag{1.13b}$$

$$L_{zz}(\Omega) = \frac{2n_2(\Omega)\cos\beta}{n_1(\Omega)\cos\gamma + n_2(\Omega)\cos\beta}\left(\frac{n_1(\Omega)}{n'(\Omega)}\right)^2 \tag{1.13c}$$

where $n'(\Omega)$ is the refractive index of the interface, β is the incidence angle of the field, and γ is the refracted angle such that $n_1(\Omega)\sin\beta = n_2(\Omega)\sin\gamma$.[68]

The second-order nonlinear susceptibility in the laboratory coordinate system, $\chi^{(2)}$, can be related to the molecular second-order nonlinear polarizability or hyperpolarizability, $\alpha^{(2)}$, through the following coordinate transform:

$$\chi_{ijk}^{(2)} = N_s \sum_{lmn} \left\langle (\hat{\mathbf{i}}\cdot\hat{\xi})(\hat{\mathbf{j}}\cdot\hat{\eta})(\hat{\mathbf{k}}\cdot\hat{\zeta}) \right\rangle \alpha_{lmn}^{(2)} \tag{1.14}$$

where N_s is the surface number density of molecules, (**i,j,k**) are unit vectors in the lab coordinates, and (ξ,η,ζ) are the unit vectors in the molecular coordinates.

When the IR frequency, ω_2, is close to a vibrational resonance in the medium being studied, the hyperpolarizability, $\alpha^{(2)}$, and the second order nonlinear susceptibility, $\chi^{(2)}$, can be written as

$$\alpha^{(2)} = \alpha_{NR}^{(2)} + \sum_q \frac{\alpha_q}{\omega_2 - \omega_q + i\Gamma_q} \tag{1.15}$$

and

$$\chi^{(2)} = \chi_{NR}^{(2)} + \sum_q \frac{\chi_q}{\omega_2 - \omega_q + i\Gamma_q} \tag{1.16}$$

where "NR" refers to the nonresonant component of $\alpha^{(2)}$ and $\chi^{(2)}$. The second part of the terms refer to the resonant components of $\alpha^{(2)}$ or $\chi^{(2)}$, and α_q or χ_q, ω_q, and Γ_q denote the resonant strength, resonant frequency, and damping constant of the qth vibrational mode, respectively.[66, 69] By obtaining the second-order nonlinear susceptibility from fitting the peaks of SFG spectra according to equation (1.16), the orientation information of a chemical group may be deduced if the hyperpolarizability is known by using ratios of the $\chi^{(2)}$ tensor elements.[66,67,69]

The resonant part of equation (1.15) is proportional to the product of the IR dipole derivative, $\frac{\partial \mu_{IR}}{\partial Q}$, and the Raman polarizability tensor, $\frac{\partial \alpha_{Raman}}{\partial Q}$, of vibrational mode q as described by

$$\alpha_R^{(2)} \propto \frac{\partial \mu_{IR}}{\partial Q} \frac{\partial \alpha_{Raman}}{\partial Q}. \tag{1.17}$$

Thus, to be SFG-active, a vibrational mode must be both IR-active and Raman-active.

1.2.3 Experimental

The schematic of the EKSPLA SFG system used in all SFG experiments is shown in Figure 1.2. The system is based on a 20 ps, 20 Hz mode-locked Nd:YAG laser with a fundamental output of 1064 nm. The fundamental output is sent to the harmonics unit where two K^*DP nonlinear crystals produce the second and third harmonics of 532 nm and 355 nm, respectively. The second harmonic of 532 nm is the visible beam for the SFG experiment while the third harmonic of 355 nm is mixed with the fundamental 1064 nm beam in the optical parametric generation/optical parametric amplification/difference frequency generation (OPG/OPA/DFG) system based on LBO and $AgGaS_2$ crystals. The

IR beam generated from the OPG/OPA/DFG system is tunable from 2.3 to 10 μm, or 1000 to 4300 cm^{-1}.

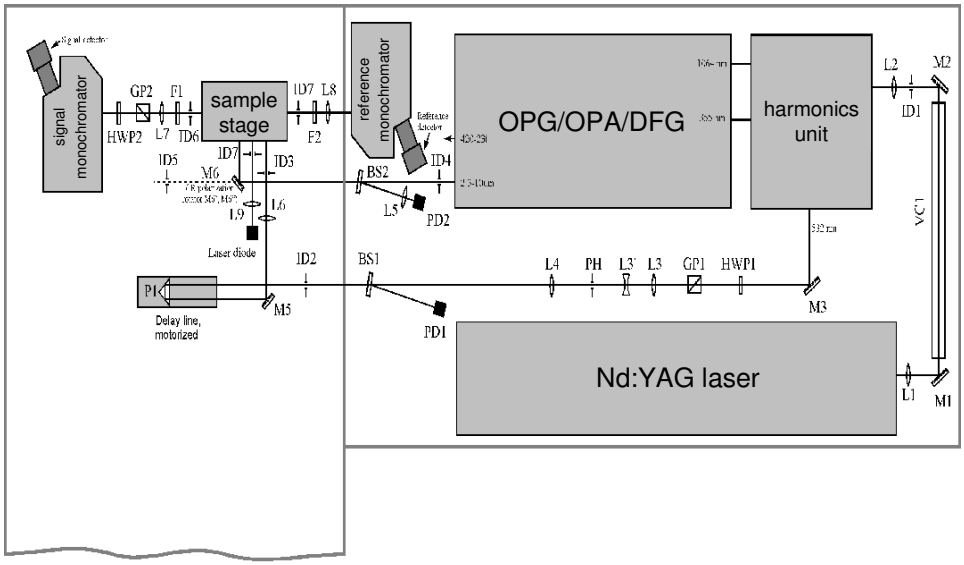

Figure 1.2 Set-up of custom built EKSPLA SFG system

In SFG experiments using the system shown in Figure 1.2, the visible and IR beams are overlapped both temporally and spatially on the sample at incident angles of 60° and 54°, respectively, with respect to the surface normal of the experimental set-up shown in Figure 1.1. Both input beams have diameters of approximately 500 μm, and the input visible and IR energies are ~200 μJ and ~100 μJ, respectively. The SFG spectra can be normalized to the input powers because the input IR and visible powers are monitored by two photodiodes. The SFG signal is sent through a monochromator, collected by a photomultiplier tube and processed with a gated integrator. SFG intensity is plotted as a function of the input IR frequency, yielding a vibrational spectrum of the sample's

surface or interfacial chemical groups. Different elements of the $\chi^{(2)}$ tensor can be probed by changing the polarizations of the input and output beams to take SFG spectra with different polarization combinations such as ssp (s-polarized SFG output, s-polarized visible input, and p-polarized IR input), sps, and ppp.

SFG spectra presented in this work were obtained using the face-down window geometry, as shown in Figure 1.3. A thin polymer film can be prepared by spin-coating a polymer solution onto an IR-transparent window. Then, SFG spectra can be obtained from the polymer thin film surface in either face-up or face-down geometry. Face-down is preferentially used because it allows one to study not only polymer surfaces but also polymer/liquid or polymer/polymer buried interfaces. Further, it has been demonstrated that SFG signals from face-down geometry are larger than those from face-up geometry because of larger Fresnel factors.[49]

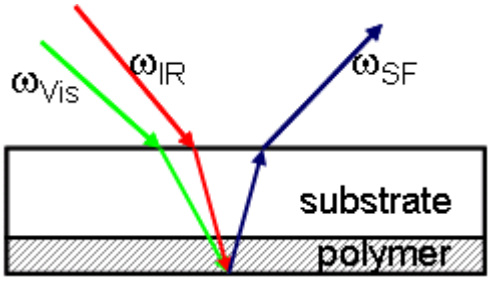

Figure 1.3 Face down window geometry for SFG experiments

1.3 Prior Work

1.3.1 Absolute Orientation and Hydrogen Bonding of Silanes at Polymer/Silane Interfaces

Earlier work studying interactions between polymers and silanes used as adhesion promoters in our research group showed that silanes with different backbone and end group chemistry oriented differently at the poly(ethylene terephthalate) (PET) interface.

The buried interfacial structures of a trimethoxysilane with an amino-functionalized endgroup, 3-aminopropyltrimethoxysilane (ATMS) was compared to those of a trimethoxysilane with an epoxy-functionalized end group, (3-glycidoxypropyl) trimethoxysilane (γ-GPS), and a trimethoxy silane with a methyl end group, n-butyltrimethoxysilane (BTMS).

Studies of the carbonyl stretching region of PET in contact with the three silanes showed evidence of hydrogen bonding between the polymer surface and the ATMS silane. As seen in Figure 1.4, the PET carbonyl stretch shifted to a lower frequency when contacted to ATMS, while this was not observed when the PET was contacted to γ-GPS or BTMS. This shift to a lower frequency was characteristic of hydrogen bonding. Of the silanes studied, only ATMS was capable of forming hydrogen bonds with the PET. As hydrogen bonding is known to be an adhesion mechanism for polymer adhesion, this study showed that SFG can be used to monitor interfacial interactions that promote polymer adhesion.[55]

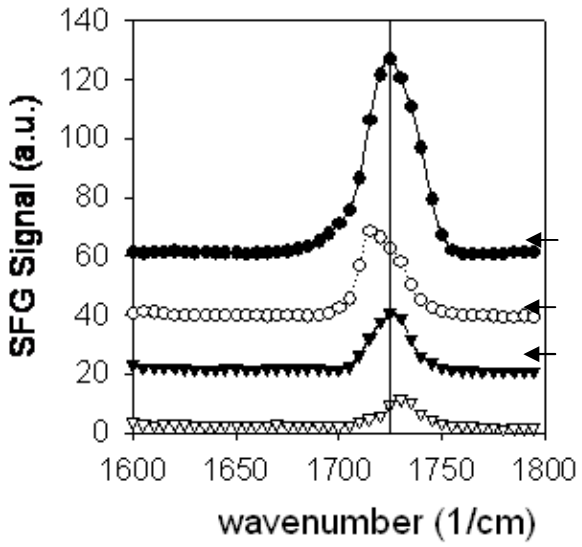

Figure 1.4 SFG spectra of PET in contact with air (closed circles), ATMS (open circles), γ-GPS (closed triangles) and BTMS (open triangles) in the carbonyl stretching region. Baselines of spectra are indicated by arrows on right.

In the same study, the absolute orientations of the two silanes at deuterated PET (d_4-PET) interface were deduced to further show that ATMS formed hydrogen bonds with PET. In this study, a titanium dioxide interlayer was used to provide nonresonant signal that could interfere with the resonant signal from the d_4-PET/silane interface, according to equation (1.16). By determining how the resonant signals from the various d_4-PET/silane interfaces interfere with the nonresonant signal from the TiO_2 interlayer, the relative absolute orientations of the three silanes could be determined. That is, it could be determined if chemical groups from each silane were facing "up" toward the polymer or "down" away from the polymer.

Figure 1.5 shows SFG spectra of d_4-PET in contact with ATMS and BTMS in the C-H stretching region. The peaks centered around 2835 cm^{-1} were from the silane methoxy symmetric stretches, indicating that the silane methoxy groups of both ATMS and BTMS were present and ordered at the d_4-PET interface. Figure 1.6 shows the same

interfaces when the TiO_2 interlayer was used to provide nonresonant signal. When the TiO_2 interlayer was used, the methoxy signal from the ATMS was enhanced while the methoxy signal from the BTMS was attenuated, indicating that the signals interfered differently with the nonresonant background and therefore had different absolute orientations. Because it had been shown that ATMS formed hydrogen bonds with PET, the amino-end groups of ATMS must have faced toward the polymer, meaning that methoxy groups of ATMS must have faced away from the polymer. Therefore, because the BTMS methoxy groups had the opposite absolute orientation at the polymer interface, the BTMS methoxy groups must have faced toward the polymer.[55]

This study showed that it was possible to determine the relative absolute orientation of silane adhesion promoter molecules at polymer interfaces, which can affect adhesion mechanisms, and laid the groundwork for research presented in Chapter 2, Section 2.3.2.

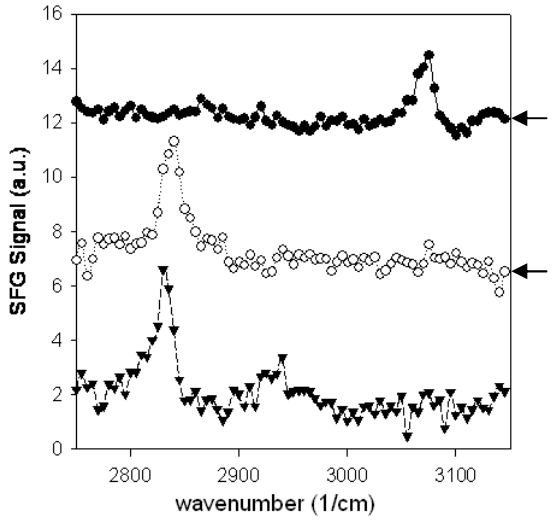

Figure 1.5 SFG spectra of d_4-PET in contact with air (closed circles), ATMS (open circles) and BTMS (closed triangles). Baselines of spectra are indicated by arrows on right.

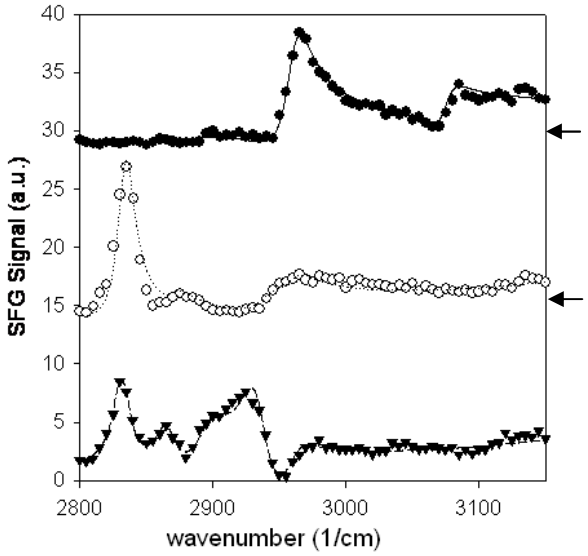

Figure 1.6 SFG spectra of d_4-PET in contact with air (closed circles), ATMS (open circles) and BTMS (closed triangles) with the TiO_2 interlayer. Baselines of spectra are indicated by arrows on right.

1.3.2 Buried Interfacial Structures of a Silane Adhesion Promoting Mixture at the PET Interface

As will be detailed in Chapter 2, Section 2.1, mixtures of an organosilane and a siloxanol have been shown to greatly enhance the adhesion of silicone elastomer to polymeric substrates. Specifically, a mixture of γ-GPS and a methylvinylsiloxanol (MVS) enhances the adhesion of silicone to PET, while alone neither the γ-GPS nor the MVS enhances adhesion. In this study, SFG was used to investigate the buried interfacial structures between d_4-PET and the mixture of γ-GPS and MVS.

In this initial investigation of the γ-GPS/MVS mixture, the structures of γ-GPS, MVS and the mixture were studied at the d_4-PET interface. Figure 1.7 shows SFG spectra of d_4-PET in contact with MVS and with γ-GPS, and Figure 1.8 shows SFG spectra of d_4-PET in contact with the γ-GPS/MVS mixture at initial contact and after the

spectral features stabilized. It can be seen in Figure 1.7 that weak signal from the γ-GPS methoxy groups was generated, and weak C-H signal from the MVS was detected. However, the spectra were different when the γ-GPS and MVS are mixed. As seen in Figure 1.8, after the spectral features stabilized, the symmetric methoxy stretching signal from the γ-GPS was enhanced. This showed that the MVS acted to order the γ-GPS methoxy groups at the polymer interface. Because the γ-GPS/MVS mixture acts as an adhesion promoter, this study was the first indication that the interfacial ordering enhancement of the γ-GPS methoxy groups by the MVS may contribute to adhesion promotion.[57]

This work provided a framework for the results presented in Chapters 2 and 3. Because enhancement of the γ-GPS interfacial ordering was observed only when the γ-GPS was mixed with MVS, it was important to determine if this behavior was universal to all silanes or if it was unique to the adhesion promoting mixture. It was also important to determine if this enhanced interfacial ordering occurred not only at the polymer/liquid silane or silane/MVS mixture interface but also at the silicone elastomer/silane interface and the polymer/silicone elastomer interface.

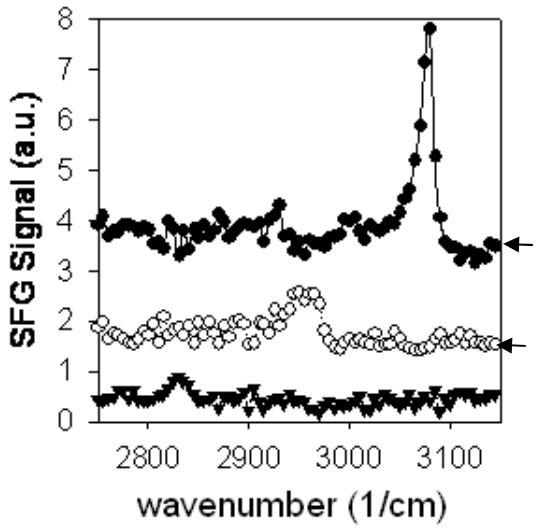

Figure 1.7 SFG spectra of d_4-PET in contact with air (closed circles), MVS (open circles) and γ-GPS (closed triangles). Note spectra are off-set. . Baselines of spectra are indicated by arrows on right.

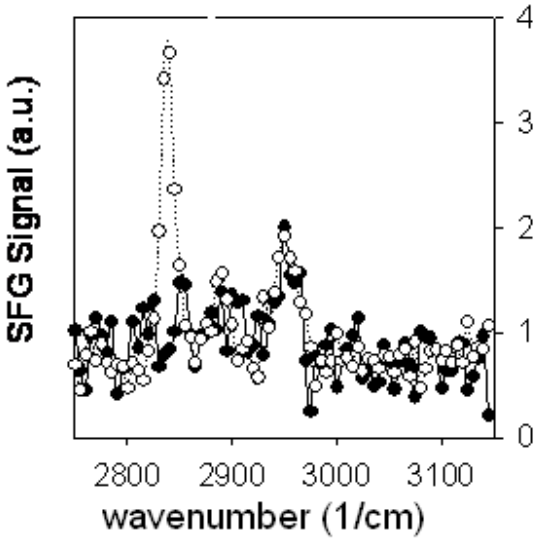

Figure 1.8 SFG spectra of d_4-PET in contact with the γ-GPS/MVS mixture at initial contact (black circles) and after the spectral features stabilized (open circles).

1.3.3 Diffusion of Silanes into a Polymer

Prior work has also shown that silane adhesion promoters can diffuse into certain polymers. Being able to probe these interfacial interactions is important because inter-diffusion is a known adhesion mechanism.

In a prior study, SFG was used to monitor the diffusion of the silane adhesion promoting mixture of γ-GPS and MVS into a thin film of deuterated poly(methyl methacrylate) (*d*-PMMA). It was known that γ-GPS and the γ-GPS/MVS mixture dissolved polystyrene (PS), so an experiment was designed to monitor the diffusion of γ-GPS and the γ-GPS/MVS mixture through the *d*-PMMA. A PS/*d*-PMMA bilayer was deposited on a fused silica substrate such that the *d*-PMMA was the outer layer contacting the silanes, and the PS was the inner layer next to the substrate. As the silane or silane/MVS mixture diffused through the *d*-PMMA, it would reach the PS layer and dissolve it. Both the silane and PS signal could be monitored.

Figure 1.9 shows SFG spectra of the PS/*d*-PMMA bilayer in contact with γ-GPS over time. The silane methoxy signal was present after approximately five minutes of contact, but the signal disappeared after fifteen minutes, along with the signal from the PS. This indicated that the silane diffused through the *d*-PMMA, dissolved the inner PS layer and disordered. Figure 1.10 shows SFG spectra of the PS/*d*-PMMA bilayer in contact with the mixture of γ-GPS and MVS. Initially, the only signal present was attributed to the inner PS layer. After forty five minutes of contact time, the γ-GPS methoxy signal emerged, and disappeared approximately ten minutes later, along with the PS signal. Thus, the γ-GPS in the γ-GPS/MVS mixture was not ordered while diffusing through the *d*-PMMA layer, but briefly became ordered at the PS interface before dissolving it.[58]

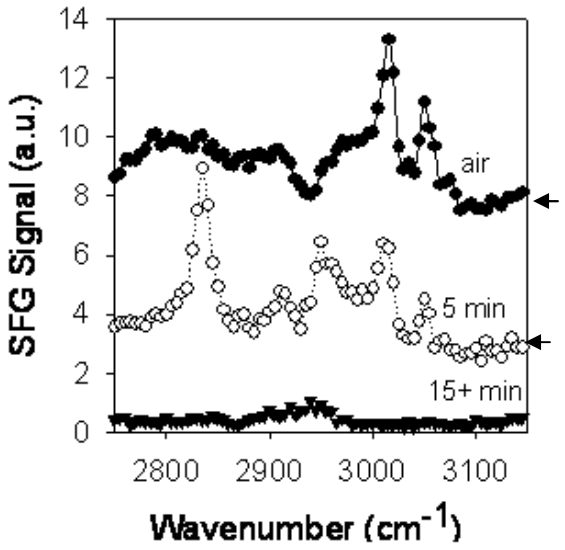

Figure 1.9 SFG spectra of PS/*d*-PMMA bilayer in contact with γ-GPS over time. . Baselines of spectra are indicated by arrows on right.

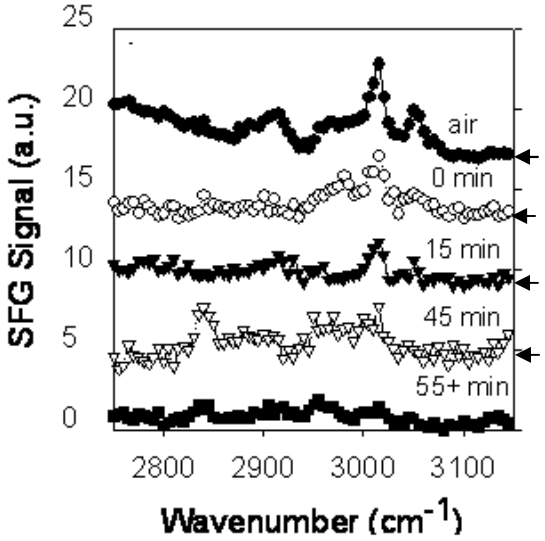

Figure 1.10 SFG spectra of PS/*d*-PMMA bilayer in contact with γ-GPS/MVS mixture over time. Baselines of spectra are indicated by arrows on right.

Further, solubility parameters based on empirical estimates of cohesive energy density were used to explain why γ-GPS and the γ-GPS/MVS mixture dissolved PS, diffused into *d*-PMMA and formed stable interfaces with PET. It was found that the solubility parameter difference between PET and the liquids was consistently higher than

that for PS or PMMA, helping to explain why the liquids could diffuse into or dissolve PMMA and PS but not PET.[58]

This work was important in further showing the ability of SFG to monitor interfacial interactions that can affect adhesion, such as diffusion. Also, the use of solubility parameters provided evidence as to why the silanes did not diffuse into or dissolve PET, which is important in determining how these silanes interact at the PET interface.

1.4 Presented Research

The presented research continues the study of surface and interfacial polymer structures affecting polymer adhesion. The inherent surface and interface sensitivity of SFG will be used to understand how the structures of polymer surfaces and the structures of the interfaces between polymer adhesives and their adherends can help deduce prerequisite conditions needed for adhesion.

In Chapter 2, the buried interfacial structures between d_4-PET and the silane adhesion promoting mixture of γ-GPS and MVS will be studied at the polymer/silane (or silane mixture) interface, the polymer/uncured silicone elastomer interface and the polymer/cured silicone elastomer interface. The behaviors of the γ-GPS and the γ-GPS/MVS mixture at the polymer interface will be compared to those of two other silanes not used as adhesion promoters, as well as their mixtures with MVS. It will be determined that the MVS acts to further order the γ-GPS molecules at the polymer interface, while this behavior is not observed for the other silanes/MVS mixtures. Further, silane behavior at the polymer/silicone interface does not directly correlate to silane behavior at the polymer/silane interface. The ability of γ-GPS in the γ-GPS/MVS

mixture to order at these interfaces may be a prerequisite condition for adhesion promotion for this system.[61]

The work in Chapter 2 infers that the silicone elastomer may affect the ordering of silanes in silane/MVS mixtures at polymer interfaces, and Chapter 3 will further investigate this by studying silicone elastomer/silane (or silane/MVS mixture) interfaces. Again, only the γ-GPS maintains interfacial order at the silicone interface when mixed with MVS. As MVS is necessary for adhesion promotion, this study is further evidence that the ability of a silane to exhibit interfacial orientational order at polymer interfaces when mixed with MVS may be a necessary prerequisite condition for adhesion promotion mechanisms.[62]

In some applications, such as those in microfluidics, the use of adhesion promoters is not advantageous and silicone surfaces are enhanced with reactive silanol groups by oxidative surface treatments to improve adhesion. It is known that removing extractable materials from silicone improves the effect of oxidative surface treatments, but the reason is poorly understood. In Chapter 4, the effect of removing extractable materials from silicone surfaces will be investigated and it will be shown that the extracted silicone surface becomes similar to that of a highly crosslinked silicone surface. This change in silicone surface structure may improve the effectiveness of oxidative treatments for adhesion enhancement.

Lastly, Chapter 5 will expand these studies to a different class of polymer adhesives. In this work, surfaces and buried interfaces of epoxy resins used as underfills in semiconductor devices will be investigated. It will be shown that the substrate composition affects how bisphenol-type epoxy films deposit, which may have important

implications for the deposition of underfills in flip-chip devices. Further, changes in bisphenol-type epoxy surface structure during cure are detected, which might affect adhesion of these epoxies as they cure *in situ* in flip-chip devices. Lastly, the effect of moisture on both surface and buried interfacial structures is investigated and correlated to adhesion testing results.

The presented work investigates how polymer adhesive surface and buried interfacial structures can affect polymer adhesion in a variety of industrial applications. By correlating surface and buried interfacial structures to adhesion, these studies provide evidence that surface and buried interfacial structures of polymer adhesives can impact adhesion properties, and lay the foundation for future work using SFG to further elucidate adhesion mechanisms.

1.5 References

1. Mittal, K. L. *Adhesion Measurement of Thin Films, Thick Films, and Bulk Coatings;* American Society for Testing and Materials: Philadelphia, 1978.

2. Kookoostedes, G. J. In *Polymeric Materials for Electronics Packaging and Interconnection*; Lupinski, J. H., Moore, R. S., Eds.; American Chemical Society: Washington, D.C., 1989; pp 230-239.

3. Charles, H. K. Jr. *Engineered Materials Handbook Vol. 3: Adhesives and Sealants;* ASM International: Materials Park, Ohio, 1990.

4. Kinloch, A. J. *Adhesion and Adhesives Science and Technology;* Chapman and Hall: London, 1987.

5. Newby, B. M. Z.; Chaudhury, M. K.; Brown, H. R. *Science* **1995**, *269*, 1407-1409.

6. Pocius, A. V. *Adhesion and Adhesives Technology, An Introduction;* Hanser/Gardner Publications, Inc.: Cincinnati, 1997.

7. Harding, P. H.; Berg, J. C. *J. Appl. Polym. Sci.* **1998**, *67*, 1025-1033.

8. Yacobi, B. G.; Martin, S.; Davis, K.; Hudson, A.; Hubert, M. *J. Appl. Phys.* **2002**, *91*, 6227-6262.

9. Suzuki, T.; Kasuya, A. *J. Adhes. Sci. Technol.* **1989**, *3*, 463-473.

10. McDonald, J.C.; Whitesides, G.M. *Acct. Chem. Res.* **2002**, *35*, 491-499.

11. Esteves, A.C.; Brokken-Zijp, J.; Laven, J.; Huinick, H.P.; Reuvers, N.J.W.; Van de With, M.P. *Polymer.* **2009**, *50,* 3955-3966.

12. McDonald, J.C.; Duffy, D.C.; Anderson, J.R.; Chiu, D.T.; Wu, H; Schueller, O.A.; Whitesides, G.M. *Electrophoresis*, **2002**, *21*, 27-40.

13. Ye, H.; Gracias, D.H. *Langmuir*, **2006**, *22*, 1863-1868.

14. Plueddemann, E. P. *Silane Coupling Agents;* Plenum Press: New York, 1991.

15. Mine, K.; Nishio, M.; Sumimura, S. U.S. Patent 4,033,924, July 5, 1977.

16. Schulz, J. B. U.S. Patent 4,087,585, May 2, 1978.

17. Gray, T. E.; Lutz, M. A. U.S. Patent 5,595,826, January 21, 1997.

18. Ardebili, H.; Wong, E.H.; Pecht, M. *IEEE Trans.* **2003**, *26*, 206-214.

19. Arvanitopoulos, C.; Koenig, J. *Applied Spec.* **1996**, *50*, 11-18.

20. Ferguson, T.P.; Qu, J. *IEEE Trans.* **2006**, *29*, 105-111.

21. Liu, M.; Wu, P.; Ding, Y.; Chen, G.; Li, S. *Macromolecules* **2002**, *35*, 5500-5507.

22. Musto, P.; Ragosta, G.; Mascia, L. *Chem. Mater.* **2000**, *12*, 1331-1341.

23. Brown, H. R. *Science* **1994**, *263*, 1411-1413.

24. Dai, C. A.; Dair, B. J.; Dai, K. H.; Ober, C. K.; Kramer, E. J.; Hui, C. Y.; Jelinski, L. W. *Phys. Rev. Lett.* **1994**, *73*, 2472-2475.

25. Russell, T. P. *Physica B* **1996**, *221*, 267-283.

26. Russell, T. P. *Science* **2002**, *297*, 964-967.

27. Simmons, E. R.; Chakraborty, A. K. *J. Chem. Phys.* **1998**, *109*, 8667-8676.

28. Schnell, R.; Stamm, M.; Creton, C. *Macromolecules* **1998**, *31*, 2284-2292.

29. Edgecombe, B. D.; Stein, J. A.; Frechet, J. M. J.; Xu, Z. H.; Kramer, E. J. *Macromolecules* **1998**, *31*, 1292-1304.

30. Schulze, J. S.; Moon, B.; Lodge, T. P.; Macosko, C. W. *Macromolecules* **2001**, *34*, 200-205.

31. Khongtong, S.; Ferguson, G. S. *J. Am. Chem. Soc.* **2001**, *123*, 3588-3594.

32. Cole, K.; Ajji, A.; Pellerin, E. *Macromolecules.* **2002**, *35*, 770-784.

33. Shull, K. R. *Macromolecules* **2002**, *35*, 8631-8639.

34. Chiang, C. H.; Ishida, H.; Koenig, J. L. *J. Colloid Interface Sci.* **1980**, *74*, 396-404.

35. Bertelsen, C. M.; Boerio, F. J. *Prog. Org. Coat.* **2001**, *41*, 239-246.

36. Gracias, D. H.; Chen, Z.; Shen, Y. R.; Somorjai, G. A. *Acc. Chem. Res.* **1999**, *32*, 930-940.

37. Opdahl, A.; Somorjai, G. A. *Langmuir* **2002**, *18*, 9409-9412.

38. Kweskin, S. J.; Komvopoulos, K.; Somorjai, G. A. *Langmuir* **2005**, *21*, 3647-3652.

39. Chen, Z.; Shen, Y. R.; Somorjai, G. A. *Annu. Rev. Phys. Chem.* **2002**, *53*, 437-465.

40. Oh-E, M.; Lvovsky, A. I.; Wei, X.; Shen, Y. R. *J. Chem. Phys.* **2000**, *113*, 8827-8832.

41. Gautam, K. S.; Schwab, A. D.; Dhinojwala, A.; Zhang, D.; Dougal, S. M.; Yeganeh, M. S. *Phys. Rev. Lett.* **2000**, *85*, 3854-3857.

42. Harp, G. P.; Gautam, K. S.; Dhinojwala, A. *J. Am. Chem. Soc.* **2002**, *124*, 7908-7909.

43. Briggman, K. A.; Stephenson, J. C.; Wallace, W. E.; Richter, L. J. *J. Phys. Chem. B* **2001**, *105*, 2785-2791.

44. Miyamae, T.; Yamada, Y.; Uyama, H.; Nozoye, H. *Appl. Surf. Sci.* **2001**, *180*, 126-137.

45. Liu, Y.; Messmer, M. C. *J. Am. Chem. Soc.* **2002**, *124*, 9714-9715.

46. Ye, S.; Morita, S.; Li, G. F.; Noda, H.; Tanaka, M.; Uosaki, K.; Osawa, M. *Macromolecules* **2003**, *36*, 5694-5703.

47. Wang, J.; Woodcock, S. E.; Buck, S. M.; Chen, C. Y.; Chen, Z. *J. Am. Chem. Soc.* **2001**, *123*, 9470-9471.

48. Wang, J.; Chen, C. Y.; Buck, S. M.; Chen, Z. *J. Phys. Chem. B* **2001**, *105*, 12118-12125.

49. Wang, J.; Paszti, Z.; Even, M. A.; Chen, Z. *J. Am. Chem. Soc.* **2002**, *124*, 7016-7023.

50. Chen, C. Y.; Wang, J.; Even, M. A.; Chen, Z. *Macromolecules* **2002**, *35*, 8093-8097.

51. Chen, C. Y.; Even, M. A.; Wang, J.; Chen, Z. *Macromolecules* **2002**, *35*, 9130-9135.

52. Chen, C. Y.; Even, M. A.; Chen, Z. *Macromolecules* **2003**, *36*, 4478-4484.

53. Chen, C. Y.; Loch, C. L.; Wang, J.; Chen, Z. *J. Phys. Chem. B* **2003**, *107*, 10440-10445.

54. Chen, C. Y.; Wang, J.; Loch, C. L.; Ahn, D.; Chen, Z. *J. Am. Chem. Soc.* **2004**, *126*, 1174-1179.

55. Loch, C. L.; Ahn, D.; Chen, C. Y.; Wang, J.; Chen, Z. *Langmuir* **2004**, *20*, 5467-5473.

56. Loch, C. L.; Ahn, D.; Chen, C. Y.; Chen, Z. *J. Adhes.* **2005**, *81*, 319-345.

57. Loch, C. L.; Ahn, D.; Chen, Z. *J. Phys. Chem. B* **2006**, *110*, 914-918.

58. Loch, C.L.; Ahn, D.; Vázquez, A.V.; Chen, Z. *J. Colloid Interface Sci.* **2007**, *308* 170-175.

59. Chen, Z. *Polymer International.* **2006**, *56* 577-587.

60. Ye, S.; McClelland, A.; Majumdar, P.; Stafslien, S.; Daniels, J.; Chisholm, B.; Chen, Z. *Langmuir*, **2008**, *24*, 9686-9694.

61. Vázquez, A.V.; Shephard, N.E.; Steinecker, C.L.; Ahn, D.; Spanninga, S.; Chen, Z. *J. Colloid Interface Sci*. **2009**, *331*, 408-416.

62. Vázquez, A.V.; Boughton, A.P.; Shephard, N.E.; Rhodes, S.L.; Chen, Z. *ACS Applied Mater. Interf.* **2010**, *2*, 96-103.

63. Shen, Y. R. *The Principles of Nonlinear Optics;* Wiley: New York, 1984.

64. Bain, C. D. *J. Chem. Soc., Faraday Trans.* **1995**, *91*, 1281-1296.

65. Eisenthal, K. B. *Chem. Rev.* **1996**, *96*, 1343-1360.

66. Lambert, A.G.; Davies, P.B.; Neivandt, D. *J. Applied. Spectroscopy Reviews.* **2005**, *40*, 103-145.

67. Buck, M.; Himmelhaus, M. *J. Vac. Sci. Technol., A* **2001**, *19*, 2717-2736.

68. Zhuang, X.; Miranda, P. B.; Kim, D.; Shen, Y. R. *Phys. Rev. B* **1999**, *59*, 12632-12640.

69. Superfine, R.; Huang, J. Y.; Shen, Y. R. *Chem. Phys. Lett.* **1990**, *172*, 303-306.

CHAPTER 2

RELATING THE MOLECULAR STRUCTURES OF SILANES AT BURIED POLYMER INTERFACES TO ADHESION PROMOTION

2.1 Introduction

Strong adhesion of elastomeric adhesives to various polymer substrates is an important aspect of many engineering applications in the electronics, automotive and aviation fields. Elastomeric adhesives are often preferred over mechanical fasteners because they are lighter, which can improve fuel economy, and also because they distribute the load on the adhesive joint more evenly. Addition-cured silicone elastomers are frequently used in engineering applications because they exhibit unique rheological properties and have high thermal stabilities in both high and low temperature regimes.[1-4] However, these silicone elastomers lack intrinsic reactive or polar functional groups that would allow for strong adhesion to polymeric substrates. Often oxidative surface treatments are used to alter the polarity of the surface of the silicone elastomer prior to application to polymer substrates. However, in some industrial settings, these pretreatments can be expensive and time-consuming. Small molecule adhesion promoters that can be incorporated in to the silicone elastomer prior to application to the substrate have been developed for a wide variety of inorganic and polymeric substrates, eliminating the need for surface pretreatments.[3,5-11]

It has been demonstrated that a mixture of an organosilane and a siloxanol enhances the adhesion between silicone elastomer and polymer substrates. Specifically, a mixture of (3-glycidoxypropyl)trimethoxysilane (γ-GPS) and a hydroxyl-terminated methylvinylsiloxanol (MVS) is a known effective adhesion promoting mixture for improving adhesion between silicone and poly(butylene terephthalate) (PBT). When small amounts of the γ-GPS/MVS mixture are incorporated into the silicone elastomer prior to application to the PBT substrate, adhesion is enhanced. Alone, neither the γ-GPS nor the MVS acts as adhesion promoters.[9,10]

It is expected that adhesion promoters facilitate some type of interfacial interactions between adhesive and substrate to improve adhesion. However, such mechanisms are difficult to study with most analytical techniques because they occur at buried interfaces that are not accessible to most surface sensitive techniques. Here, the ability of SFG to probe buried interfaces was exploited to study the buried interfaces between polymer substrate and neat silanes and silane mixtures, as well as the buried interfaces between polymer substrate and cured and uncured silicone elastomer to gain insight into the function of the silane adhesion promoting mixture of γ-GPS and MVS.

As discussed in Chapter 1, Section 1.3, earlier SFG results studying the polymer/silane or polymer/silane mixture interface have shown that γ-GPS methoxy groups ordered at the interface of poly(ethylene terephthalate) (PET), a polymer analogous to PBT. Further, when γ-GPS was mixed with MVS, the ordering of the γ-GPS methoxy groups was enhanced.[12] This study aimed to further understand why the γ-GPS/MVS mixture is an effective adhesion promoter compared to other silanes not used as adhesion promoters.

In this study, the behavior of γ-GPS and its mixture with MVS were first studied at PET interface. The behavior of the γ-GPS and the adhesion promoting mixture of γ-GPS and MVS were compared to those of two other silanes not used as adhesion promoters, N-octadecyltrimethoxysilane (OTMS) and (tridecalfluoro-1,1,2,2-tetrahydroctyl)trimethoxysilane (TDFTMS), as well as their mixtures with MVS. Both OTMS and TDFTMS have trimethoxy head groups, but have different backbones and end groups than γ-GPS. OTMS has a methylene backbone and a methyl end group, while TDFTMS has a fluoroalkyl backbone and a CF_3 end group. The presence and absolute orientation of the silane methoxy groups were deduced at the d_4-PET interface. More importantly, for the first time, the behavior of the silanes and silane/MVS mixtures were investigated at the PET/silicone elastomer buried interfaces. Both the PET/uncured silicone interface and the PET/cured silicone interface with small amounts of incorporated silane or silane/MVS mixture were investigated. Further, X-ray photoelectron spectroscopy (XPS) was used to investigate the exposed PET surface resulting from peeling the PET/cured silicone elastomer with incorporated TDFTMS interface and the PET/cured silicone with incorporated TDFTMS/MVS mixture interface.

To confirm that only the γ-GPS/MVS mixture significantly enhanced adhesion between PET and silicone elastomer, 90^o peel adhesion tests were performed. Adhesion test specimens were prepared using a high throughput thermal gradient press. The temperature for curing (T_{cure}) and adhesion, as defined by the threshold temperature for cohesive failure (T_{CF}) were determined for all systems studied. The SFG results were correlated to the adhesion testing results to develop an understanding of how interfacial silane ordering affects adhesion.

2.2 Experimental

2.2.1 Sample Preparation

Poly(ethylene terephthalate) (PET, Mv = 18,000) was obtained from Sigma-Aldrich, Inc. PET with deuterated ethylene glycol subunits (d_4-PET, Mv = 72,000) was purchased from Polymer Source, Inc. The d_4-PET was used in SFG studies to avoid any spectral confusion in the C-H stretching region. N-octadecyltrimethoxysilane (OTMS) and (tridecafluoro-1,1,2,2-tetrahydroctyl)trimethoxysilane (TDFTMS) were ordered from Gelest, Inc. Methylvinylsiloxanol with hydroxyl endgroups (MVS), (3-glycidoxypropyl)trimethoxysilane (γ-GPS) and Sylgard 184 silicone elastomer kit were obtained from Dow Corning Corp. All chemicals were used as received.

The Sylgard 184 silicone elastomer was prepared in a 10:1 base/curing agent ratio, as directed by the manufacturer. The base and curing agent were mixed vigorously to the point of visual homogeneity. When added, 1.5 wt% γ-GPS, 3 wt% 1:1 (wt/wt) γ-GPS/MVS mixture, 1.5 wt% OTMS, 3 wt% 1:1 OTMS/MVS mixture, 3 wt% TDFTMS or 4.5 wt% 2:1 (wt/wt) TDFTMS/MVS mixture was manually mixed into the silicone elastomer formulation to the point of visual homogeneity prior to cure. A larger concentration of TDFTMS was used to ensure that all systems had similar molar ratios of silanes. When MVS was added, a SiH-functional PDMS was added to maintain a 1.5:1 SiH/vinyl molar ratio.

To prepare thin films of d_4-PET for SFG analysis, a 1 wt% solution of d_4-PET in 2-chlorophenol (99%, Sigma-Aldrich, Inc) was spin cast using a spin-coater from Specialty Coating Systems onto fused silica windows (1-in diameter, 1/8-in thickness, ESCO Products, Inc). The fused silica windows were cleaned by etching in warm

chromic acid solution prior to use. The films were placed under vacuum for at least 18 h prior to analysis to ensure that the solvent was removed. When the buried interface between d_4-PET and cured silicone elastomer was studied, thick films of silicone elastomer (with incorporated silane or silane/MVS mixture) were applied to the polymer thin film and were cured in an oven for 1 h at 150^{o} C prior to analysis.

Adhesion testing specimens were prepared on microscope slides. Microscope slides were cleaned by etching in warm chromic acid solution prior to use. A thin film of PET was spin cast from a 1 wt% solution in 2-chlorophenol. The film was placed under vacuum for at least 18 h prior to analysis to remove solvent. A thick film (approximately 1 cm) of silicone elastomer (with incorporated silane or silane/MVS mixture) was applied to the polymer thin film. A piece of aluminum foil (Fisher Scientific, Inc) was applied to the top of the silicone elastomer film to provide a flexible backing for adhesion testing. The samples were cured in the high throughput thermal gradient press, as will be described below.

For XPS experiments, thin films of PET were prepared by spin coating a 1 wt% solution in 2-chlorophenol on glass microscope slides that had been etched in warm chromic acid, and were then placed under vacuum for 18 h. Thick films of silicone elastomer with 3 wt% TDFTMS or 4.5 wt% 2:1 (wt/wt) TDFTMS/MVS mixture were applied to the PET films and were cured in an oven for 1 h at 150^{o}C. An interfacial crack was initiated and the interface was peeled to expose the two resulting surfaces (the PET and the silicone elastomer). The resulting PET surface was examined using XPS.

Structures of PET and the silanes in this study are shown in Figure 2.1.

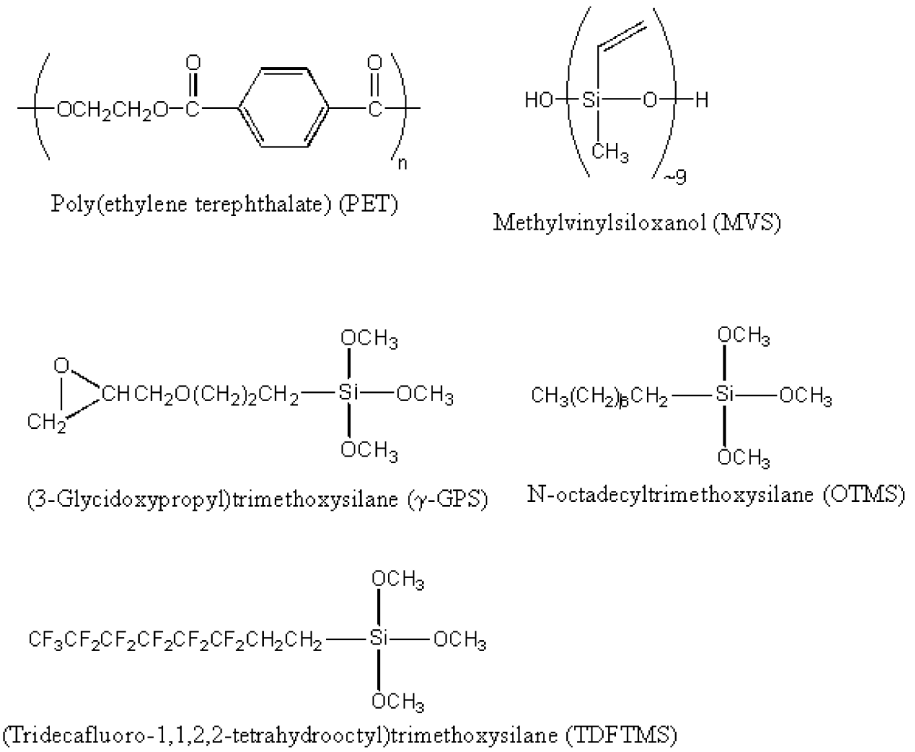

Figure 2.1. Chemical structures of PET, MVS and silanes.

2.2.2 TiO_2 Film Preparation

To study the absolute orientation of the silanes at the d_4-PET interface, nonresonant SFG signal from TiO_2 was used to interfere with resonant SFG signal from the silanes. A 150 nm Ti film was deposited onto fused silica substrates by electron beam evaporation. The fused silica substrates were cleaned by etching in warm chromic acid prior to deposition. The procedure was performed at a pressure of 2 x 10^{-6} mbar with a deposition rate of 0.2 nm/s. The substrates were heated in a furnace at 700^{o}C for 12 h to form a translucent layer of TiO_2.

2.2.3 SFG Experiments

The theory of SFG is well-developed and has been detailed in Chapter 1, Section 1.2.3.[13-17] The SFG system and experimental geometry used in this investigation were detailed in Chapter 1, Section 1.2.3.[12, 18-22] Briefly, the visible and infrared (IR) input

beams overlap spatially and temporally on the polymer surface, polymer/liquid interface or the polymer/cured elastomer interface with input angles of 60° and 54°, respectively and pulse energies of 200 μJ and 100 μJ, respectively. The beam diameters are approximately 500 μm. Prior results indicate that SFG signals are dominated by polymer surface or interface with negligible contribution from the polymer bulk or the polymer/substrate interface. In this investigation, all SFG spectra were obtained in the ssp polarization combination (s-polarized sum frequency output, s-polarized visible input and p-polarized IR input). Other polarization combinations, such as sps and ppp, did not yield SFG signal for these studies.

2.2.4 XPS Experiments

For XPS sample characterization, a Kratos AXIS Ultra DLD X-ray photoelectron spectrometer (Kratos Analytical Ltd., Manchester, England) with a monochromatic aluminum source (AlKalpha = 1486.6 eV) at a vacuum pressure of 10^{-8} – 10^{-9} Torr was used. Initial survey scans were run with a pass energy of 160 eV, and characteristic region scans of the C 1s, O 1s, and F 1s used a pass energy of 20 eV with a step of 0.1 eV.

2.2.5 Adhesion Testing Experiments

Adhesion test specimens were prepared on the high throughput thermal gradient press developed at Dow Corning Corp. for 90° peel tests. For the samples described above, the silicone was cured on a programmable linear temperature gradient, allowing both T_{cure} and T_{CF} to be determined in a single adhesion test experiment.[23] Samples were prepared on a linear temperature gradient from 50 to 180° C with a ramp time of 8 min, a soak time of 52 min and a cool time of 15 min. To perform the 90° peel test, an interfacial crack was initiated on the cool side of the slide, and the silicone (with the

aluminum foil backing) was peeled at 90^{o} until it was arrested by a transition to cohesive failure. The position on the slide was related to cure temperature by a linear regression. The position on the slide where the silicone elastomer transitioned from a viscous liquid to an elastomeric solid was correlated to T_{cure}, and the position on the slide where the sample transitioned from interfacial to cohesive failure was correlated to T_{CF}.

2.3 Results and Discussion

2.3.1 SFG Studies of *d_4*-PET in Contact with Neat Silanes and Silane/MVS Mixtures

In earlier studies, SFG spectra were obtained from the interfaces between *d_4*-PET and neat γ-GPS and *d_4*-PET and the 1:1 (wt/wt) γ-GPS/MVS mixture to determine which chemical groups of the γ-GPS ordered at the polymer interface. These results are reproduced in Figure 2.2.[12] In the SFG spectrum of the *d_4*-PET in contact with γ-GPS, a peak centered at 2835 cm^{-1} was detected and assigned to the symmetric C-H stretch of the γ-GPS methoxy groups at the *d_4*-PET interface.[12] The intensity of the peak increased over 30 minutes of contact time, and was then stable. The spectrum of *d_4*-PET in contact with the 1:1 γ-GPS/MVS mixture also exhibited the symmetric silane methoxy stretch. However, the γ-GPS methoxy peak strength was greater for the silane/siloxanol mixture than it was for the neat silane, indicating that the MVS acted to increase the order of the γ-GPS molecules at the polymer interface. In the spectrum of *d_4*-PET in contact with the γ-GPS/MVS mixture, a peak at 2960 cm^{-1} was attributed to the MVS.[12]

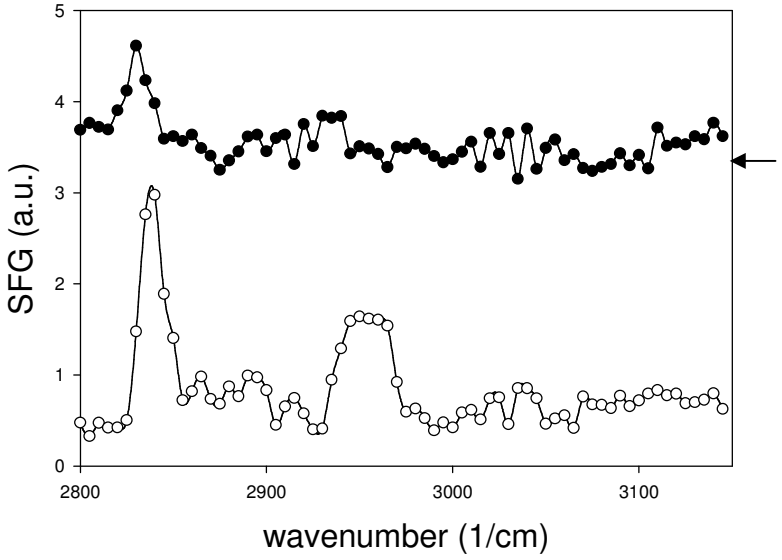

Figure 2.2. SFG spectra of d_4-PET in contact with γ-GPS (closed circles) and d_4-PET in contact with the γ-GPS/MVS mixture (open circles). . Baselines of spectra are indicated by arrows on right.

As discussed in the introduction, Section 2.1, the mixture of the silane γ-GPS and the siloxanol MVS act as an adhesion promoting mixture for the adhesion of silicone to PET. It can be inferred from the earlier study that perhaps the improvement of adhesion with the γ-GPS/MVS mixture is correlated to the improved interfacial ordering of the γ-GPS methoxy groups at the PET interface. However, it is important to determine if the ordering of the silane methoxy groups at the PET interface, and the enhancement of this ordering when the silane is mixed with MVS, is a general phenomenon or one that is unique to γ-GPS and the γ-GPS/MVS adhesion promoting mixture. Therefore, the interfaces between d_4-PET and two other silanes with different backbones and end groups, OTMS and TDFTMS, as well as their mixtures with MVS were investigated with SFG for comparison.

SFG spectra of d_4-PET in contact with neat OTMS and the OTMS/MVS mixture are in Figure 2.3. In the spectrum of d_4-PET in contact with neat OTMS, the characteristic silane methoxy symmetric C-H stretching peak was observed at 2835 cm^{-1}, indicating that the OTMS methoxy head groups exhibited some orientational order at the polymer interface. Unlike the γ-GPS, this signal was stable with time. There was also signal at 2950 cm^{-1}, which was most likely from the OTMS methylene backbone. This showed that, unlike the γ-GPS, the OTMS backbone may also be present at the d_4-PET interface. The SFG spectrum of d_4-PET in contact with the 1:1 OTMS/MVS mixture also exhibited a stable peak at 2835 cm^{-1}, from the OTMS methoxy groups. However, when the OTMS was mixed with MVS, the strength of the OTMS methoxy peak was markedly weaker than that of the neat OTMS. Because SFG is sensitive to orientational ordering, this difference in strength may have implied that the MVS caused the OTMS to lose some of its interfacial order, weakening the intensity of the OTMS signal. The attenuation of the OTMS methoxy signal strength may also have resulted from simple bulk dilution effects. If the OTMS silane lacked strong attractive interactions with the polymer surface, the MVS may have also segregated to the polymer interface. In this case, the interfacial concentration of OTMS would have decreased, and the SFG signal from the OTMS would also decrease. However, as seen in Figure 2.3, no strong, discernable signal that could be attributed to MVS was detected from the interface between d_4-PET and the 1:1 OTMS/MVS mixture, so there was no evidence of MVS segregating with order to the polymer interface. Therefore, the most likely explanation is that the MVS disordered the OTMS at the interface.

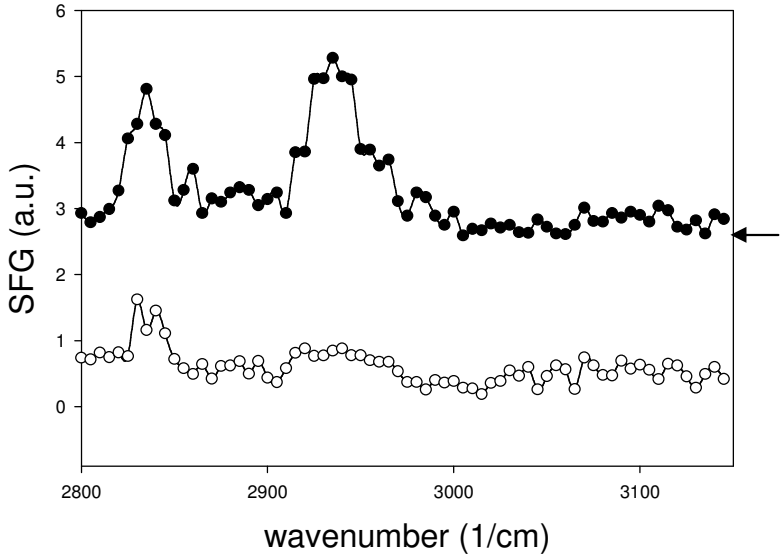

Figure 2.3. SFG spectra of d_4-PET in contact with OTMS (closed circles) and d_4-PET in contact with the OTMS/MVS mixture (open circles). . Baselines of spectra are indicated by arrows on right.

Lastly, SFG spectra of d_4-PET in contact with neat TDFTMS and the 2:1 TDFTMS/MVS mixture are presented in Figure 2.4. Like the previous SFG spectra of d_4-PET in contact with the neat silanes, the spectrum of d_4-PET in contact with neat TDFTMS exhibited a peak at 2835 cm^{-1}, from the C-H symmetric stretch of the TDFTMS methoxy head groups. This shows that the silane methoxy head groups were present with orientational order at the polymer interface. Small spectral features were also observed at 2910 cm^{-1} and 2950 cm^{-1}, which must have originated from the methylene portion of the TDFTMS backbone at the polymer interface. The SFG spectrum of d_4-PET in contact with the TDFTMS/MVS mixture exhibited the characteristic silane methoxy peak at 2835 cm^{-1}, but unlike the γ-GPS, the MVS did not act to enhance the TDFTMS methoxy signal.

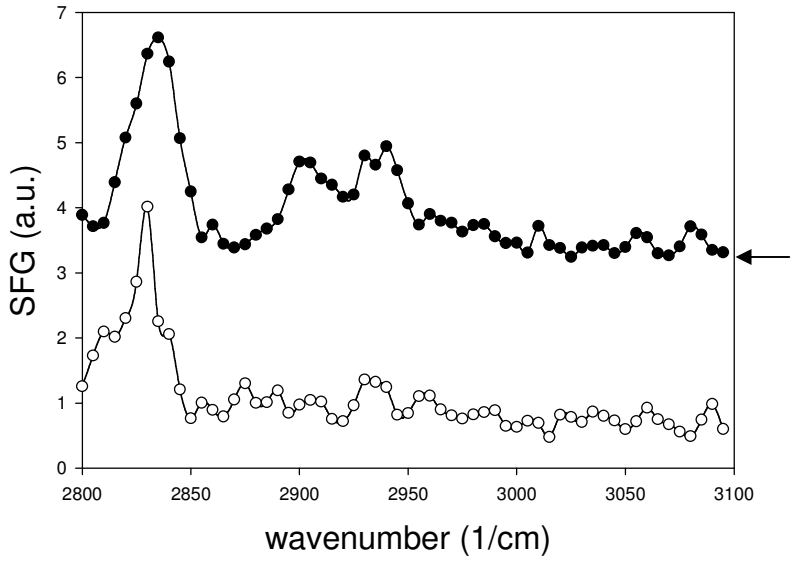

Figure 2.4. SFG spectra of d_4-PET in contact with TDFTMS (closed circles) and d_4-PET in contact with the TDFTMS/MVS mixture (open circles). Baselines of spectra are indicated by arrows on right.

The SFG studies of d_4-PET in contact with neat liquid silanes and the silane/MVS mixtures showed that the methoxy head groups of three silanes with distinctly different backbones and end groups can order at the interface between the polymer and the neat silane. This is evidenced by the silane methoxy signal observed from all three neat silanes. The backbones of neat OTMS and TDFTMS also appeared to show some orientational ordering at the d_4-PET interface. The different signal strengths of the silane methoxy signals may have been affected by the different backbones and end groups. This implies that the backbone and end groups may have influenced the orientational ordering of the methoxy head groups at the polymer interface.

The SFG spectra of d_4-PET in contact with the silane/MVS mixtures show that the silanes were affected differently by the presence of MVS, because the silane methoxy signals from the different silanes were affected differently by the presence of MVS. As

can be seen in Figure 2.2, the γ-GPS methoxy signal was enhanced when mixed with MVS, indicating that the silane methoxy groups became more ordered at the polymer interface when MVS was present. It is seen in Figure 2.3 and Figure 2.4 that, unlike γ-GPS, mixing with MVS did not increase the interfacial ordering of OTMS or TDFTMS.

It is important to recall that of all the silanes and silane mixtures studied, only the γ-GPS/MVS mixture acts as an adhesion promoter for the PET/silicone elastomer system. Therefore, interfacial behavior that is unique to the γ-GPS/MVS mixture may provide insights as to why this is an effective adhesion promoter. From this study, it can be inferred that the enhancement of the γ-GPS methoxy group ordering at the polymer interface when mixed with MVS may be an important part of its adhesion promoting activity. Some known adhesion-promoting mechanisms, such as chemical reaction or inter-diffusion may require the interfacial orientational ordering of certain chemical groups to occur. Thus, the MVS may act to order the γ-GPS interfacial molecules so the γ-GPS can then participate in one of these adhesion-promoting mechanisms. Conversely, the MVS may act to disorder the OTMS and TDFTMS, or the MVS may not be compatible with these two silanes.

2.3.2 Determination of the Absolute Orientation of Silane Molecules at the d_4-PET Interface

The SFG results discussed in section 2.3.1 indicated that the methoxy groups of all neat silanes studied ordered at the d_4-PET interface. However, these results could not determine if the three silanes exhibited the same or different absolute orientations (up or down) at the polymer interface. For example, the silane methoxy groups were ordered at the polymer interface, but some of these groups may have been ordered facing the

polymer interface (up), while other silane methoxy groups may have been ordered facing away from the polymer interface (down). The SFG signal detected in section 2.3.1 could not distinguish between these possibilities. To determine the absolute orientation of the different silanes at the d_4-PET interface, d_4-PET films were prepared on fused silica windows with TiO_2 interlayers, which provide nonresonant signal that can interfere with the resonant signal from the silanes. In the reflected direction, SFG intensity can be written as:

$$I(\omega) \alpha \left| \chi_{eff}^{(2)} \right|^2 \tag{2.1}$$

with $I(\omega)$ being the SFG intensity at a given frequency, and $\chi_{eff}^{(2)}$ being the effective second order nonlinear susceptibility. In an SFG experiment, if the IR frequency (ω_{IR}) is close to a surface or interfacial vibrational resonance, $\chi_{eff}^{(2)}$ can be written as:

$$\chi_{eff}^{(2)} = \chi_{nr} + \sum \frac{A_q}{\omega_{IR} - \omega_q + i\Gamma_q} \tag{2.2}$$

with χ_{nr} being the nonresonant background signal, and A_q, ω_q and Γ_q being the strength, frequency and damping coefficient of vibrational mode q, respectively. The nonresonant background signal is independent of the frequency, and is characteristic of the substrate. Fused silica yields no discernable nonresonant signal, but TiO_2 gives nonresonant signal that can interfere with the resonant signal from the interfacial silane methoxy groups. By comparing the signal from the interface between d_4-PET and the neat silanes with and without the TiO_2 interlayer, the relative phases of these signals and the absolute orientation of the interfacial species can be determined.

The SFG spectra of the interfaces between d_4-PET and the neat silanes with the TiO_2 interlayer are shown in Figure 2.5. When compared to Figure 2.2, the spectrum of d_4-PET in contact with γ-GPS with the TiO_2 showed a marked decrease in the γ-GPS methoxy signal with the TiO_2 interlayer. This indicated that the resonant γ-GPS methoxy signal interfered destructively with the nonresonant TiO_2 signal. The silane methoxy signal of OTMS and TDFTMS also decreased with the TiO_2 interlayer, as compared to Figures 2.3 and 2.4, respectively. Therefore, the OTMS and TDFTMS signals also destructively interfered with the TiO_2 nonresonant signal, and all silanes have the same absolute orientation. However, from just this data, it is not possible to determine what that absolute orientation is.

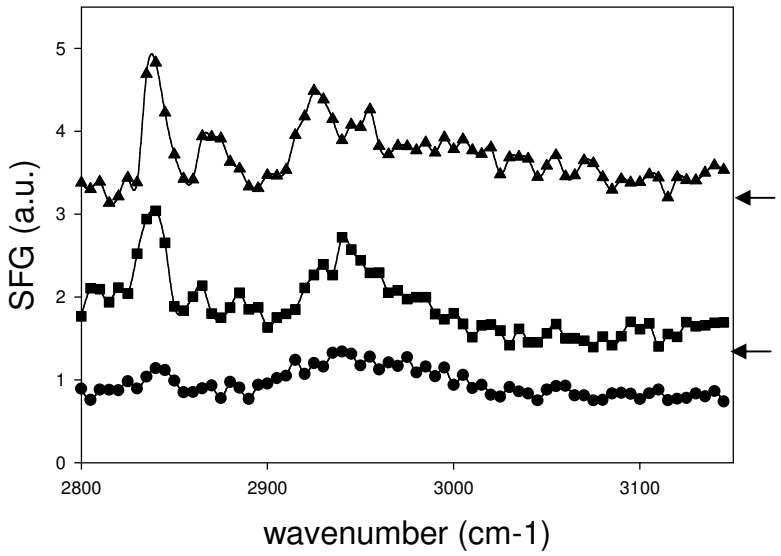

Figure 2.5. SFG spectra of d_4-PET in contact with γ-GPS (circles), OTMS (squares) and TDFTMS (triangles) with a TiO_2 interlayer. . Baselines of spectra are indicated by arrows on right.

In previous work described in Chapter 1, Section 1.3, a TiO_2 interlayer was used in SFG experiments to determine the absolute orientation of silanes at various PET/silane

interfaces. The silanes used were aminopropyltrimethoxysilane (ATMS) and butyltrimethoxysilane (BTMS). These silanes have the same methoxy head groups but different end groups. It was known that the amino end groups or ATMS formed hydrogen bonds to the PET carbonyl surface groups, and it was therefore assumed that the ATMS amino end groups faced the PET surface and the ATMS methoxy end groups faced away from the PET surface. In the experiments, it was found that the ATMS methoxy signal was enhanced with the TiO_2 interlayer, indicating that the resonant ATMS methoxy signal constructively interfered with the nonresonant TiO_2 signal. Since it was expected that the ATMS methoxy groups faced away from the PET interface, it could be determined that constructive interference corresponded to a "down" absolute orientation of silane methoxy groups. For the interface between PET and BTMS, the BTMS methoxy signal was attenuated with the TiO_2 interlayer, indicating that the resonant BTMS methoxy signal destructively interfered with the nonresonant TiO_2 signal. This showed that the BTMS molecules adopted the opposite absolute orientation as the ATMS molecules, namely facing "up" toward the PET surface.[24] Because the silane OTMS is very similar in structure to BTMS, it is expected that OTMS would have a similar absolute orientation to BTMS at the PET (or d_4-PET) interface. Therefore, because the resonant signal from OTMS, as well as the signal from γ-GPS and TDFTMS, destructively interfered with the nonresonant signal from TiO_2, it can be determined that the methoxy groups of all silanes in this study faced toward the polymer interface.

2.3.3 SFG Studies of d_4-PET in Contact with Uncured Silicone with Incorporated Silanes or Silane/MVS Mixtures

While the studies in sections 2.3.1 and 2.3.2 gave insight into the potential importance of silane methoxy ordering at the polymer interface for adhesion promotion, the interfaces between polymer and liquid silane or silane/MVS mixtures are not an accurate representation of systems used in industry. In industrial settings, small amounts of silane adhesion promoters or silane/MVS adhesion promoting mixtures are incorporated into silicone elastomer prior to application to the polymer substrate. It is therefore important to also study the ordering of silanes and silane/MVS mixtures at the buried interface between d_4-PET and silicone elastomer to determine if the behavior of the silanes is the same when incorporated into silicone as it is when not mixed with silicone. Here, first, buried interfaces between PET and uncured silicone elastomer with incorporated silanes or silane/MVS mixtures were studied to investigate the interfacial behavior of silanes prior to silicone cure. In section 2.3.4, the buried interfaces between PET and cured silicone elastomer with silanes or silane/MVS mixtures were studied to determine if the interfacial behavior of silanes changes after the silicone cure process.

Figure 2.6 shows the SFG spectra of d_4-PET in contact with uncured silicone elastomer without any silanes or silane/MVS mixtures incorporated both at initial contact and after the spectral features stabilized, after approximately 15 minutes. The very weak signal between 2910 and 2950 cm^{-1} were attributed to the silicone elastomer.[22] No significant signal was detected, indicating that the silicone elastomer was mostly disordered at the polymer interface without any silane or silane/MVS mixture present.

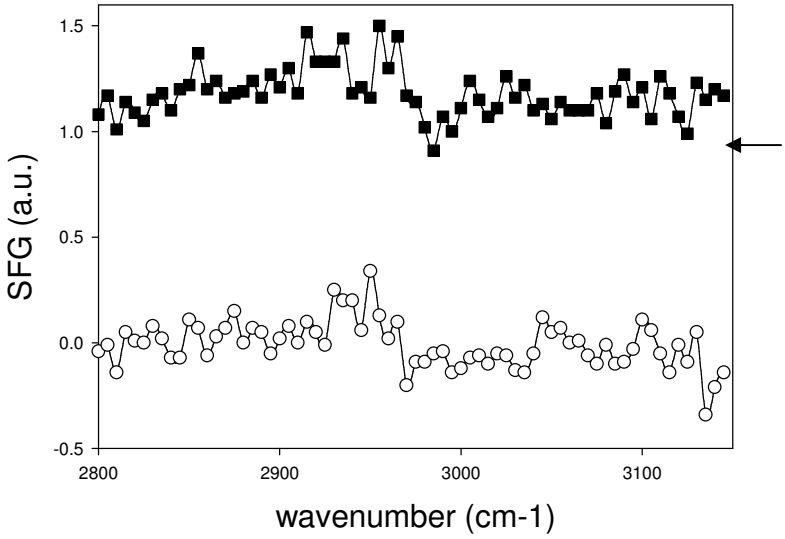

Figure 2.6. SFG spectra of d_4-PET in contact with uncured silicone elastomer at initial contact (open circles) and once spectral features have stabilized (closed circles). . Baselines of spectra are indicated by arrows on right.

Figure 2.7 shows SFG spectra of d_4-PET in contact with uncured silicone elastomer with 1.5 wt% γ-GPS and with 3 wt% γ-GPS/MVS mixture. The spectra are shown after the spectral features stabilized. The SFG spectrum of d_4-PET in contact with uncured silicone with 1.5 wt% γ-GPS showed no signal over one hour, showing that either the γ-GPS molecules did not segregate to the polymer interface from the silicone bulk, or the interfacial γ-GPS molecules were not ordered. This result was different from the buried interface between d_4-PET and neat γ-GPS, shown in Figure 2.2, in which the γ-GPS molecules did exhibit some orientational order at the polymer interface. It is possible that interactions between the silicone elastomer and the silane prohibited the silane from reaching and/or ordering at the polymer interface. However, SFG spectra of d_4-PET in contact with uncured silicone with 3 wt% γ-GPS/MVS mixture were different. In these spectra, the characteristic silane methoxy peak at 2835 cm^{-1} was present, as was

a peak at 2950 cm^{-1}, which was assigned to either the MVS or the silicone elastomer. The spectral features increased in intensity over thirty minutes and then stabilized. Therefore, when mixed with MVS, the γ-GPS could migrate from the bulk silicone to the polymer interface, and segregated with orientational order at the polymer interface. This result was similar to that of the interface between d_4-PET and the γ-GPS/MVS mixture, in which the interfacial ordering of γ-GPS was enhanced by the presence of MVS. Here, even with very small amounts of γ-GPS and MVS in the silicone, interfacial γ-GPS methoxy signal was still detected, showing that γ-GPS could still segregate with order to the d_4-PET interface when mixed with uncured silicone.

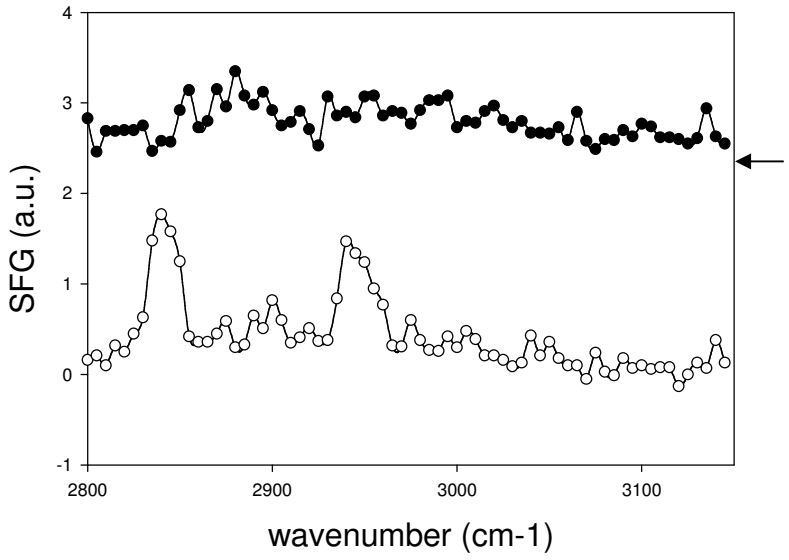

Figure 2.7. SFG spectra of d_4-PET in contact with uncured silicone elastomer with 1.5 wt% γ-GPS (closed circles) and with 3 wt% γ-GPS/MVS mixture (open circles). . Baselines of spectra are indicated by arrows on right.

The SFG spectra of d_4-PET in contact with uncured silicone with 1.5 wt% OTMS and 3 wt% OTMS/MVS mixture are shown in Figure 2.8, and the SFG spectra of d_4-PET in contact with uncured silicone with 3 wt% TDFTMS and 4.5 wt% TDFTMS/MVS

mixture are shown in Figure 2.9. As can be seen in these spectra, these buried interfaces yielded no signal that could be attributed to the silanes over one hour. Small signal at 2910 and 2950 cm^{-1} were attributed to the silicone elastomer. Therefore, there was no evidence of either the OTMS or TDFTMS segregating with order at the polymer interface, alone or when mixed with MVS. Either the silanes were not able to diffuse through the bulk silicone to the interface, or the silanes were present at the interface but lacked orientational order.

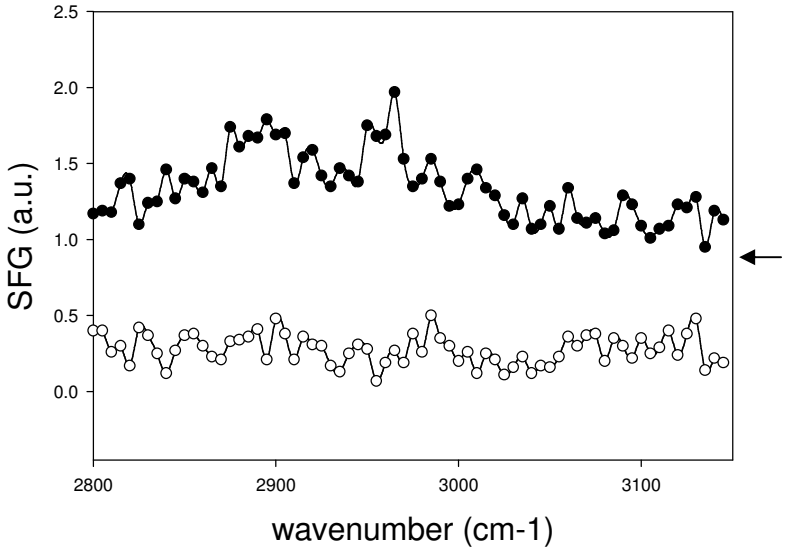

Figure 2.8. SFG spectra of d_4-PET in contact with uncured silicone elastomer with 1.5 wt% OTMS (closed circles) and with 3 wt% OTMS/MVS mixture (open circles). . Baselines of spectra are indicated by arrows on right.

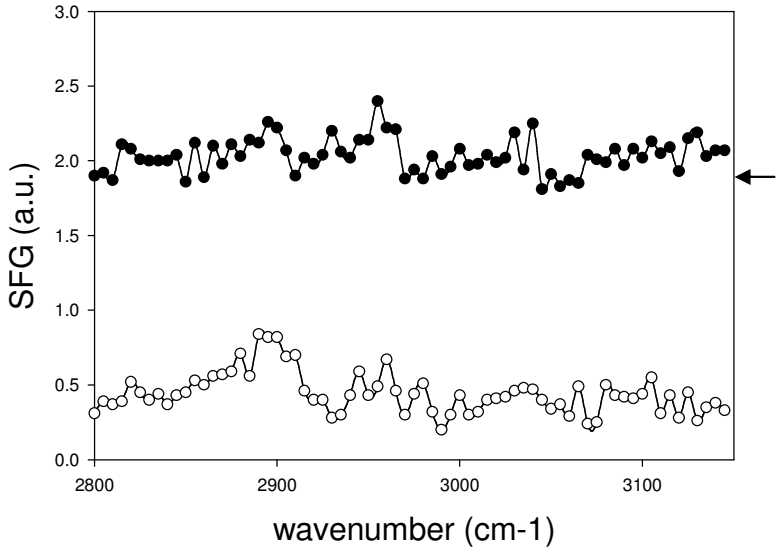

Figure 2.9. SFG spectra of d_4-PET in contact with uncured silicone elastomer with 3 wt% TDFTMS (closed circles) and with 4.5 wt% TDFTMS/MVS mixture (open circles). . Baselines of spectra are indicated by arrows on right.

The studies of d_4-PET in contact with uncured silicone with incorporated silane or silane/MVS mixture illustrated that only the γ-GPS in the γ-GPS/MVS mixture significantly segregated with order at the buried interface. Although the other silanes studied could segregate with order at the interface between the polymer and the neat liquid silane, neither OTMS nor TDFTMS showed evidence of this when mixed with uncured silicone. As previously discussed, only the γ-GPS/MVS mixture acts as an adhesion promoter for this system, and therefore the ability of the γ-GPS in the γ-GPS/MVS mixture to segregate with order at the interface between the polymer and silicone may be necessary for it to promote adhesion. It is possible that the OTMS and TDFTMS could not order at the interface because of interactions between these silanes and the uncured silicone elastomer. Therefore, this part of the study showed that

interactions between silanes and the silicone, not just interactions between silanes and the polymer substrate may influence the behavior of silane molecules.

2.3.4 SFG Studies of d_4-PET in Contact with Cured Silicone with Incorporated Silanes or Silane/MVS Mixtures

Lastly, it was important to determine how the silane molecules behaved at the buried interfaces between d_4-PET and silicone elastomer with incorporated silanes or silane/MVS mixtures after the silicone was cured. In industrial applications, silane adhesion promoters are mixed with silicone, and the silicone is applied to the polymer substrate and cured. Thus, adhesion promoters must work after the system is fully cured, and it is important to study how the segregation of silane adhesion promoters is affected by curing the silicone, because heat or other cure conditions may influence silane behavior. In this section, the buried interfaces between d_4-PET and cured silicone elastomer with incorporated silanes or silane/MVS mixtures were studied with SFG.

Figure 2.10 show SFG spectra of d_4-PET in contact with cured silicone with 1.5 wt% γ-GPS and with 3 wt% γ-GPS/MVS mixture. The characteristic silane methoxy stretch at 2835 cm^{-1} was observed from the buried interface between d_4-PET and cured silicone with 1.5 wt% γ-GPS. Another spectral feature at 2950 cm^{-1} was assigned to the silicone elastomer. Interestingly, this was different from what was observed at the interface between d_4-PET and uncured silicone with incorporated γ-GPS, where no silane signal was observed. The elevated temperature during the cure process may have facilitated the interfacial segregation and ordering of the silane molecules. The SFG spectra of d_4-PET in contact with cured silicone with incorporated γ-GPS/MVS mixture showed a weaker peak at 2835 cm^{-1}, from the silane methoxy groups. This indicated that

in the silane/MVS mixture, the silane molecules exhibited some interfacial orientational order. However, the signal from the γ-GPS in the γ-GPS/MVS mixture was weaker than that from the γ-GPS alone in the cured silicone. This contrasts with the results from the buried interface between d_4-PET and the liquid γ-GPS/MVS mixture, as well as the results from the buried interface between d_4-PET and uncured silicone with incorporated γ-GPS/MVS. This may be because the samples were cured above the T_{CF} for samples with the γ-GPS/MVS mixture, as will be detailed in section 2.3.5. Because the system was cured above T_{CF}, any adhesion-promoting mechanism that the silane is involved in has likely taken place. The higher temperature above T_{CF} may have induced a chemical reaction or inter-diffusion of the silane into the polymer surface. These cure temperature-dependent mechanisms would have decreased the silane signal. In the case of a chemical reaction between the silane and polymer, the silane would have been chemically altered, decreasing SFG signal. In the case of diffusion, the buried interface would have become less ordered, also decreasing SFG signal.

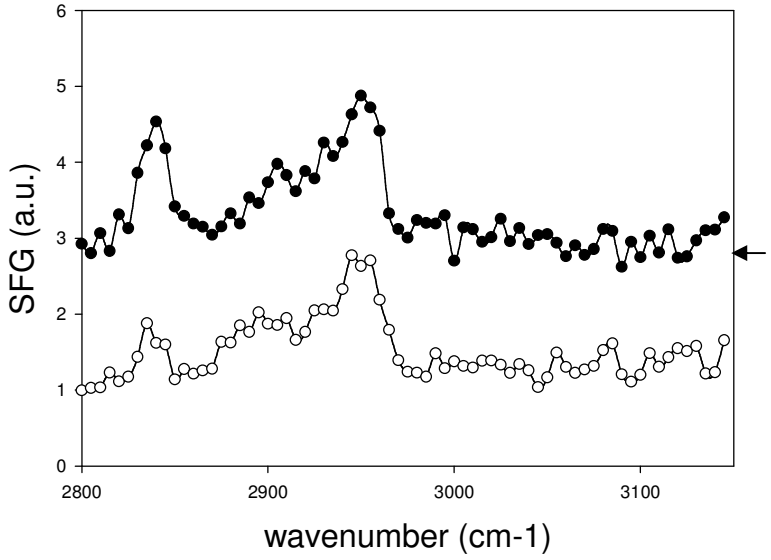

Figure 2.10 SFG spectra of d_4-PET in contact with cured silicone with 1.5 wt% γ-GPS (closed circles) and with 3 wt% γ-GPS/MVS mixture (open circles). Baselines of spectra are indicated by arrows on right.

The SFG spectra of d_4-PET in contact with cured silicone with 1.5 wt% OTMS and with 3 wt% OTMS/MVS mixture are shown in Figure 2.11. A peak at 2910 cm^{-1} was observed and assigned to the silicone matrix. Unlike the γ-GPS and the γ-GPS/MVS mixture, there was no evidence of the silane methoxy groups ordering at the polymer interface. The addition of MVS did not appear to affect the interfacial behavior of the OTMS. This behavior was like that of the interface between d_4-PET and the uncured silicone elastomer with OTMS and the OTMS/MVS mixture. This behavior was, however, different than the interfacial behavior of OTMS and the OTMS/MVS mixture at the buried interface between d_4-PET and the liquid neat silane or liquid silane mixture, in which the silane did order at the polymer interface. There are two different possible explanations for this difference in behavior. First, the lack of signal may have been the silane molecules were present but disordered at the interface. Also, because the OTMS hyrdrocarbon backbone may have been more compatible with silicone than the other two

silanes, there may have been fewer bulk repulsive interactions between the silicone and the silane to drive the silane to the interface.

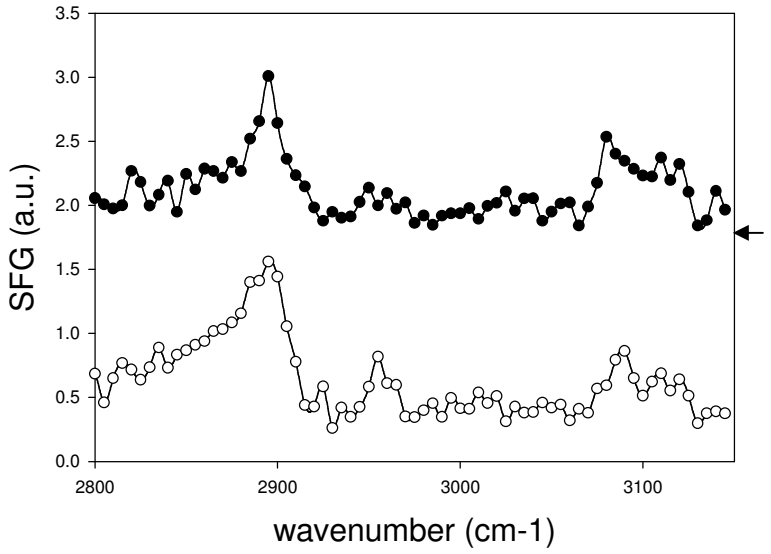

Figure 2.11. SFG spectra of d_4-PET in contact cured silicone with 1.5 wt% OTMS (closed circles) and with 3 wt% OTMS/MVS mixture (open circles). Baselines of spectra are indicated by arrows on right.

Figure 2.12 shows SFG spectra of d_4-PET in contact with cured silicone with 3 wt% TDFTMS and with 4.5 wt% TDFTMS/MVS. Like the OTMS and the OTMS/MVS mixture, no spectral features from the silane were detected. A peak at 2910 cm^{-1} was attributed to the silicone elastomer. Thus, there was no evidence of the silane ordering at the polymer interface. The behavior of TDFTMS was similar to that of OTMS. Either the silane did not diffuse through the silicone bulk to the d_4-PET interface during the cure process, or the TDFTMS was present at the buried interface without orientational order. Section 2.3.4 will describe an XPS study of the exposed surface from the interface between PET and silicone with incorporated TDFTMS or TDFTMS/MVS mixture, which determined if TDFTMS diffused through the silicone matrix to the PET interface.

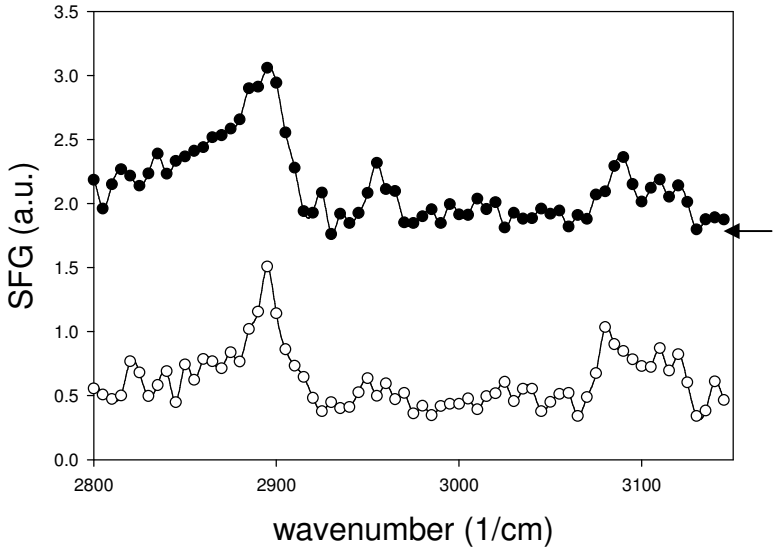

Figure 2.12. SFG spectra of d_4-PET in contact with cured silicone with 3 wt% TDFTMS (closed circles) and with 4.5 wt% TDFTMS/MVS mixture (open circles). Baselines of spectra are indicated by arrows on right.

The SFG studies of the buried interfaces between d_4-PET and cured silicone with incorporated silanes or silane/MVS mixtures showed that only γ-GPS, both alone and in its mixture with MVS, segregated with order at the d_4-PET interface. The other two silanes, OTMS and TDFTMS, as well as their mixtures with MVS, showed no evidence of ordering at the polymer interface, which was markedly different behavior from that of the buried interfaces between d_4-PET and liquid silanes or silane/MVS mixtures. This suggests that interactions between the silanes and the silicone matrix play a role in the interfacial behavior of silanes.

It is important to observe that interfacial SFG signal was detected from very small amounts of γ-GPS and the γ-GPS/MVS mixture in both the uncured and cured silicone elastomer. This shows that the methoxy groups of the γ-GPS in the γ-GPS/MVS mixture were able to order at the buried polymer interface before and after the cure process. To

act as an effective adhesion promoter, the silane methoxy groups may need to interact with the polymer surface before, during and after the silicone cure process.

As previously mentioned, the silicone cure temperature used for sample preparation was 150°C. From the adhesion testing results discussed in section 2.3.5 and shown in Table 2.2, this cure temperature is around or below T_{CF} for all samples except for that with the γ-GPS/MVS mixture. The cure temperature above T_{CF} for the γ-GPS/MVS mixture may have helped to drive the silane molecules from the silicone bulk to the interface to participate in an adhesion promotion mechanism such as chemical reaction or diffusion. If an adhesion promotion mechanism had already taken place after cure at 150°C, the silane signal would have decreased in the mixture with MVS, as was observed.

2.3.4 XPS Studies of Exposed Surfaces from the Buried Interface Between PET and Cured Silicone with Incorporated TDFTMS and TDFTMS/MVS Mixture

SFG is sensitive to orientational order in addition to the presence of chemical species. Therefore, the lack of SFG signal for the samples with OTMS and TDFTMS discussed in sections 2.3.2 and 2.3.3 may have been due to two different factors. First, the silanes could have been present but disordered at the interface. Also, the silanes may not have been present at the interface at all. To distinguish between these two possibilities for TDFTMS and the TDFTMS/MVS mixture at the buried interface between PET and cured silicone, XPS analysis was performed to supplement the SFG studies. TDFTMS and the TDFTMS/MVS mixture was analyzed instead of OTMS and the OTMS/MVS mixture because the fluorinated signal from the TDFTMS backbone could be used as a signature for the silane, while the OTMS signal could not be easily

distinguished from the polymer. Although XPS cannot be directly applied to buried interfaces, it can be used to probe the surfaces that result from breaking the buried adhesive interface.

The interfaces between PET and cured silicone with incorporated 3 wt% TDFTMS and with incorporated 4.5 wt% TDFTMS/MVS mixture were prepared and then the interfaces were manually broken. The resulting PET surface was subjected to XPS analysis to determine if TDFTMS was present. If TDFTMS fluorine signal was detected, then it could be concluded that the TDFTMS did segregate to the polymer interface, but did not exhibit orientational order.

Figure 2.13 shows XPS spectra in the F 1s binding energy region from the PET side of the broken interfaces. Table 2.1 shows the surface compositions of the samples in atomic percent. Samples without MVS were referenced to the CF_2 peak at 292.5 eV, and samples with MVS were referenced to the C-Si peak at 284.4 eV. As seen in Figure 2.15, significant fluorine signal was observed,[25] indicating that the TDFTMS was present at the polymer interface. The fluorine signal was stronger when it was alone than when mixed with MVS. Further, atomic composition data in Table 2.1 indicated that fluorine from TDFTMS was on the PET surface, and there was significantly more fluorine when TDFTMS was not mixed with MVS. When combined with SFG results, it is believed that the TDFTMS segregated to the interface between PET and silicone, but did not adopt an orientational order, so there was no SFG signal from the buried interface.

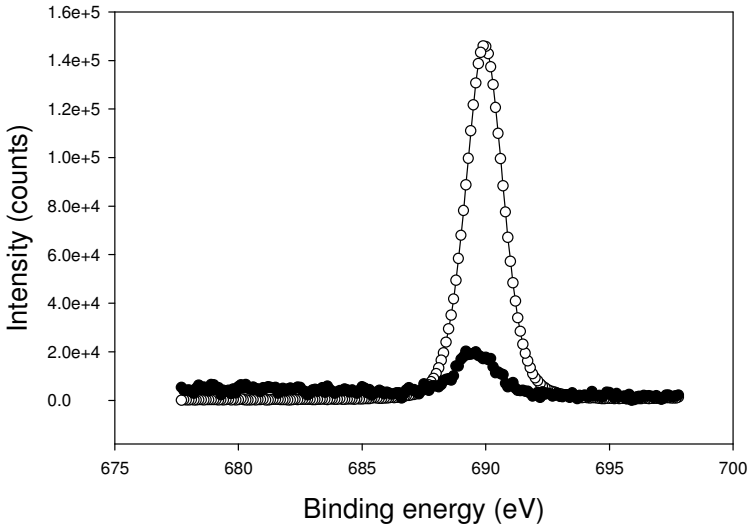

Figure 2.13. XPS spectra of the exposed PET surface from the buried interface between PET and cured silicone with 3 wt% TDFTMS (open circles) and from the buried interface between PET and cured silicone with 4.5 wt% TDFTMS/MVS mixture, multiplied by a factor of 10 (closed circles).

Sample	F	O	C	Si	Na	Ca	Sum
PET from PET/silicone with 3% TDFTMS	41.9%	10.8%	42.1%	5.1%	0.1%	0.0%	100.0%
PET from PET/silicone with 4.5% 2:1 TDFTMS/MVS	1.1%	26.7%	51.7%	20.4%	0.1%	0.0%	100.0%

Table 2.1 Atomic composition from XPS experiments.

2.3.5 Adhesion Testing of Interfaces Between PET and Cured Silicone with Incorporated Silanes or Silane/MVS Mixtures

Adhesion test specimens were prepared in the high throughput thermal gradient press described in section 2.2.5, and adhesion tests were performed with a 90^{o} peel test initiated from a manual crack on the cool end of the specimens. The positions where the silicone transitioned from a viscous liquid to a solid and the position where the mode of

failure transitioned from interfacial to cohesive were related by a linear regression to the T_{cure} and the T_{CF}, respectively. Results from adhesion tests are shown in Table 2.2. It was observed that only the γ-GPS/MVS mixture significantly improved adhesion, as measured by a lowered T_{CF}. Therefore, it was confirmed that only the γ-GPS/MVS mixture was an effective adhesion promoter of the systems studied. Further, it is of interest to note that the cure temperatures of all samples with MVS were increased due to the coordination of the platinum catalyst in the silicone formulation to the vinyl groups in the MVS.

Sample	Cure Temperature	Adhesion Temperature
PET/silicone + 1.5% γ-GPS	50 ±1°C	148 ± 2°C
PET/silicone + 3% 1:1 γ-GPS/MVS mix	81 ± 2°C	86 ± 3°C
PET/silicone + 1.5% OTMS	57 ± 2°C	169 ± 2°C
PET/silicone + 3% 1:1 OTMS/MVS mix	78 ± 1°C	163 ± 2°C
PET/silicone + 3% TDFTMS	54 ± 3°C	169 ± 1°C
PET/silicone + 4.5% 2:1 TDFTMS/MVS mix	84 ± 2°C	152 ± 3°C

Table 2.2. Adhesion testing results by 90° peel testing.

2.4 Conclusions

In these studies, SFG was correlated to adhesion testing results to compare the interfacial structures of a known adhesion promoting mixture of γ-GPS and MVS with other silanes and silane/MVS mixtures not used as adhesion promoters. SFG was used to

probe buried interfaces between polymer and liquid silanes or liquid silane/MVS mixtures, polymer and uncured silicone with incorporated silanes or silane/MVS mixtures, and polymer and cured silicone with incorporated silanes or silane/MVS mixtures. The SFG spectra of d_4-PET in contact with liquid silanes all showed evidence of interfacial silane ordering. However, the addition of MVS to the silanes changed the different interfaces differently. The methoxy groups of γ-GPS in the γ-GPS/MVS mixture exhibited greater order, while this did not occur when the OTMS and TDFTMS were mixed with MVS. It was also shown that the silanes all adopted a similar absolute orientation at the d_4-PET interface, namely that the methoxy groups face toward the polymer surface.

However, the behavior of the silanes at the interface between the polymer and the liquid silanes or silane/MVS mixtures did not directly correlate to the silane behavior at the interfaces between the polymer and uncured and cured silicone elastomer. Only the γ-GPS in the γ-GPS/MVS mixture remained ordered at both the interface between d_4-PET and uncured silicone as well as at the interface between d_4-PET and cured silicone. No other silane or silane mixture exhibited evidence of interfacial ordering at the buried interface between d_4-PET and uncured silicone and between d_4-PET and cured silicone. Therefore, neither OTMS nor TDFTMS segregated with order at the interface between the polymer and silicone. However, XPS experiments confirmed that TDFTMS did segregate at the polymer interface, but did not exhibit interfacial orientational order.

Adhesion testing confirmed that only the γ-GPS/MVS mixture was an effective adhesion promoter for the adhesive interface between PET and silicone elastomer. Therefore, when the SFG results were correlated to the adhesion testing results, it was

inferred that the substantial segregation and ordering of the silane methoxy groups at the PET interface, before, during and after the silicone cure, as seen with the γ-GPS/MVS mixture, was necessary for adhesion promotion in this system.

This research demonstrated that SFG can be used to study interfacial segregation and ordering of small molecules at buried interfaces between solids and liquids and between two solids. Further, interfacial signal of the silane molecules was detected from the buried interfaces between two solids, even when only a very small amount of silane was present. The interfacial ordering of these silane molecules was successfully correlated to adhesion promotion properties as determined by cure temperature-dependent adhesion testing.

2.5 References

1. Kinloch, A.J. *Adhesion and Adhesives Science and Technology*; Chapman and Hall: London, 1987.
2. Mittal, K.L. *Adhesion Measurements of Thin Films, Thick Films and Bulk Coatings*; American Society for Testing and Materials: Philadelphia, 1978.
3. Yacobi, B.G.; Martin, S.; Davis, K.; Hudson, A.; Hubert, M. *J. Appl. Phys.* **2002**, *91*, 6227-6262.
4. Charles, H.M. *Engineered Materials Handbook Vol. 3: Adhesives and Sealants*; ASM International: Materials Park, OH, 1990.
5. Feresenbet, E.; Raghavan, D.; Holmes, G.A. *J. Adhes.* **2003**, *79*, 643-665.
6. Sathyanarayana, M.N.; Yaseen, M. *Prog. Org. Coat.* **1995**, *26*, 275-313.
7. Suzuki, T.; Kasuya, A. *J. Adhes. Sci. Technol.* **1989**, *3*, 463-473.
8. Walker, P. *Adhesion Promoters, 1st Ed.*; Elsevier: London, 1987.
9. Mine, K.; Nishio, M.; Sumimura, S. US Patent 4,033,924, July 5, 1977.
10. Schulz, J. B. US Patent 4,087,585, May 2, 1978.
11. Gray, T.E.; Lutz, M. A. US Patent 5,595,836, Jan 21, 1997.
12. Loch, C.L.; Ahn, D.; Chen, Z. *J. Phys. Chem. B.* **2006**, *110*, 914-918.
13. Bain, C.D. *J. Chem. Soc. Faraday Trans.* **1995**, *91*, 1218-1296.
14. Buck, M.; Himmelhaus, M. *J. Vac. Sci. Technol. A.* **2001**, *19*, 2717-2736.
15. Lambert, A.G.; Davies, P.B.; Neivandt, D. *J. Appl. Spectrosc. Rev.* **2005**, *40*, 103-145.
16. Shen, Y.R. *The Principles of Nonlinear Optics*; Wiley: New York, 1984.
17. Shen, Y.R. *Nature*, **1989**, *337*, 519-525.

18. Chen, C.; Wang, J.; Loch, C.L.; Ahn, D.; Chen, Z. *J. Am. Chem. Soc.* **2004**, *126*, 1174-1179.

19. Wang, J.; Woodcock, S.E.; Buck, S.M.; Chen, C.; Chen, Z. *J. Am. Chem. Soc.* **2001,** *308*, 9470-9471.

20. Wang, J.; Chen, C.; Buck, S.M.; Chen, Z. *J. Phys. Chem. B.* **2001**, *105*, 12118-12125.

21. Loch, C.L.; Ahn, D.; Chen, C.; Chen, Z. *J. Adhes.* **2005**, *81*, 319-345.

22. Chen, C.; Wang, J.; Chen, Z. *Langmuir*. **2004**, *20*, 10186-10193.

23. Ahn, D.; Shephard, N.E.; Olney, P.A.; McMillan, C.S. *Macromolecules.* **2007**, *40*, 3904-3906.

24. Loch, C.L.; Ahn, D.; Chen, C.; Wang, J.; Chen Z. *Langmuir*, **2004**, *20*, 5467-5473.

25. Beamson, G.; Briggs, D. *High Resolution XPS of Organic Polymers: The Scienta ESCA300 Database*; Wiley: 2002.

CHAPTER 3

MOLECULAR STRUCTURES OF BURIED INTERFACES BETWEEN SILICONE ELASTOMER AND SILANE ADHESION PROMOTERS

3.1 Introduction

Silicone elastomeric adhesives are widely used in many industrial applications as a more inexpensive alternative to mechanical fasteners. Specifically, addition-cured silicone elastomers are often used as adhesives because they have unique elastomeric properties, high thermal stability and simple, controllable cure chemistry.[1-4] However, these elastomers lack polar or reactive functional groups that allow for easy adhesion to other polymeric materials. Often, surface treatments are used to oxidize the silicone surface to improve adhesion. However, these pretreatments are not ideal in many industrial applications.

Adhesion promoters are often used to avoid the need for oxidative surface treatments in many applications, and alkoxysilane adhesion promoters have been developed to improve the adhesion of elastomers to various polymer substrates. Small amounts of silane adhesion promoters can be mixed into the silicone elastomer prior to application to the substrate, or silane adhesion promoters can be used as an interlayer between the substrate and the elastomer.[3,5-11]

As detailed in Chapter 2, it has been demonstrated that using a mixture of an organosilane and a siloxanol greatly improves the adhesion between polymer substrates and addition-cured silicone elastomer. A mixture of (3-glycidoxypropyl)trimethoxysilane (γ-GPS) and a hydroxyl-terminated methylvinylsiloxane (MVS) has been shown to promote adhesion between poly(butylene terephthalate) (PBT) and addition-cured silicone elastomer. Alone, neither γ-GPS nor MVS promotes adhesion.[10,11]

The ability of SFG to probe buried polymer interfaces was exploited in the research described in Chapter 2. In that work, SFG was used to study the interactions between the adhesion promoting mixture of γ-GPS and MVS and poly(ethylene terephthalate), a polymer analogous to PBT. SFG spectra of d_4-PET in contact with γ-GPS and the γ-GPS/MVS mixture showed that the γ-GPS methoxy groups ordered at the d_4-PET/γ-GPS interface, and that the interfacial ordering of γ-GPS was increased when mixed with MVS.[12,13] When compared to two other trimethoxy silanes with different backbones and end groups, OTMS and TDFTMS, it was found that the other silanes exhibited different interfacial behavior.

Further, SFG studies of the buried interfaces between d_4-PET and silicone elastomer with incorporated silanes or silane/MVS mixtures indicated that only the γ-GPS methoxy groups ordered at the interface when mixed with MVS both before and after the silicone was cured. Because the other silanes (alone or mixed with MVS) did not exhibit this behavior, it was determined that the ordering of the silane methoxy groups at the buried interface between PET and silicone elastomer must be necessary for a silane to act as an adhesion promoter in this system. Further, because the silanes

behaved differently at the buried interface between PET and liquid silanes or silane/MVS mixtures than they did at the buried interface between PET and the silicone elastomer with incorporated silanes or silane/MVS mixtures, it was demonstrated that interactions between the silanes and silicone may compete with interactions between silanes and PET to influence the ordering of silanes at the PET/silicone buried interface.[13]

The earlier research on interfacial behavior of silane adhesion promoters has focused on interactions between the polymer substrate and adhesion promoters. However, interactions between the silicone elastomer and adhesion promoter were shown to also affect how a silane or silane/MVS mixture behave at the interface between a polymeric substrate and a silicone elastomer. This can be true both when the adhesion promoter is incorporated into the silicone elastomer, like the experiments in Chapter 2, and also when the silane adhesion promoter is used as an interlayer between the polymer substrate and silicone.

This study aimed to investigate interactions between cured silicone elastomer and γ-GPS, as well as the silane adhesion-promoting mixture of γ-GPS and MVS using both SFG and molecular dynamics (MD) simulations. The interfacial structures of the two other silanes not used as adhesion promoters, OTMS and TDFTMS, as well as their mixtures with MVS, were compared to those of γ-GPS and γ-GPS in the γ-GPS/MVS mixture. SFG was used to study the molecular structures at the buried interfaces between silicone elastomer and the neat silanes or the silane/MVS mixtures. However, from SFG alone, information about interfacial orientation distribution could only be inferred. Therefore, MD simulations were performed to calculate the orientation distribution of silane methoxy groups at the silicone interface to supplement the SFG results. MD

results were used to determine if the silanes exhibited a narrow or broad interfacial orientation distribution.

3.2 Experimental

3.2.1 Sample Preparation

A Sylgard 184 silicone elastomer kit, (3-glycidoxypropyl) trimethoxy silane (γ-GPS), and hydroxyl-terminated methylvinylsiloxane (MVS) were obtained from Dow Corning Corporation. The two other silanes, *n*-octadecyltrimethoxysilane (OTMS) and (tridecafluoro-1,1,2,2-tetrahydrooctyl)trimethoxysilane (TDFTMS) were purchased from Gelest, Inc. All chemicals were used as received.

The Sylgard 184 silicone elastomer was prepared in a 10:1 base/curing agent ratio, as directed by the manufacturer. The base and curing agent were mixed vigorously to the point of visual homogeneity.

When the silanes were mixed with MVS, the following solutions were prepared: 1:1 (wt/wt) γ-GPS/MVS, 1:1 (wt/wt) OTMS/MVS, and 2:1 (wt/wt) TDFTMS/MVS. The solutions were mixed to the point of visual homogeneity prior to being contacted to silicone thin films.

To prepare thin films of Sylgard 184 silicone elastomer for SFG analysis, a 5 wt% solution of Sylgard 184 in toluene (Sigma-Aldrich, Inc) was spin cast using a spin-coater from Specialty Coating Systems onto fused silica windows (1-in diameter, 1/8-in thickness, ESCO Products, Inc). The fused silica windows were cleaned by etching in warm chromic acid solution prior to use. The thin films were then cured in an oven at 150^{o}C for 1 h. The films were cooled to room temperature prior to analysis.

To compare the signal of the epoxy-functionalized silane γ-GPS to that of a different sample with epoxy groups, a thin film of 1-4-butanediol diglycidyl ether (BDDGE, Sigma-Aldrich, Inc) was spin cast from a 1 wt% solution in chloroform (Sigma-Aldrich, Inc) onto fused silica windows that were etched in a warm chromic acid solution prior to use. The thin films were dried overnight prior to SFG analysis.

Chemical structures of silicone [poly(dimethylsiloxane) (PDMS)], the silanes, MVS and BDDGE are shown in Figure 3.1.

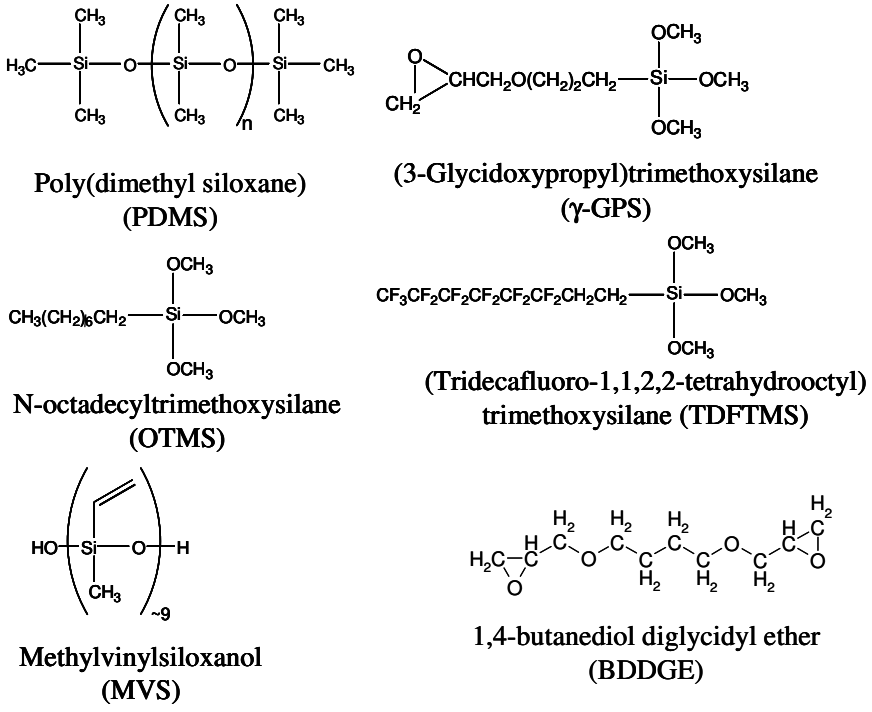

Figure 3.1. Chemical structures of silicone, silanes, MVS and BDDGE.

3.2.2 SFG Experiments

SFG theory has been well-developed and is discussed in Chapter 1, Section 1.2.2. Also, the experimental set-up and geometry used in these experiments was detailed in the literature and discussed in Chapter 1, Section 1.2.3.[12, 14-17] In experiments, a fixed-

frequency visible beam and a frequency-tunable IR beam are overlapped spatially and temporally at the polymer/liquid interface at 60° and 54°, respectively, with energies of 100 μJ and 200 μJ, respectively, with beam diameters of 500 μm. Previous work has shown that the SFG signal is dominated by the signal from the polymer/liquid interface rather than the polymer bulk or polymer/fused silica substrate interface.[12,15,16] In this study, the ssp (s-polarized SFG output signal, s-polarized visible input light, p-polarized IR input light) polarization combination was used to obtain all spectra. Other polarization combinations, such as ppp and sps, did not yield appreciable signal.

3.2.3 Molecular Dynamics Simulations

Molecular dynamics (MD) simulations were performed using Materials Studio 4.3 (Accelyrs, Inc.), using the Amorphous Cell (AC) and Forcite modules. NVT (constant number of molecules, constant volume and constant temperature) MD simulations were run at 298 K using the Anderson thermostat. The Condensed-phase Optimized Molecular Potentials for Atomic Simulation Studies (COMPASS) force field was used for all calculations. COMPASS is a Class II force field optimized for atomistic condensed-phase simulations.[18] The AC module was used to simulate a 17-monomer chain of vinyl-terminated silicone (poly(dimethylsiloxane) (PDMS)) with periodic boundaries. The AC module was also used to simulate periodic cells of the following: 16 molecules of γ-GPS, 16 molecules of the 1:1 γ-GPS/MVS mixture (8 molecules γ-GPS, 8 molecules MVS), 16 molecules OTMS and 16 molecules TDFTMS. All periodic cells had a cutoff size of 12.5 Å. Each cell was equilibrated in the following manner. An initial geometric optimization was performed using the conjugate gradient method with a root mean square (RMS) atomic force cutoff of 0.1 kcal/mol Å. Then, 50 ps of NVT MD at 298K with a 1

fs time step was performed using the Velocity Verlet algorithm and the COMPASS force field. The 50 ps simulation time was sufficient for the potential energy to equilibrate, and was consistent with other reported polymer simulations.[19] Longer (100 ps) simulations were performed for some of the silanes with little effect on the equilibrated potential energy. After the 50 ps NVT MD, the cells were subjected to a second geometric optimization with the conjugate gradient method and an RMS atomic force cutoff of 0.01 kcal/mol Å.[19,20] Interfaces were simulated using the Layer Builder Tool, creating interfacial systems with two-dimensional periodicity. The following interfaces were simulated: PDMS/γ-GPS, PDMS/1:1 γ-GPS/MVS mixture, PDMS/OTMS and PDMS/TDFTMS. The interfaces were equilibrated in the same manner as described above.

The equilibrium orientation distribution of the silane methoxy groups was calculated for each silane studied. The coordinates of each methoxy group of a single final trajectory frame were analyzed from five different simulations using different initial random seed values. The final results from the multiple simulations of the each system were consistent for all similar trajectories. The angle distributions of the individual CH_3 groups of the silane methoxy groups were calculated with respect to the surface normal of the plane of the silicone/silane (or silane/MVS mixture) interface. A correction factor was included to remove the error from variation in the solid angle.[21]

3.3 Results and Discussion

3.3.1 Silicone Elastomer in Contact with Neat γ-GPS and the γ-GPS/MVS Mixtures Studied with SFG

SFG spectra were obtained from the buried interface between cured silicone elastomer and neat silanes or silane/MVS mixtures. Spectra were taken immediately after contact between the silicone thin film and the liquid silane or silane/MVS mixture. The laser was then blocked for 15 min to allow the system to equilibrate, and another spectrum was obtained. This was repeated every 15 minutes for 60 minutes. However, no spectral changes were observed after 30 min contact time for any of the systems studied, so only spectra taken over 30 min are reported.

SFG spectra from the thin film of silicone elastomer in contact with neat γ-GPS and in contact with the 1:1 γ-GPS/MVS mixture are shown in Figure 3.2 and Figure 3.3, respectively. In the spectra of silicone in contact with γ-GPS, a peak was observed at 2835 cm^{-1} which is characteristic of the γ-GPS methoxy symmetric stretch.[12] The peak was stable over 30 minutes contact time, indicating that the chemical structures at the interface between silicone and neat γ-GPS were stable. The silane signal was only obtained from the ssp polarization combination, meaning that the silane methoxy groups were most likely ordered at the silicone interface with a broad angular distribution. However, SFG alone cannot prove this, and MD simulation results will be discussed in section 3.3.4 that agreed with this interpretation. Also, peaks at 2960 cm^{-1} and 2910 cm^{-1} were observed and were stable with time. These peaks were assigned to the silicone methyl asymmetric and symmetric stretches, respectively.[22] The presence of silicone signal indicated that the silicone methyl groups were present and ordered at the interface.

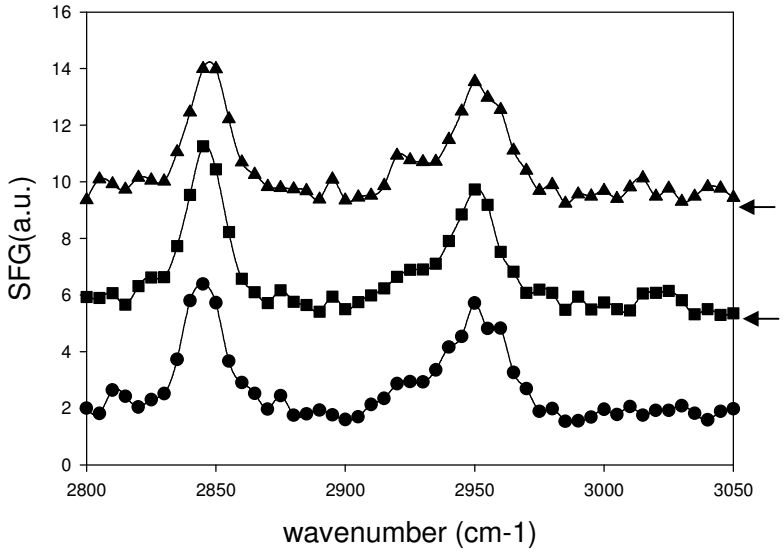

Figure 3.2. SFG spectra of silicone elastomer thin film in contact with neat γ-GPS at initial contact (circles), 15 min contact (squares) and 30 min contact (triangles). Baselines of spectra are indicated by arrows on right.

SFG spectra of silicone in contact with the 1:1 γ-GPS/MVS mixture are shown in Figure 3.3. In these spectra, stable signal at 2835 cm^{-1}, characteristic of the silane symmetric methoxy stretch, was present. Like the neat γ-GPS, only signal in the ssp polarization combination was obtained, implying that the γ-GPS methoxy groups are present at the interface with a broad interfacial orientation distribution. However, the signal from the silane methoxy groups was lower in strength in the mixture than it was for the neat silane. This contrasts with the results discussed in Chapter 2, in which the γ-GPS signal was enhanced at the d_4-PET interface when mixed with MVS.[12,13] Because the neat γ-GPS and the γ-GPS/MVS mixture have similar refractive indices, it was not expected that the difference in intensity was due to differences in refractive indices at the different interfaces. Therefore, the decrease in silane methoxy signal intensity must have been due to a physical phenomenon at the interface. Unlike at the d_4-PET interface, the

MVS may have acted to disorder the γ-GPS molecules at the cured silicone elastomer interface. This would have led to a decrease in silane methoxy signal because SFG is sensitive to interfacial orientational ordering of chemical groups. Another possibility is that the MVS preferentially interacted with the silicone and therefore diluted the γ-GPS at the silicone interface. If there was less γ-GPS at the buried interface between silicone and the γ-GPS/MVS mixture, the signal would have decreased because SFG is also sensitive to interfacial number density. It is not possible to differentiate between these two possibilities with SFG. Also, a stable peak at 2960 cm^{-1} with a shoulder at 2910 cm^{-1} was attributed to the silicone elastomer with possible contribution from the MVS.[13] Because the silicone signal was similar at both the γ-GPS/MVS mixture interface and the neat γ-GPS interface, it can be concluded that silicone methyl group orientation was unaffected by the presence of MVS.

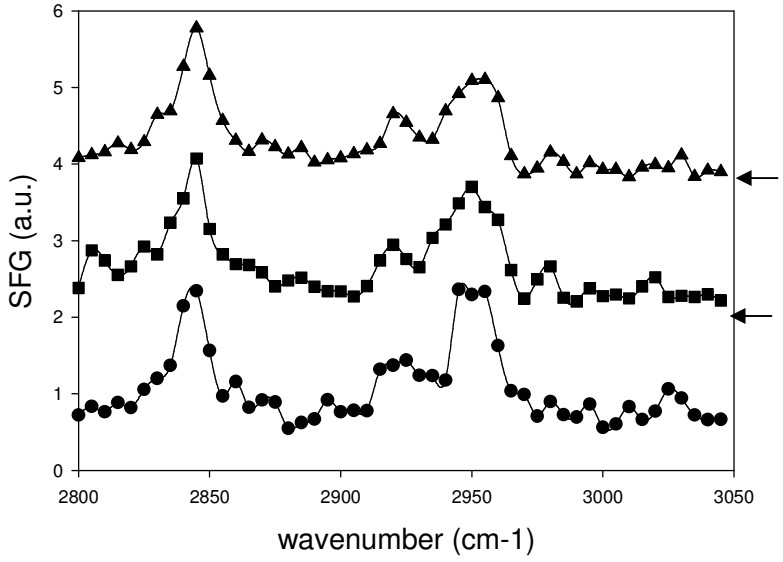

Figure 3.3. SFG spectra of silicone elastomer thin film in contact with the γ-GPS/MVS mixture at initial contact (circles), 15 min contact (squares) and 30 min contact (triangles). Baselines of spectra are indicated by arrows on right.

While only methoxy signal has been detected from γ-GPS and γ-GPS in the γ-GPS/MVS mixture, other functional groups that could be involved in adhesion promotion were present in the system. Specifically, the epoxy groups from the γ-GPS end groups and the vinyl groups from the MVS could be involved in adhesion promoting mechanisms. Because both epoxy and vinyl groups can participate in the silicone cross-linking mechanism, it would be expected to observe signal from these groups at the silicone interface. However, no apparent signal from either the silane epoxy end groups or the MVS vinyl groups was observed. The vinyl signal may have been indiscernible from the silicone signal in the C-H stretching region. Also, because the silicone elastomer thin film was cured prior to contact with the silane/MVS mixtures, there may have been less driving force for the MVS vinyl groups to segregate with order at the cured silicone interface. If the MVS vinyl groups were not attracted to the cured silicone thin film, the groups would not have ordered at the interface and no SFG signal would have been observed.

The lack of epoxy signal from the γ-GPS end groups can also be due to different factors. Figure 3.4 shows an SFG spectrum in the ssp polarization combination of a thin film of BDDGE, an epoxy-containing compound. Among other C-H stretches in the spectrum, a strong peak at 3000 cm^{-1} characteristic of the C-H stretching mode of the epoxy ring was observed.[23] Here, because the thin film of BDDGE had an ordered surface in air, the epoxy ring structure was ordered at the surface and exhibited signal in the C-H region. This spectrum shows that it is possible to observe epoxy ring signal in the C-H stretching region with SFG.

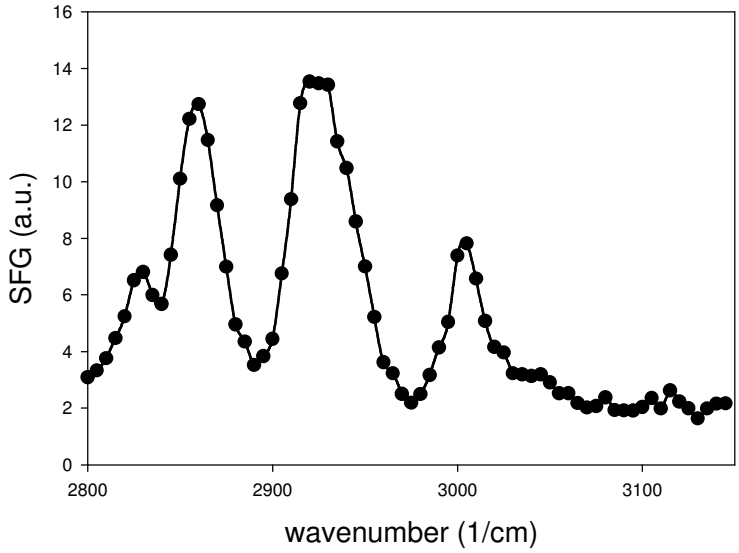

Figure 3.4. SFG spectrum of thin film of BDDGE.

Because no epoxy signal was observed from the γ-GPS, it can be concluded that either the γ-GPS epoxy end groups were not present at the interface or the γ-GPS epoxy end groups were present but disordered at the interface. From the SFG results shown in Figures 3.2 and 3.3, it was inferred that the γ-GPS methoxy groups were ordered at the interface with a broad orientation. Because the interface was dominated by the ordered methoxy groups, it was most likely that the γ-GPS epoxy end groups were not present at the interface with a large number density and were not well-ordered at the interface. The epoxy groups simply could not reach the already crowded silicone interface. Therefore, no signal was observed from the epoxy end groups. Like the MVS vinyl groups, the epoxy end groups may have not strongly ordered at the silicone interface because the silicone was cross-linked prior to contact with the silane or silane/MVS mixture. Therefore, there would be little driving force for the epoxy groups to migrate to the interface.

To summarize, SFG spectra of silicone elastomer thin films in contact with neat γ-GPS and the silane adhesion-promoting mixture of γ-GPS and MVS exhibited stable signal from both the γ-GPS methoxy groups and the silicone methyl groups, indicating that a stable interface was formed. Because only ssp signal was obtained for these systems, it was inferred that the silane methoxy groups adopted an orientation at the silicone interface with a broad angle distribution. The γ-GPS methoxy signal decreased when mixed with MVS, indicating that either the MVS preferentially interacted with the silicone, diluting the γ-GPS at the interface, or the MVS acted to disorder the interfacial γ-GPS methoxy groups. Unfortunately SFG cannot be used to distinguish between these two possibilities. Further, no evidence of other chemical groups that could participate in adhesion promotion, specifically the epoxy end groups of γ-GPS and the vinyl groups of MVS, were detected at the interface, indicating that they were not present with order at the interface.

3.3.2 Silicone Elastomer in Contact with Neat OTMS and the OTMS/MVS Mixtures Studied with SFG

As discussed previously, the γ-GPS/MVS mixture is a known adhesion promoter for enhancing the adhesion between silicone elastomer and PBT or PET. In section 3.3.1, it was demonstrated that the γ-GPS methoxy groups order at the silicone interface both alone and when mixed with MVS. It is important to determine if this behavior is unique to the silane adhesion promoting mixture, or if other silanes with different backbones and end groups behave in the same way at the silicone interface. Here, the behavior of γ-GPS and γ-GPS in the γ-GPS/MVS mixture were compared to that of OTMS, a silane with a methylene backbone and methyl end group, as well as OTMS in an OTMS/MVS mixture.

SFG spectra of thin films of silicone in contact with neat OTMS and in contact with the 1:1 OTMS/MVS mixture are shown in Figures 3.5 and 3.6. In Figure 3.5, the SFG spectra of silicone in contact with neat OTMS exhibited a weak stable signal at 2835 cm^{-1}, characteristic of the symmetric stretch of the silane methoxy groups. The weak ssp signal indicated that the silane methoxy groups were present at the silicone interface, and were weakly ordered, most likely with a broad angle distribution. The silane signal from the OTMS was weaker in strength than that from γ-GPS, as seen in Figure 3.3. This showed that the OTMS was less ordered at the silicone elastomer interface than γ-GPS, possibly because specific favorable interactions between γ-GPS and the silicone surface caused the γ-GPS methoxy groups to exhibit stronger order. Also, stable, weak signal was detected at 2960 cm^{-1} and was attributed to the silicone elastomer. This was consistent with what was observed at the interface between silicone and neat γ-GPS, indicating that the interfacial silicone methyl groups remained ordered when contacted to OTMS.

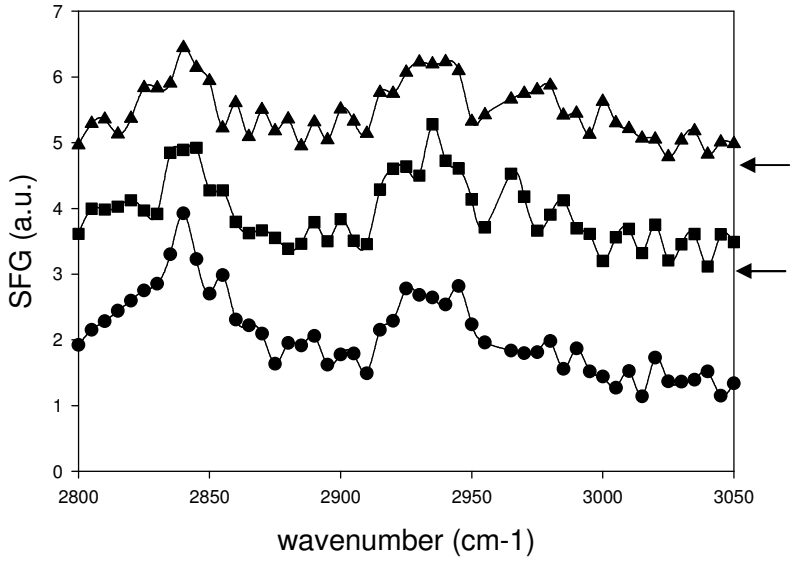

Figure 3.5. SFG spectra of silicone elastomer thin film in contact with neat OTMS at initial contact (circles), 15 min contact (squares) and 30 min contact (triangles). Baselines of spectra are indicated by arrows on right.

SFG spectra of silicone elastomer in contact with the OTMS/MVS mixture are seen in Figure 3.6. From these spectra, there was no indication that the OTMS methoxy groups were present at the silicone interface with orientational order, because there was no signal at 2835 cm^{-1} from the silane methoxy groups. There were, however, stable weak signal at 2910 cm^{-1} and 2960 cm^{-1}, characteristic of the silicone methyl symmetric and asymmetric stretches, respectively. The silicone methyl groups were still present and ordered at the interface with the OTMS/MVS mixture. There may have also been contribution from MVS in this signal as well, but it is not possible to deconvolute the signal.

The lack of signal from the OTMS methoxy groups in the OTMS/MVS mixture may have two possible explanations. First, MVS may have caused the OTMS to become disordered at the silicone interface. If the OTMS lost its orientational order, SFG signal would be lost. Second, MVS may have preferentially interacted with the silicone surface,

and therefore would have covered the interface. If MVS mostly covered the interface, there would not be enough interfacial OTMS molecules to generate signal. Because signal was generated in the C-H stretching region that could be attributed to MVS, this possibility cannot be ruled out. Because no specific signal from MVS can be distinguished in these experiments, SFG cannot be used to differentiate between these two possibilities.

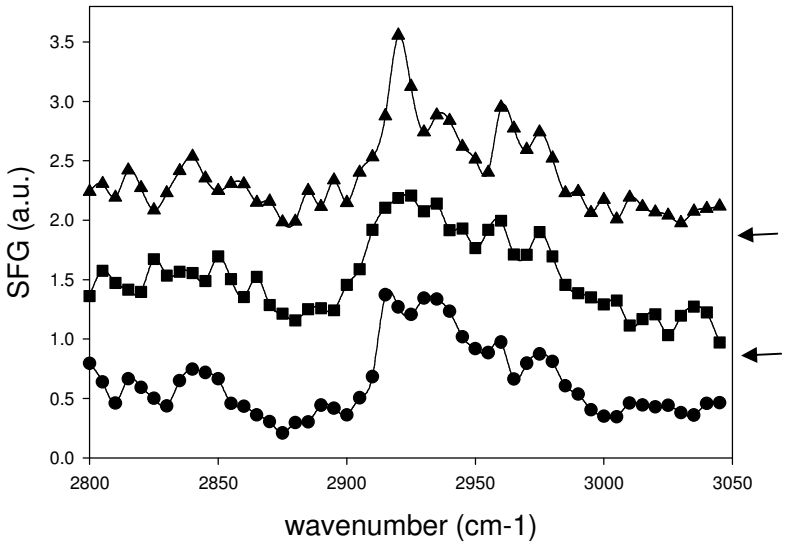

Figure 3.6. SFG spectra of silicone elastomer thin film in contact with 1:1 OTMS/MVS mixture at initial contact (circles), 15 min contact (squares) and 30 min contact (triangles). Baselines of spectra are indicated by arrows on right.

The SFG spectra of silicone thin films in contact with OTMS and the OTMS/MVS mixture were significantly different from those of silicone thin films in contact with γ-GPS and the silane adhesion promoting mixture of γ-GPS and MVS. For the neat OTMS, the OTMS methoxy groups were less ordered at the silicone interface than those of the γ-GPS, showing that interactions between the silicone and the γ-GPS may have been stronger than those between the silicone and the OTMS. At the interface

between silicone and the γ-GPS/MVS mixture, silane methoxy signal was observed, while there was no evidence of the OTMS in the OTMS/MVS mixture at the silicone interface. As discussed above, this may have been due to MVS acting to disorder the interfacial OTMS, or this may have simply been a dilution effect.

It is important to note that MVS is a necessary component of adhesion promoters for silicone elastomer, because the vinyl groups participate in the cross-linking curing reaction of the silicone. Therefore, if a neat silane can adopt a specific interfacial orientation necessary for adhesion promotion, it must also remain in that orientation when mixed with MVS to effectively enhance adhesion. The interfacial γ-GPS methoxy groups remained ordered when mixed with MVS, while the OTMS methoxy groups did not remain ordered when mixed with MVS. Since the γ-GPS/MVS mixture is the only known adhesion promoter of the systems studied, the ability of γ-GPS to maintain its interfacial molecular orientation may be part of the reason why it acts as an effective adhesion promoter when mixed with MVS.

3.3.3 Silicone Elastomer in Contact with Neat TDFTMS and the TDFTMS/MVS Mixtures Studied with SFG

Lastly, to compare the behavior of the epoxy-functionalized silane γ-GPS with other silanes not used as adhesion promoters, the behavior of a silane with a fluoro-alkyl backbone and CF_3 end groups, TDFTMS, was investigated. Here, SFG spectra of silicone elastomer in contact with TDFTMS and a mixture of TDFTMS and MVS are shown in Figures 3.7 and 3.8, respectively. In Figure 3.7, like the other silanes, SFG signal was observed at 2835 cm^{-1}, characteristic of the silane methoxy symmetric stretch. The signal was observed immediately upon contact between the silicone thin film and the

silane. However, the peak strength decreased after approximately 15 minutes of contact, and then remained stable for one hour.

The decrease in strength of the silane peak was different than what was observed for neat γ-GPS and neat OTMS, and may be because of different interfacial mechanisms. The decrease in signal over 15 minutes may have been due to a slower interfacial equilibration than was observed for the other two neat silanes. Over approximately 15 minutes, the TDFTMS molecules at the interface may have relaxed to equilibration. In this case, the TDFTMS methoxy groups would have slightly disordered/reoriented at the interface, which could decrease the TDFTMS signal. The γ-GPS and the OTMS may have equilibrated much more quickly at the silicone interface, such that the equilibration process was complete before the initial SFG scan was taken and no drop in silane signal intensity was observed. A second possible explanation is that the TDFTMS slowly diffused into the silicone elastomer thin film. In this case, as TDFTMS diffused into the silicone thin film, the interfacial TDFTMS would have become less ordered and the SFG signal from TDFTMS would have decreased. Further, there was no signal from silicone at the buried interface between silicone and neat TDFTMS, as there was at the buried interfaces between silicone and the other silanes. This indicates that the silicone methyl groups laid down at the interface with neat TDFTMS due to unfavorable interactions with the fluoro-alkyl backbone of the silane.

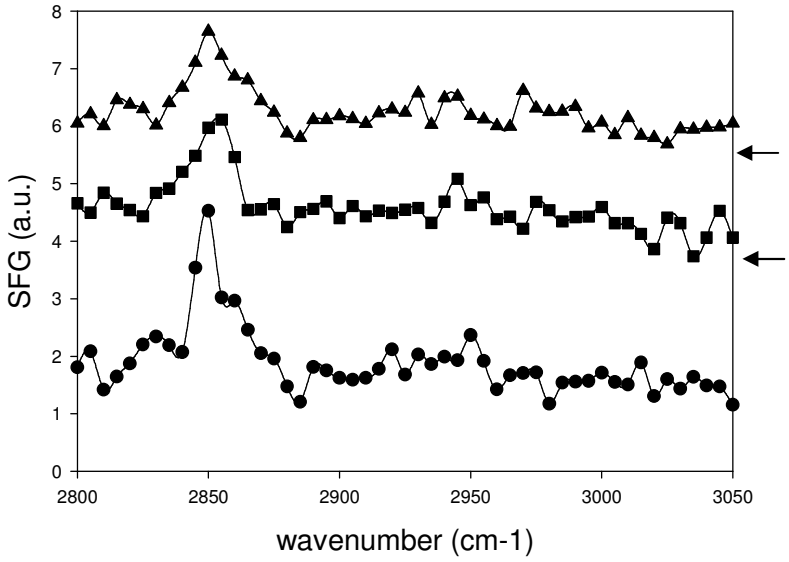

Figure 3.7. SFG spectra of silicone elastomer thin film in contact with neat TDFTMS at initial contact (circles), 15 min contact (squares) and 30 min contact (triangles). Baselines of spectra are indicated by arrows on right.

SFG spectra of silicone elastomer in contact with the TDFTMS/MVS mixture are shown in Figure 3.8. As can be seen, no discernable signal was observed over one hour from either the silane or the silicone elastomer. There was no silicone elastomer signal for the same reason as there was no silicone signal at the neat TDFTMS interface. The silicone methyl groups laid down because of the fluoro-alkyl backbone of the silane. The lack of silane methoxy signal can be explained with the same reasoning as the OTMS/MVS mixture. The MVS may have acted to disorder the TDFTMS methoxy groups at the silicone interface, causing the TDFTMS signal to decrease. Also, the MVS may have preferentially interacted with the silicone interface, which would dilute the TDFTMS at the interface. This would have decreased the interfacial number density of TDFTMS, attenuating the SFG signal. However, this explanation is not likely because there was no signal that could be attributed to interfacial MVS. A third explanation is that

MVS facilitated the faster interfacial diffusion of TDFTMS into the silicone elastomer thin film, disordering the interface and causing a loss in SFG signal.

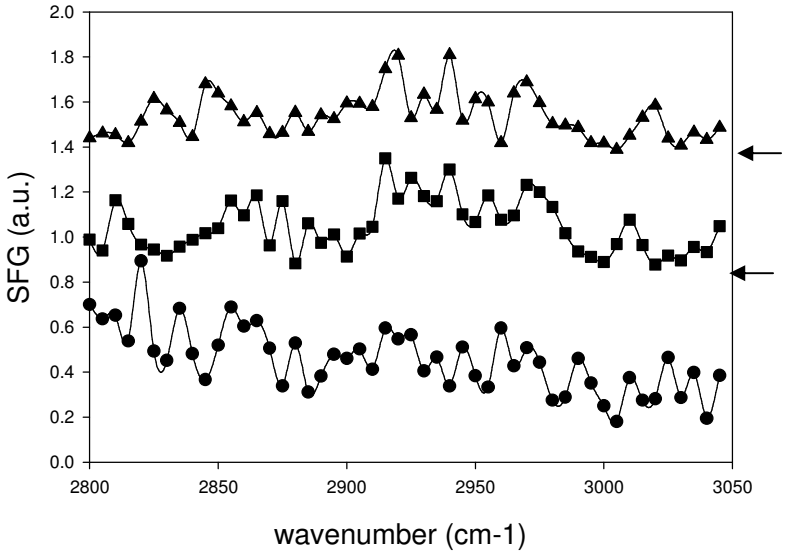

Figure 3.8. SFG spectra of silicone thin film in contact with TDFTMS/MVS mixture at initial contact (circles), 15 min contact (squares) and 30 min contact (triangles). Baselines of spectra are indicated by arrows on right.

The interfaces formed between thin films of silicone elastomer and TDFTMS and the TDFTMS/MVS mixture behaved differently than those with γ-GPS and the γ-GPS/MVS mixture or OTMS and the OTMS/MVS mixture. Unlike the other silanes, the TDFTMS showed evidence of either a slow interfacial diffusion or slow interfacial equilibration because the silane signal decreased over fifteen minutes and then became stable. Also unlike the other interfaces studied, the silicone methyl groups appeared to lay down when contacted to the fluorinated silane and its mixture with MVS. Like the OTMS/MVS mixture, there was no evidence of the TDFTMS methoxy groups segregating with order to the silicone interface when mixed with MVS.

Of all the silane/MVS mixtures studied, only the mixture of γ-GPS and MVS promotes adhesion between silicone elastomer and PET and PBT. Therefore, because

neither OTMS nor TDFTMS ordered at the interface when mixed with MVS, there is further corroboration that interfacial ordering of the γ-GPS methoxy groups when mixed with MVS is a necessary condition for the γ-GPS/MVS mixture to enhance the adhesion of silicone. It is possible that the silane molecules must adopt a specific orientation in order to participate in a specific adhesion mechanism, such as chemical bonding, inter-diffusion or the formation of an interpenetrating network.

3.3.4 Interfacial Silane Orientation Distribution Studied by MD Simulations

Histograms of the calculated silane methoxy orientation distributions for γ-GPS, γ-GPS in the γ-GPS/MVS mixture, OTMS and TDFTMS at the silicone interface are shown in Figure 3.9. The histograms incorporate the correction factor for variation in solid angle. Histograms for the OTMS in the OTMS/MVS mixture and the TDFTMS in the TDFTMS/MVS mixture were not calculated because there was no evidence of these silanes ordering at the silicone interface. As seen in Figure 3.9, the methoxy groups for all silanes exhibited similar broad, random orientation distributions in these simulations. This indicates that none of the silanes' methoxy groups exhibited strong enough specific interactions with the silicone surface that would result in a narrow orientation distribution. The broad orientation distributions calculated from the simulations largely agree with the inferences made from SFG spectra that all silane methoxy groups exhibited broad interfacial angle distributions. However, the MD simulations did not account for the ordering of the silane methoxy groups seen in the SFG experiments. This may be because the MD simulations were only carried out for 50 ps, as opposed to the minutes taken to obtain an SFG spectrum. It is possible that the ordering of the silane methoxy groups at the silicone interface occurred on a longer time scale than is possible to study

with MD simulations. However, because broad, random angle distributions were observed from the MD simulations, it can be concluded that there was no strong driving force for the silane methoxy groups to order at the silicone interface with a narrow angle distribution.

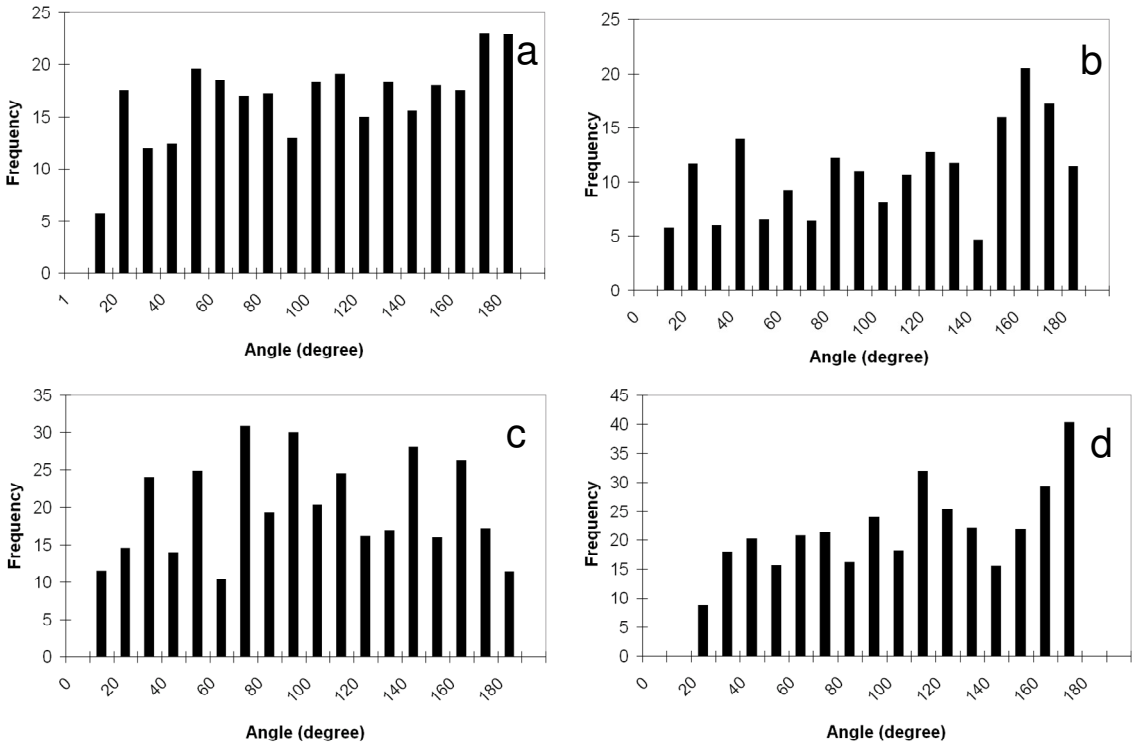

Figure 3.9. Histograms of silane methoxy orientation at the silicone interface for γ-GPS (a), γ-GPS in the γ-GPS/MVS mixture (b), OTMS (c) and TDFTMS (d).

3.4 Conclusions

The molecular structures of buried interfaces between silicone elastomer thin films and silanes or silane/MVS mixtures were investigated with SFG and MD simulations. The silane γ-GPS and the known adhesion promoting mixture of γ-GPS and MVS were compared to two other silanes not used as adhesion promoters, OTMS and TDFTMS, as well as their mixtures with MVS. It was found that the methoxy groups of all silanes exhibited some interfacial order at the silicone elastomer interface, although

TDFTMS appeared to either slowly reorient or slowly diffuse into the silicone thin film. However, only the γ-GPS methoxy groups exhibited interfacial order when mixed with MVS. MVS is necessary to promote adhesion between silicone elastomer and polymeric substrates because the MVS vinyl groups can participate in the cross-linking reaction of the silicone. Therefore, if a neat silane adopts an interfacial orientation that is necessary for an adhesion promotion mechanism to occur, the silane must also adopt this orientation when mixed with MVS. Because the methoxy groups of γ-GPS maintained interfacial orientational order at both the silicone interface and the PET interface, as described in Chapter 2,[13] the interfacial ordering of silane methoxy groups may be a prerequisite condition for the γ-GPS in the γ-GPS/MVS mixture to promote adhesion. This orientation may be needed for a specific adhesion promotion mechanism, such as chemical reaction, formation of an interpenetrating network or interfacial diffusion, to occur. Further, MD simulation studies confirmed that the silane methoxy groups exhibited broad orientation angle distributions at the silicone elastomer interface.

3.5 References

1. Kinloch, A. J. *Adhesion and Adhesives Science and Technology*; Chapman and Hall: London, 1987.
2. Mittal, K.L. *Adhesion Measurement of Thin Films, Thick Films and Bulk Coatings.* American Society for Testing and Materials: Philadelphia, PA, 1978.
3. Yacobi, B.G.; Martin, S.; Davis, K.; Hudson, A.; Hubert, M. *J. Appl. Phys.* **2002**, *91*, 6227-6262.
4. Charles, H.M. *Engineered Materials Handbook Volume 3: Adhesives and Sealants*: ASM International: Materials Park, OH, 1990.
5. Feresenbet, E.; Raghavan, D.; Holmes, G.A. *J. Adhesion* **2003**, *79*, 643-665.
6. Sathyanarayana, M. N.; Yaseen, M. *Prog. Org. Coat.* **1995**, *26*, 275-313.
7. Suzuki, T.; Kasuya, A. *J. Adhes. Sci. Technol.* **1989**, *3*, 463-473.
8. Walker, P. *Adhesion Promoters, 1st ed.*; Elsevier: London, 1987.
9. Mine, K.; Nishio, M.; Sumimura, S. US Patent 4,033,924, July 5, 1977.
10. Schulz, J.B. US Patent 4,087,585, May 2, 1978.
11. Gray, T.E.; Lutz, M.A. US Patent 5,595,836, Jan 21, 1997.
12. Loch, C.L.; Ahn, D.; Chen, Z. *J. Phys. Chem. B* **2006**, *110*, 914-918.
13. Vázquez, A.V.; Shephard, N.E.; Steinecker, C.L.; Ahn, D.; Spanninga, S.; Chen, Z. *J. Colloid Interface Sci.* **2009**, *331*, 408-416.
14. Chen, C.; Wang, J.; Loch, C.L.; Ahn, D.; Chen, Z. *J. Am. Chem. Soc.* **2004**, *126*, 1174-1179.
15. Wang, J.; Woodcock, S.E.; Buck, S.M.; Chen, C.; Chen, Z. *J. Am. Chem. Soc.* **2001**, *308*, 9470-9471.

16. Wang, J.; Chen, C.; Buck, S.M.; Chen, Z. *J. Phys. Chem. B.* **2001**, *105*, 12118-12125.

17. Loch, C.L.; Ahn, D.; Chen, C.; Chen, Z. *J. Adhesion* **2005**, *81*, 319-345.

18. Hwang, M.; Stockfisch, T.P.; Hagler, A.T. *J. Am. Chem. Soc.* **1994**, *116*, 2515-2525.

19. Deng, M.; Tan, V.B.C.; Tay, T.E. *Polymer* **2004**, *45*, 6399-6407.

20. Kornherr, A.; Hansal, S.; Hansal, W.E.G.; Besenhard, J.O.; Kronberger, H.; Nauer, G.E.; Zifferer, G. *J. Chem. Phys.* **2003**, *119*, 9719-9728.

21. Lee, C.Y.; McCammon, J.A.; Rossky, P. *J. Chem. Phys.* **1984**, *80*, 4448-4455.

22. Chen, C.; Wang, J.; Chen, Z. *Langmuir* **2004**, *20*, 10186-10193.

23. Carrasco, F.; Pages, P.; Lacorte, T.; Briceno, K. *J. Appl. Polym. Sci.* **2005**, *98*, 1524-1535.

CHAPTER 4

EFFECT OF SOLVENT EXTRACTIONS ON COMMERCIAL SILICONE SURFACE STRUCTURE

4.1 Introduction

Silicone elastomer adhesives are widely used in a variety of applications in the electronics, automotive, aviation and microfluidics fields. In particular, addition-cured silicone elastomer based on poly(dimethylsiloxane) (PDMS) is valuable for its high thermal stability, unique elastic behavior, and resistance to chemical corrosion.[1-6] Specifically for microfluidics applications, PDMS is valued because it is clear in the UV-visible region, where detection for biological and medical applications usually occurs, and it is nontoxic for medical applications.[7]

While PDMS is an ideal material for microfluidics, some of its properties pose complications for these applications. The surface of PDMS is hydrophobic, and thus has a very low energy. This can diminish its adhesion to other polymeric substances.[6] To improve adhesion, PDMS can be made more hydrophilic by subjecting its surface to oxidative treatments using oxygen plasma or UV irradiation. Surface silanol groups are formed, which then condense with certain polymers or glass surfaces to improve adhesion.[7,8] Generally, the PDMS surface is exposed to plasma or UV irradiation for approximately one minute and is then immediately brought into contact with the adherend. This is most effective when the surface is smooth on a micron scale.[4]

In microfluidics applications, PDMS often needs to be sealed, meaning that two PDMS pieces must be adhered together. PDMS sealing can either be reversible or irreversible. Reversible sealing occurs because PDMS is flexible and can therefore bond through van der Waal forces when two PDMS surfaces are contacted.[7] Irreversible sealing occurs by the formation of chemical bonds after the PDMS surfaces are rendered hydrophilic through oxidative treatments. However, this oxidative activation is a temporary effect because hydrophobic recovery quickly occurs, in which the PDMS surface returns to its low energy, hydrophobic state. Hydrophobic recovery decreases the adhesion of surface-modified PDMS if it is not contacted to the adherend immediately after surface modification. This unfavorable process can be slowed by extracting uncrosslinked, low molecular weight oligomers from the PDMS polymer.[9] However, it is not well-understood why extracting low molecular weight oligomers slows hydrophobic recovery.

A commonly used commercial PDMS is Sylgard 184 (Dow Corning Corporation). Sylgard 184 consists of vinyl-terminated dimethylsiloxane oligomers, platinum catalyst, dimethylvinyl and trimethyl silica fillers, dimethylhydrogen siloxane crosslinker, and a tetramethyltetravinyl cyclotetrasiloxane inhibitor.[10] The most common formulation is a 10:1 (wt/wt) base/curing agent ratio for Sylgard 184. However, after this formulation is cured, it has been shown that up to 5 wt % of the total material can be uncured oligomer, and the amount of uncured oligomer can be even greater for a thin film of silicone.[11] Further, the degree of crosslinking that occurs in PDMS can be affected by the concentration of crosslinker in the formulation, the temperature at which the system was cured and the thickness of the film.[6] During the cure process, secondary reactions

involving the Si-H groups of the crosslinker can occur, creating shorter chain fragments that are physically entangled rather than chemically bonded to the PDMS network. It has been demonstrated that the secondary reactions occur more frequently in thin films of PDMS. These physically entangled oligomers can be extracted from the PDMS film[6] and may be partially responsible for fast hydrophobic recovery after oxidative surface treatments.

Because hydrophobic recovery after surface oxidative treatments is slowed by the removal of short chain oligomers from the PDMS network, it can be assumed that surface-specific chemical changes occur with the extraction of these materials that affect the rate of hydrophobic recovery. To better understand the effect of solvent extractions on the hydrophobic recovery of PDMS surfaces after oxidative treatments, it is necessary to understand how solvent extractions affect the surface structure of PDMS thin films. Because of its surface-sensitivity and ability to deduce the orientation of surface chemical groups, SFG is an ideal technique to study such surfaces.

PDMS surfaces have been studied with SFG in prior publications. Ye and Gracias studied the effect of surface modifications on the surface structure of Sylgard 184 samples with different crosslink densities.[8] Prior to surface modifications, it was found that the less-crosslinked Sylgard 184 surface methyl groups exhibited an orientation angle of approximately 40^{o} with respect to the surface normal, which agreed with work by Chen et al.[12] The more-crosslinked Sylgard 184 surface methyl groups exhibited approximately a 45^{o} orientation angle, meaning that the surface methyl groups laid down more with greater crosslink density because there were more crosslinked methylene links.[8] Therefore, crosslink density was shown to influence the surface orientation of

PDMS methyl groups. We believe that removing extractable materials, including unreacted short-chain oligomers and other additives, would increase the overall crosslink density of the PDMS, since surface un-crosslinked material would be removed. Therefore, similar changes in methyl orientation may be expected.

The current study investigated the surface restructuring of Sylgard 184 thin films before and after extractable materials were removed. The orientation of the PDMS surface methyl groups before and after extractions was determined, and compared to the work of Ye and Gracias.[8] Any change in the orientation of the surface methyl groups may affect the efficacy of oxidative surface treatments. For example, a change in surface orientation of the PDMS methyl groups may help explain why extracted PDMS surfaces experience slower hydrophobic recovery after oxidative surface treatments. The change in surface structure may change the surface energy of the PDMS, or the ability of the PDMS surface to form silanol groups after oxidative treatments. Also, extractions may affect the roughness of the PDMS surface. It has been shown that smoother PDMS surfaces are more amenable to oxidative treatments.[4] Therefore, if removing the extractable short-chain segments from PDMS smoothes the surface, this may also improve the efficacy of oxidative surface treatments.

In this study, the effect of solvent extractions on Sylgard 184 PDMS surfaces was investigated by three different methods. First, SFG studies were performed on Sylgard 184 thin films before and after solvent extractions. Spectral fitting was performed and the orientation of the surface methyl groups before and after solvent extractions was calculated. This was used to determine if and how the functional groups on PDMS surfaces reoriented after solvent extractions, and to determine if extracted PDMS had

similar surface structure to the highly cross-linked PDMS studied by Ye and Gracias. Further, water contact angle measurements were performed before and after extractions to determine if and how the hydrophobicity of the PDMS was affected by the removal of short chain oligomers. Lastly, atomic force microscopy (AFM) images were obtained of PDMS surfaces to determine how the root mean squared (RMS) surface roughness was affected by solvent extractions.

4.2 Experimental

4.2. Sample Preparation

A Sylgard 184 silicone elastomer kit was obtained from Dow Corning Corporation and was used as received. The Sylgard 184 silicone elastomer was prepared in a 10:1 base/curing agent ratio, as directed by the manufacturer. The base and curing agent were mixed vigorously to the point of visual homogeneity.

To prepare thin films of Sylgard 184 silicone elastomer for SFG analysis, a 5 wt% solution of Sylgard 184 in toluene (Sigma-Aldrich, Inc) was spin cast using a spin-coater from Specialty Coating Systems onto fused silica windows (1-in diameter, 1/8-in thickness, ESCO Products, Inc). The fused silica windows were cleaned by etching in warm chromic acid solution prior to use. The thin films were then cured in an oven at 150^{o}C for 1 h. The films were cooled to room temperature prior to analysis.

Extractions were performed by placing the Sylgard 184 thin film in toluene (Sigma-Aldrich, Inc) for 30 min. The same volume of fresh toluene was used for each extraction to ensure consistency among samples. The solvent was then removed by drying the Sylgard 184 films under nitrogen prior to analysis.

4.2.2 SFG Experiments

SFG theory has been well-developed and is discussed in Chapter 1, Section 1.2.2. Also, the experimental design used in these experiments was detailed in the literature and discussed in Chapter 1, Section 1.2.3.[12, 13-16] Briefly, a fixed-frequency visible beam and a tunable-frequency IR beam are overlapped spatially and temporally at the polymer surface at 60° and 54°, respectively, with energies of 100 and 200 μJ, respectively, with beam diameters of 500 μm. Previous work has shown that the SFG signal is dominated by the signal from the polymer/air interface rather than the polymer bulk or polymer/fused silica substrate interface.[13,14,15] In this study, the ssp (s-polarized SFG output signal, s-polarized visible input light, p-polarized IR input light) and sps (s-polarized SFG output signal, p-polarized visible input light, s-polarized IR input light) polarization combinations were used to obtain all spectra.

4.2.3 Calculation of the Orientation of Surface Methyl Groups

As discussed in Chapter 1, Section 1.2.2, SFG signal in the ssp polarization combination can be written as the sum of the resonant part of the second order nonlinear susceptibility, $\chi^{(2)}_{R,ssp}$ and the non-resonant part of the second-order nonlinear susceptibility, $\chi^{(2)}_{NR,ssp}$:

$$\chi^{(2)}_{ssp} = \chi^{(2)}_{R,ssp} + \chi^{(2)}_{NR,ssp} = \sum_q \frac{A_{q,yyz}}{\omega_{IR} - \omega_q + i\Gamma_q} + \chi^{(2)}_{NR,yyz} \tag{4.1}$$

where $A_{q,yyz}$, ω_{IR}, ω_q and Γ_q are the strength of the vibrational mode q, the infrared frequency, the frequency of mode q and the damping constant of mode q, respectively.[15,17,18]

Because of the relationship between the macroscopic second-order nonlinear susceptibility, $\chi^{(2)}$, and the microscopic second-order nonlinear polarizability or hyperpolarizaibility, $\alpha^{(2)}$, the orientation of surface and/or interfacial functional groups can be deduced by fitting SFG spectra obtained using different polarization combinations of input and output beams. The PDMS methyl groups have C_{3v} symmetry, so the orientation of these methyl groups can be evaluated by measuring the values of the ratio of $\frac{|\chi_{yyz,as}|}{|\chi_{yzy,as}|}$.[12,15] The second-order nonlinear susceptibility ratio can be related to the methyl group orientation angle with respect to the surface normal, θ, by the following relation:

$$\frac{|\chi_{yyz,as}|}{|\chi_{yzy,as}|} = \left| \frac{\langle \cos\theta \rangle - \langle \cos^3\theta \rangle}{\langle \cos^3\theta \rangle} \right| \tag{4.2}$$

where the brackets are the averages of methyl group tilt angles such that

$$\langle \cos^n\theta \rangle = \int_0^{\pi} \cos^n\theta f(\theta) \sin\theta d\theta \tag{4.3}$$

and $f(\theta)$ is a Gaussian distribution function describing the surface methyl angle distribution. The Gaussian distribution can be set from a δ-distribution to a wider Gaussian distribution depending on the surface being studied. In plotting equation (4.2), various Gaussian distributions can be plotted to understand how different distributions of surface methyl angles may affect surface orientation.

The values of $|\chi_{yyz,as}|$ and $|\chi_{yzy,as}|$ are determined by spectral fitting using Equation (4.1). The $|\chi_{yyz,as}|$ term is related to the ssp spectrum and the $|\chi_{yzy,as}|$ term is related to the sps spectrum. By matching the calculated values from equation (4.1) to values on the

curve plotted of equation (4.2), it is possible to then determine the orientation angle for various Gaussian angle distributions for the surface PDMS methyl groups.[12]

4.2.4 Contact Angle Goniometry Experiments

Static contact angle goniometry measurements were performed using a CAM 100 Optical Contact Meter (KSV Instruments) contact angle goniometer. Three samples of PDMS were studied before solvent extractions, after one solvent extraction, and after two solvent extractions. Four to five measurements were performed for each sample.

4.2.5 AFM Experiments

AFM images were obtained using a Molecular Imaging Picoscan system. Images were obtained using the Magnetic AC (MAC) mode with magnetically coated silicon nitride cantilevers with an average resonance frequency of 75 kHz and a force constant of 2.3 N/m. Images were obtained under ambient conditions at room temperature and were processed using the Scanning Probe Imaging Processor software (Image Metrology).[19] Images sizes were 2 μm by 2 μm.

4.3 Results and Discussion

4.3.1 SFG Studies of PDMS Thin Films with Solvent Extractions and Methyl Orientation Calculation

SFG spectra were obtained from PDMS thin film surfaces before solvent extractions, after one solvent extraction and after two solvent extractions in the ssp and sps polarization combinations. The spectra in the ssp polarization combination are seen in Figure 4.1, and the spectra in the sps polarization combination are seen in Figure 4.2.

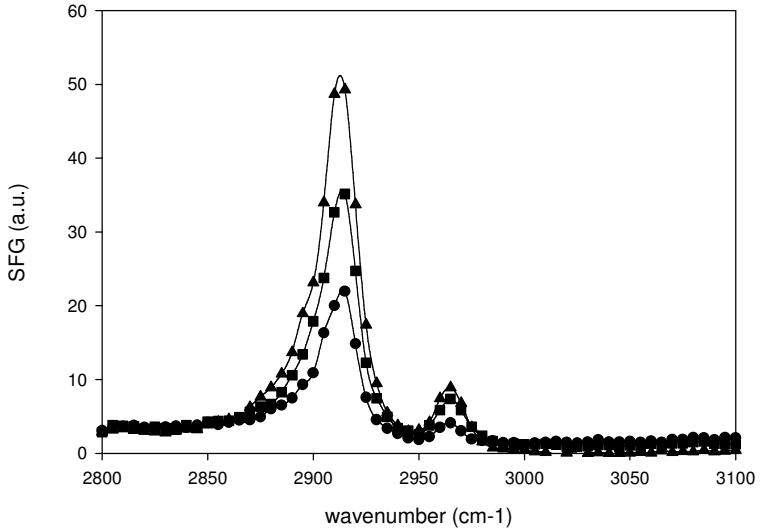

Figure 4.1. SFG spectra in the ssp polarization combination of PDMS thin films before solvent extractions (circles), after one solvent extraction (squares) and after two solvent extractions (triangles).

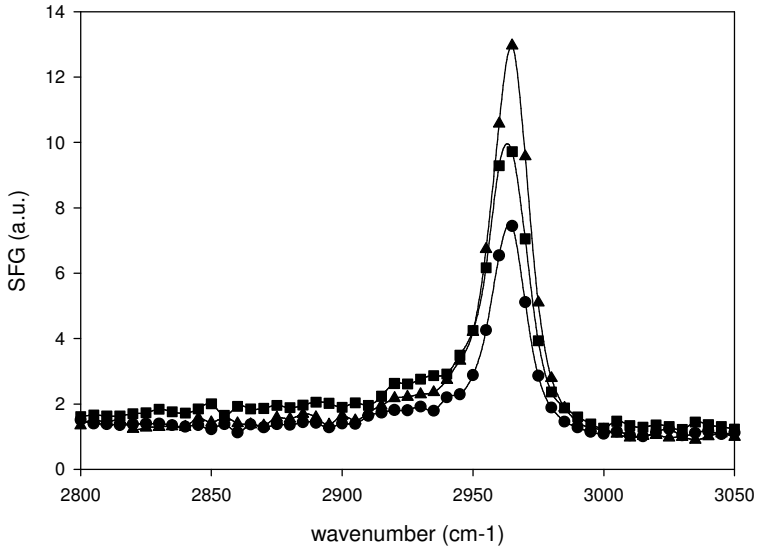

Figure 4.2. SFG spectra in the sps polarization combination of PDMS thin films before solvent extractions (circles), after one solvent extraction (squares) and after two solvent extractions (triangles).

The ssp spectra in Figure 4.1 were dominated by the symmetric methyl stretch at 2910 cm^{-1}, with some contribution from the asymmetric methyl stretch at 2960 cm^{-1},

while the sps spectra in Figure 4.2 were dominated by the asymmetric methyl stretch at 2960 cm^{-1}.[8,12] It was observed that the PDMS methyl signal increased in strength with solvent extractions in both ssp and sps polarization combinations, as seen in Figure 4.1 and 4.2. Because SFG signal is directly related to the number density of the surface functional groups, as well as the ordering and orientation of the surface groups, stronger SFG signal may signify that a greater concentration of PDMS methyl groups were present and/or ordered at the surface. With solvent extractions, fillers and additives in the Sylgard 184 formulations were removed, allowing more PDMS to go to the surface. Therefore, the signal intensity from the PDMS methyl groups increased because the density of the crosslinked PDMS at the surface increased with solvent extractions. Further, surface short-chain uncured PDMS segments would have also been extracted. These short-chain segments may not have been as orientationally ordered as the crosslinked PDMS. Thus, when these disordered short segments were removed, the more orientationally ordered crosslinked PDMS was better able to cover the surface. This also led to an increase in PDMS methyl SFG signal with solvent extractions.

In addition to the change in number density, the changes in SFG signal with solvent extractions observed in Figures 4.1 and 4.2 also indicated that there may have been a change in the PDMS surface methyl orientation. To determine if the orientation of the surface PDMS methyl groups changed after solvent extractions, the SFG spectra in Figures 4.1 and 4.2 were fit according to equation (4.1). The ratio of $\frac{\chi_{yyz,as}}{\chi_{yzy,as}}$ was calculated for PDMS samples before solvent extractions, after one solvent extraction, and after two solvent extractions from the spectra taken in the ssp and sps polarization

combinations. Before solvent extractions, the ratio of $\frac{\chi_{yyz,as}}{\chi_{yzy,as}}$ was found to be 0.701, after one solvent extraction, $\frac{\chi_{yyz,as}}{\chi_{yzy,as}}$ was 0.986, and after two solvent extractions, $\frac{\chi_{yyz,as}}{\chi_{yzy,as}}$ was calculated to be 1.023. These values were plotted on a graph based on equation (4.2), and this graph is seen in Figure 4.3.

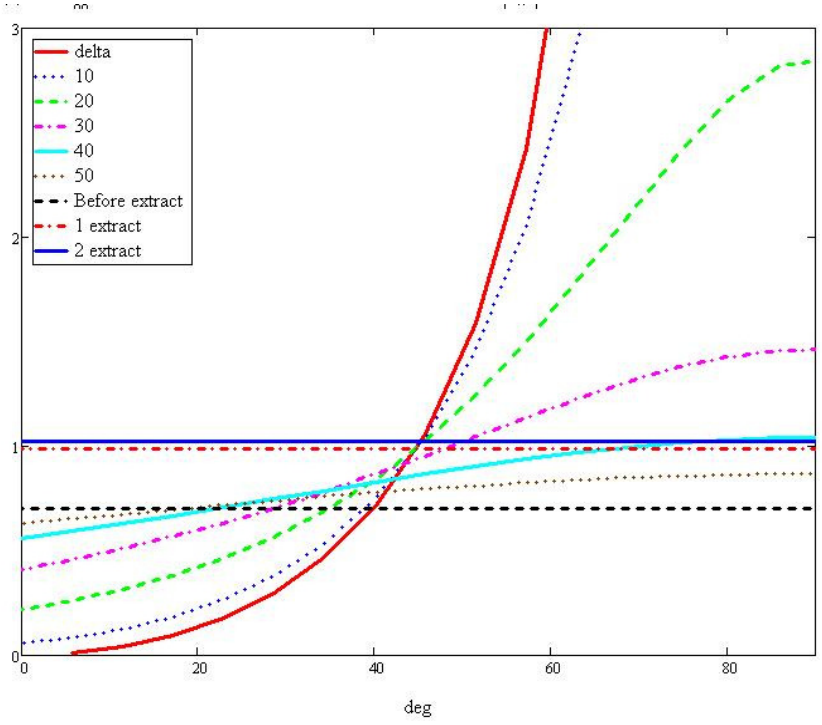

Figure 4.3. Plot of $\frac{\chi_{yyz,as}}{\chi_{yzy,as}}$ from SFG spectral fitting with respect to orientation angle of PDMS surface methyl groups versus the surface normal of the PDMS films. Curves with different colors are for different Gaussian angle distributions of the surface PDMS methyl orientations, namely a δ distribution (red), 10 degree distribution (blue dotted line), 20 degree distribution (green dotted line), 30 degree distribution (pink dotted line), 40 degree distribution (aqua line) and a 50 degree distribution (purple dotted line). The horizontal lines represent the measured ratio of $\frac{\chi_{yyz,as}}{\chi_{yzy,as}}$ for PDMS surface methyl groups before extractions (black dotted line), after one extraction (red dotted line) and after two extractions (blue line).

As can be seen in Figure 4.3, the orientation angle of the surface PDMS methyl groups increased with respect to the surface normal with solvent extractions. If a δ-distribution of surface PDMS methyl orientation angles is assumed, the methyl angle before solvent extractions was approximately 40°, which was consistent with other SFG studies of PDMS.[8, 12] After one solvent extraction, the orientation angle was found to be approximately 45°, and this orientation did not significantly change after the second solvent extraction. Although the orientation angles deduced from Figure 4.3 were very close to magic angle, we believe the orientation angle distribution was narrow because of the strong signal intensity. Interestingly, the 45° methyl orientation angle after solvent extractions matched the orientation angle of more highly crosslinked PDMS determined by Ye and Gracias.[8] Therefore, by removing the uncured short chain PDMS segments and other fillers through extractions, the remaining surface was dominated by crosslinked PDMS methyl groups. Because the orientation of the extracted PDMS methyl groups matched that of the highly crosslinked PDMS, the extractions must only removed the short-chain uncrosslinked oligomers and other fillers. That is, extractions did not dissolve and extract PDMS that was already crosslinked into the polymer network.

Additionally, the reorientation of the methyl groups gave further evidence that the number density of surface methyl groups of cross linked PDMS molecules increased after solvent extractions. The plot in Figure 4.3 showed that the PDMS methyl groups laid down more after solvent extractions. If the number density of surface methyl groups had been the same before and after solvent extractions, the signal intensity in the ssp polarization combination would have decreased because the ssp polarization combination probes vibrational transitions in the direction of the surface normal. Therefore, because

the angle of the surface PDMS methyl groups increased with solvent extractions, and the PDMS methyl signal intensity also increased with solvent extractions, the number density of ordered PDMS methyl groups must have increased to account for the signal intensity change.

The orientation change of the PDMS surface methyl groups with solvent extractions and the increase in surface PDMS methyl number density may have implications for understanding the effectiveness of surface oxidative treatments. As discussed in Section 4.1, hydrophobic recovery after oxidative surface treatments can be slowed by extracting short chain oligomers from PDMS surfaces. The orientation change of the surface PDMS methyl groups may have altered surface structure such that hydrophobic recovery would be slowed. The surface of extracted PDMS was similar to that of highly crosslinked PDMS. It is likely that after the uncured short chain segments and other additives were removed through extraction, the more ordered crosslinked PDMS surface that remained would more easily form silanol groups after being subjected to oxidative surface treatments. This may slow hydrophobic recovery, making oxidative surface treatments more effective.

4.3.2 Contact Angle Goniometry Studies of PDMS Thin Films with Solvent Extractions

It is possible that a significant change in hydrophobicity occurred when extractable materials were moved from the Sylgard 184 surface. Perhaps more hydrophobic materials were removed in the toluene extractions, rendering the surface more hydrophilic. If the extracted Sylgard 184 surface was significantly more

hydrophilic than the un-extracted surface, this may slow hydrophobic recovery and may improve the effectiveness of oxidative surface treatments.

To determine if the hydrophobicity of Sylgard 184 was significantly affected by solvent extractions, static contact angle measurements were obtained before extractions, after one extraction, and after two extractions. Measurements are shown in Table 4.1.

	Sylgard 184 before extractions	Sylgard 184 after one extraction	Sylgard 184 after two extractions
Static water contact angle	$108.6^{o} \pm 1.6$	$104.0^{o} \pm 1.9$	$102.7^{o} \pm 2.3$

Table 4.1. Static water contact angle measurements for Sylgard 184 before solvent extractions, after one solvent extraction and after two solvent extractions.

The contact angle measurements reported in Table 4.1 were all within the range of previously reported static water contact angle measurements for PDMS.[12] While the static contact angle decreased slightly with solvent extractions, indicating a small increase in hydrophilicity, the change was not significant. Thus, the material being extracted into the toluene must not have been significantly more hydrophobic than the crosslinked PDMS left behind. Therefore, it can be determined that a major change in the hydrophobicity of the surface with solvent extractions did not occur. Therefore, it does not play a significant role in slowing hydrophobic recovery after oxidative surface treatments. Other factors, such as the change in surface PDMS methyl number density and the change in surface PDMS methyl orientation described in section 4.3.1 which is caused by a more highly crosslinked PDMS surface must play a greater role in slowing hydrophobic recovery.

4.3.3 AFM Studies of PDMS Thin Films with Solvent Extractions

As previously stated, flatter PDMS surfaces have been shown to respond more favorably to oxidative treatments for adhesion enhancement.[4] It is possible that flatter PDMS films may lead to better surface enhancement of silanol groups after oxidative treatment and this may slow hydrophobic recovery. Because moieties that may cause surface disorder, such as uncrosslinked PDMS oligomers and other additives, are removed during the extraction process, the extracted PDMS surfaces are more dominated by the ordered crosslinked network of PDMS and therefore may be flatter than their un-extracted counterparts. In addition to the changes in the surface structure of PDMS after extractions described in section 4.3.1, a change in surface roughness may also help explain why extracted PDMS surfaces respond better to oxidative treatments.

Here, atomic force microscopy (AFM) images were obtained of Sylgard 184 PDMS films before extractions, after one extraction and after two extractions. The AFM image of PDMS before extractions is seen in Figure 4.4, the AFM image of PDMS after one extraction is seen in Figure 4.5, and the AFM image of PDMS after two extractions is seen in Figure 4.6.

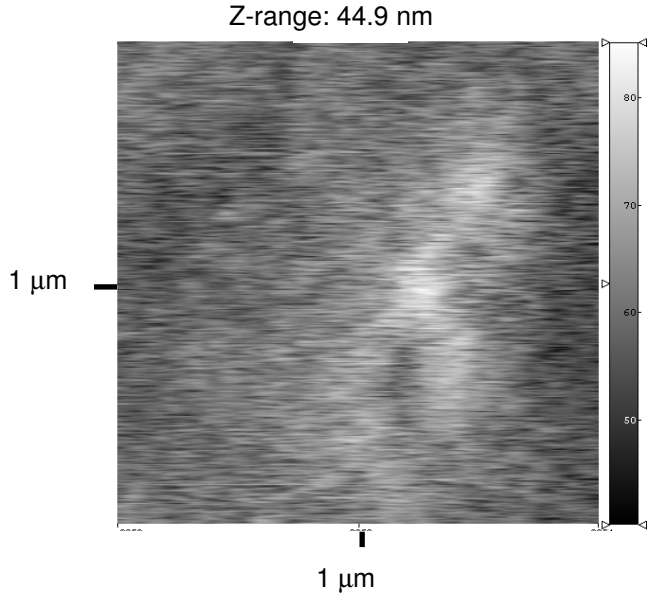

Figure 4.4. AFM image of Sylgard 184 thin film before solvent extractions.

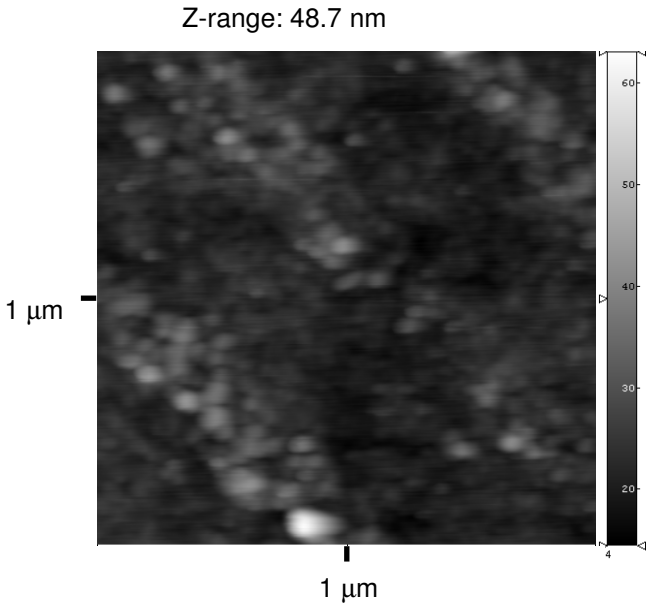

Figure 4.5. AFM image of Sylgard 184 thin film after one solvent extraction.

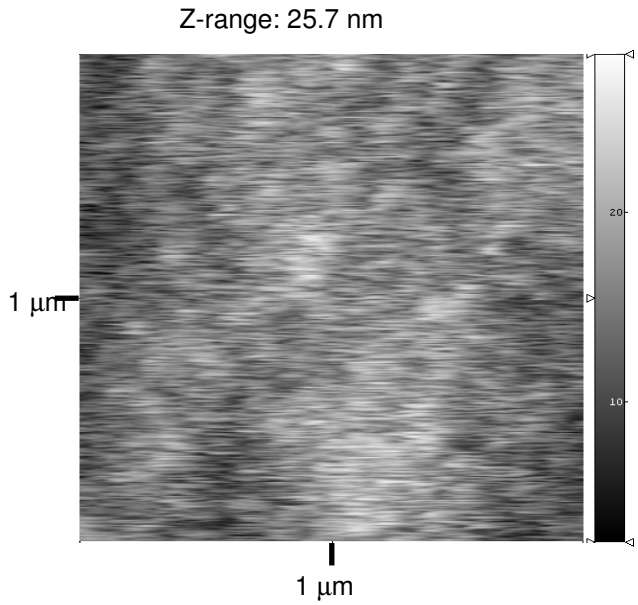

Figure 4.6. AFM image of Sylgard 184 thin film after two solvent extractions.

To compare the surface roughness of the three samples, it is necessary to calculate the root mean squared (RMS) roughness value for each sample. Table 4.2 shows the calculated RMS roughness for the three samples shown in Figure 4.4, Figure 4.5 and Figure 4.6.

	Sylgard 184 before extractions	Sylgard 184 after one extraction	Sylgard 184 after two extractions
RMS roughness (nm)	1.55	1.17	1.06

Table 4.2. RMS roughness calculated from AFM images for Sylgard 184 films before solvent extractions, after one solvent extraction and after two solvent extractions.

As can be seen in Table 4.2, the RMS roughness of the Sylgard 184 PDMS films decreased with solvent extractions. After the extractable materials were removed, the surface became less rough because disordered, short-chain oligomers and bulky additives and fillers were no longer present at the surface. Rather, the surface became dominated by the smoother, ordered, crosslinked PDMS.

4.4 Conclusions

In applications when PDMS must be sealed, it is often subjected to oxidative surface treatments. However, the efficacy of these treatments can be limited by hydrophobic recovery, in which the oxidized surface reverts back to its original hydrophobic state. It is known that extracting short-chain oligomers from PDMS can slow hydrophobic recovery, and thus improve oxidative surface treatments, but the reason why is largely unknown. Here, SFG, contact angle goniometry and AFM were used to study the effect of solvent extractions on the surface structure of Sylgard 184, a commonly used commercial PDMS. Static water contact angle measurements indicated that the hydrophobicity of the PDMS was largely unaffected by solvent extractions. However, SFG results showed that after extractions, the surface density of PDMS methyl groups increased, and that the angle with respect to the surface normal of these PDMS methyl groups decreased after one extraction. The angle of the surface PDMS methyl groups after extractions was similar to that of highly crosslinked PDMS,[8] indicating that short chain PDMS oligomers that were not part of the crosslinked network were removed in extractions. Further, AFM images showed that the RMS roughness of the PDMS samples decreased with solvent extractions.

It is important to note that only two solvent extractions were performed because when more extractions were performed, the crosslinked PDMS matrix began to dissolve. This was evidenced by visible pitting in PDMS films.

The AFM and SFG results show that the PDMS surface changed after solvent extractions. The extractable materials were removed, leaving a smoother surface dominated by PDMS in the crosslinked network. These changes in the surface of the

Sylgard 184 PDMS after extractable materials were removed may slow hydrophobic recovery after oxidative surface treatments because the surface structures may be more amenable to the formation and retention of surface silanol groups. This knowledge has important implications for the fabrication of microfluidics and other devices in which PDMS must be sealed irreversibly. It may be necessary to remove extractable materials from PDMS used in these devices prior to fabrication to improve adhesion.

4.5 References

1. Kinloch, A.J. *Adhesion and Adhesives Science and Technology*; Chapman and Hall: London, 1987.
2. Yacobi, B.G.; Martin, S.; Davis, K.; Hudson, A.; Hubert, M. *J. Appl. Phys.* **2002**, *91*, 6227-6262.
3. Mittal, K.L. *Adhesion Measurements of Thin Films, Thick Films and Bulk Coatings*; American Society for Testing and Materials: Philadelphia, 1978.
4. McDonald, J.C.; Whitesides, G.M. *Acct. Chem. Res.* **2002**, *35*, 491-499.
5. Charles, H.M. *Engineered Materials Handbook Vol. 3: Adhesives and Sealants*; ASM International: Materials Park, OH, 1990.
6. Esteves, A.C.; Brokken-Zijp, J.; Laven, J.; Huinick, H.P.; Reuvers, N.J.W.; Van de With, M.P. *Polymer.* **2009**, *50,* 3955-3966.
7. McDonald, J.C.; Duffy, D.C.; Anderson, J.R.; Chiu, D.T.; Wu, H; Schueller, O.A.; Whitesides, G.M. *Electrophoresis*, **2002**, *21*, 27-40.
8. Ye, H.; Gracias, D.H. *Langmuir*, **2006**, *22*, 1863-1868.
9. Chen, H-Y; McClelland, A.A.; Chen, Z.; Lahann, G. *Anal. Chem.* **2008**, *80*, 4119-4124.
10. Lee, J.N.; Jiang, X.; Ryan, D.; Whitesides, G.M. *Langmuir*, **2004**, *20*, 11684-11691.
11. Lee, J.N.; Park, C.; Whitesides, G.M. *Anal. Chem*, **2003**, *75*, 6544-6554.
12. Chen, C.; Wang, J.; Chen, Z. *Langmuir*, **2004**, *20*, 10186-10193.

13. Chen, C.; Wang, J.; Loch, C.L.; Ahn, D.; Chen, Z. *J. Am. Chem. Soc.*, **2004**, *126*, 1174-1179.

14. Wang, J.; Woodcock, S.E.; Buck, S.M.; Chen, C.; Chen, Z. *J. Am. Chem. Soc.*, **2001**, *308*, 9470-9471.

15. Wang, J.; Chen, C.; Buck, S.M., Chen, Z. *J. Phys. Chem. B.*, **2001**, *105*, 12118-12125.

16. Loch, C.L.; Ahn, D.; Chen, C.; Chen, Z. *J. Adhesion,* **2005**, *81*, 319-345.

17. Hirose, C.; Yamamoto, H.; Akamatsu, N.; Domen, K. *J. Phys. Chem.,* **1993**, *97*, 10064-10069.

18. Hirose, C.; Akamatsu, N.; Domen, K. *J. Chem. Phys.*, **1992**, *96*, 997-1004.

19. Woodcock, S.E.; Chen, C.; Chen, C. *Langmuir*, **2004**, *20*, 1928-1933.

CHAPTER 5

SURFACE AND INTERFACIAL STRUCTURES OF EPOXY RESINS USED IN FLIP-CHIP TECHNOLOGY

5.1 Introduction

Applications of flip-chip technology have greatly advanced the semi-conductor industry. In flip-chip devices, the semiconductor device is connected to external circuitry through solder bumps, making them smaller and faster than wire-bound devices. However, flip-chip devices require the use of an electronically insulating underfill adhesive, which is generally made of epoxy resin. Bisphenol-type epoxies are the most common material used as underfills, and additives such as aliphatic epoxies, SiO_2 and TiO_2 particle fillers, and silane adhesion promoters are often also included in formulations.[1-6] Epoxies used in underfills are generally cured with primary amines, forming hydroxyl groups in the cured network that can participate hydrogen bonding.[7]

The success of flip-chip devices largely depends on the underfill adhesive. The underfill adhesive comes into contact with a variety of substrates in semiconductor devices, including metals, semiconductors and polymeric passivation layers. If the adhesion of the underfill adhesive fails at any of these interfaces, the flip-chip device can fail.[3,4,8-11] Thus, it is extremely important to understand the adhesion of epoxies used as underfills.

The adhesion of epoxy underfills can fail for a variety of reasons. One major cause is interfacial stress. If the coefficient of thermal expansion of the epoxy is significantly different from that of the substrate it is contacting, interfacial stresses can cause adhesion failure. Because epoxies contact a variety of different adherends in flip-chip devices, this can be a significant problem. Further, epoxies shrink as they cure, and this shrinkage further adds to stresses at adhesive interfaces. Other factors that can affect the interfacial stresses include cure temperature and crosslink density. However, when designing underfills in flip-chip devices, one needs to balance minimizing interfacial stresses with optimizing mechanical properties for the system. For example, a significant change in the crosslink density of the epoxy can affect mechanical properties.[8-11]

Another major cause of adhesion failure of underfill epoxy adhesives is moisture exposure, because epoxies readily absorb water. Moisture exposure changes the dielectric constant and glass transition temperature of the epoxy, which can alter the operation temperature for the flip-chip device.[4] Further, moisture-induced epoxy swelling occurs because the water can participate in the hydrogen bonding in the cured epoxy network, increasing interfacial stresses.[3,4,10,12]

There are three different proposed mechanisms of how moisture affects epoxy surfaces and interfaces. First, as mentioned above, water can plasticize the epoxy by participating in the hydrogen bonding in cured epoxy networks. This process can be reversed if the water is sufficiently removed. The two other mechanisms are not reversible. Due to water-induced swelling, crazing can occur in which small cracks develop on the epoxy surface or at the epoxy interface. Also, water can cause hydrolysis

to occur in which short chains of the polymer detach from the network, affecting adhesion.[3,4]

Because adhesion mechanisms largely depend on interfacial structures and interactions, SFG is an ideal technique to study the buried interfaces between epoxy underfill adhesives and substrates in flip-chip devices. Further, SFG can be used to examine the effect of moisture on surface and interfacial structures to monitor for evidence of water-induced interfacial structural changes.

In the presented work, SFG was used to study model compounds for epoxy resins used as underfills in flip-chip devices. First, surfaces of model bisphenol-type and aliphatic-type epoxy resin were studied. It was important to study epoxy surfaces to develop an understanding of epoxy structure that could later be compared to buried interfacial structures. Uncured samples were investigated on two different substrates to determine how substrate affects the deposition of epoxy underfills. As discussed above, underfill materials contact many different types of materials in flip-chip devices, and if the underfill material deposits differently on different substrates, adhesion could be affected.

In the next section, the surface structures of the model epoxies were studied after they were cured. Underfills are cured *in situ* in flip-chip devices, so changes in the surface structures of the underfill adhesives during the cure process could impact adhesion. For example, a specific orientation of surface dominating functional groups may be needed for an adhesion mechanism to occur. If the surface orientation of such groups changes during the cure process, that mechanism would not be able to occur.

Also, the effect of moisture exposure on cured epoxy surfaces was investigated with SFG. As described previously, moisture exposure leads to delamination of epoxies due to plasticization, crazing or hydrolysis. Any of these mechanisms could distort the epoxy surface structure, which could alter the ability of the epoxy to participate in adhesion mechanisms. Understanding how moisture exposure changes epoxy surface structure may provide further information about how moisture exposure diminishes epoxy adhesion.

Lastly, buried interfaces between deuterated polystyrene (*d*-PS) and cured model epoxies were investigated. The *d*-PS was chosen as a model polymer surface because it was fully deuterated, avoiding any spectral confusion with the epoxies. The effect of moisture exposure on buried interfacial structures was investigated. Further, lap shear adhesion testing was performed on analogous samples to connect adhesion strength to buried interfacial structure.

5.2 Experimental

5.2.1 Sample Preparation

Bisphenol A digylcidyl ether (BADGE), 1,4-butanediol diglycidyl ether (BDDGE), ethylene diamine (EDA) and polystyrene (PS, M_V = 280,000) were purchased from Sigma-Aldrich, Inc. Deuterated polystyrene (*d*-PS, M_V = 207,500) was obtained from Polymer Source, Inc. Deuterated polystyrene was used in SFG studies to avoid spectral confusion in the C-H stretching region. All chemicals were used as received.

Thin films of uncured BADGE and BDDGE on fused silica substrates for both SFG and contact angle goniometry analysis were prepared by diluting BADGE or BDDGE to 2 wt% solutions in chloroform (Sigma-Aldrich, Inc). The diluted solutions

were spin cast on fused silica windows ((1-in diameter, 1/8-in thickness, ESCO Products, Inc) using a spin coater from Specialty Coating Systems. The fused silica windows were cleaned by etching in warm chromic acid solution prior to use. Thin films of uncured BADGE and BDDGE on *d*-PS substrates for SFG and contact angle goniometry analysis were prepared by first spin coating a 1 wt% *d*-PS solution in toluene (Sigma-Aldrich, Inc) onto fused silica windows that had been cleaned by etching in warm chromic acid. The *d*-PS films were dried in an oven for approximately 18h at 120^{o}C and were cooled to room temperature. Then, the 2 wt% solutions of BADGE or BDDGE in chloroform were spin cast on top of the *d*-PS film.

Thin films of cured BADGE and BDDGE were prepared for SFG analysis by first mixing the BADGE or BDDGE and EDA curing agent in a 2:1 molar ratio. The epoxy and curing agents were diluted to 2 wt% solutions in chloroform. The dilute solutions were spin cast on fused silica windows that had been etched in warm chromic acid solution. The samples were then cured in an oven for approximately 18 h at 80^{o}C and were cooled to room temperature prior to analysis. For cured BADGE and BDDGE samples that were exposed to moisture, the cured samples were placed in deionized water for 18 h and dried prior to SFG analysis.

Buried interfaces of *d*-PS and cured BADGE or BDDGE for SFG analysis were prepared as follows. Thin films of *d*-PS were prepared by spin coating the 1 wt% solution of *d*-PS in toluene onto fused silica windows that had been etched in chromic acid prior to sample preparation. The *d*-PS films were dried in an oven at 120^{o}C for approximately 18 h and were allowed to cool. Then, BADGE or BDDGE were mixed with the EDA curing agent in a 2:1 molar ratio. Thick layers of the undiluted BADGE

and EDA or BDDGE and EDA mixtures were deposited onto the *d*-PS thin films. These buried interface samples were cured in an oven at 80°C for approximately 18 h and were cooled to room temperature prior to SFG analysis. When exposed to moisture, the buried interface samples were placed in deionized water for 18 h and were dried prior to SFG analysis.

Adhesion lap shear samples were prepared as follows. Glass microscope slides (Fisher Scientific, Inc) were cleaned by etching in warm chromic acid solution. A thin film of PS was deposited on half the glass slides by spin coating a 1 wt% PS solution in toluene on the slides. The slides were dried in an oven at 120°C for approximately 18 h and were allowed to cool to room temperature. Cured BADGE and BDDGE were prepared by mixing BADGE and BDDGE with the EDA curing agent in a 2:1 molar ratio. Thick films of the BADGE/EDA or BDDGE/EDA mixtures were applied to the *d*-PS films and a second glass slide was placed on top of the BADGE/EDA or BDDGE/EDA thick film such that there was a ½ cm bond length. The samples were cured in an oven at 80°C for approximately 18 h and were cooled to ambient temperature prior to analysis. In lap shear testing, adhesion failure only occurred at the PS/epoxy interface, not the glass/epoxy interface.

Structures of BADGE, BDDGE and EDA are seen in Figure 5.1

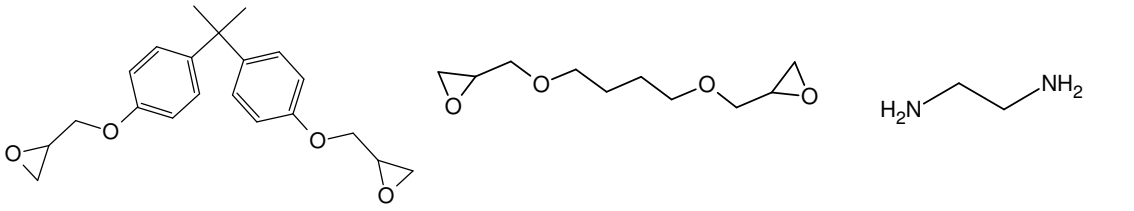

Figure 5.1 Chemical structures of materials used in this study.

5.2.2 SFG Experiments

The theory of SFG is well-developed and has been detailed in Chapter 1, Section 1.2.3.[13-17] The SFG system and experimental geometry used in this investigation were detailed in Chapter 1, Section 1.2.3.[18-24] Briefly, the visible and infrared (IR) input beams overlap spatially and temporally on the polymer surface, polymer/liquid interface or the polymer/cured epoxy interface with input angles of 60° and 54°, respectively and pulse energies of 200 μJ and 100 μJ, respectively. The beam diameters are approximately 500 μm. Prior results indicate that SFG signals are dominated by polymer surface or interface with negligible contribution from the polymer bulk or the polymer/substrate interface. In this investigation, SFG spectra were obtained in the ssp (s-polarized sum frequency output, s-polarized visible input and p-polarized IR input), ppp and sps polarization combinations.

5.2.3 Calculation of the Orientation of Surface Methyl and Methylene Groups

As discussed in Chapter 1, Section 1.2.2, SFG signal in the ssp polarization combination can be used to probe $\chi^{(2)}_{yyz}$, and $\chi^{(2)}_{yyz}$ can be written as the following:

$$\chi^{(2)}_{yyz} = \chi^{(2)}_{R,yyz} + \chi^{(2)}_{NR,yyz} = \sum_q \frac{A_{q,yyz}}{\omega_{IR} - \omega_q + i\Gamma_q} + \chi^{(2)}_{NR,yyz} \qquad (5.1)$$

where $\chi^{(2)}_{R,yyz}$ is the resonant second order nonlinear susceptibility component, $\chi^{(2)}_{NR,yyz}$ is the nonresonant second order nonlinear susceptibility component and A_q, ω_{IR}, ω_q and Γ_q are the strength of vibrational mode *q*, the infrared frequency, the frequency of vibrational mode *q*, and the damping constant of vibrational mode *q*, respectively.

The orientation of surface and/or interfacial functional groups can be deduced by fitting SFG spectra obtained using different polarization combinations of the input and

output beams because of the relationship between the second-order nonlinear susceptibility, $\chi^{(2)}$, and the second order nonlinear polarizaibility, or hyperpolarizaibility, $\alpha^{(2)}$. To avoid confusion with the orientation angle, α (2α is the angle between two methyl groups in the $(CH_3)_2C$ group in BADGE), we will use the term β for hyperpolarizabilities.

The methyl groups of BADGE can be considered part of an isopropyl group. Thus, the methyl orientation analysis performed in Chapter 4 is not appropriate for deducing the orientation of these connected methyl groups. Here, a procedure first performed by Kataoka and Cremer[25] was used in which the entire $(CH_3)_2C$ unit was treated as a single entity rather than two separate methyl groups. The two methyl groups were considered to have a fixed angle between them of $2\alpha = 112^0$ and it was assumed that the two methyl groups could rotate freely, leaving the $(CH_3)_2C$ group with quasi-C_{2v} symmetry. As such, some non-vanishing components of the second-order nonlinear susceptibility, $\chi^{(2)}$ are:

$$\begin{aligned}\chi_{yyz,sym} &= N(\beta_{aac}-\beta_{ccc})\{\ (\cos\alpha-\cos^3\alpha)\times(5+3\cos 2\psi)-2\cos\alpha\} \\ &(\cos\theta-\cos^3\theta)-2(\cos\alpha-\cos^3\alpha)\cos\theta \\ &+2N\beta_{aac}\cos\alpha\cos\theta\end{aligned} \tag{5.2}$$

$$\begin{aligned}\chi_{yzy,sym} &= N(\beta_{aac}-\beta_{ccc}) \\ &\{(\cos\alpha-\cos^3\alpha)\times(5+3\cos 2\psi)(\cos\theta-\cos^3\theta)+ \\ &2\cos\alpha\cos\theta \\ &(\cos^2\alpha+\cos^2\theta-2)\ \}\end{aligned} \tag{5.3}$$

$$\chi_{zzz,sym} = N(\beta_{aac} - \beta_{ccc}) \left(\cos\alpha - \cos^2\alpha\right)[\{2\cos^3\theta - 3(1+\cos 2\psi)(\cos\theta - \cos^3\theta)\} - 2\cos\alpha\cos^3\theta] + 2N\beta_{aac}\cos\alpha\cos\theta \quad (5.4)$$

$$\chi_{yyz,asym} = N\beta_{caa}[(\cos\alpha - \cos^3\alpha)\{-2\cos\theta + 3(\cos\theta - \cos^3\theta)(1+\cos 2\psi)\} - 2\cos^3\alpha(\cos\theta - \cos^3\theta)] \quad (5.5)$$

$$\chi_{yzy,asym} = N\beta_{caa}[3(\cos\alpha - \cos^3\alpha)\times(\cos\theta - \cos^3\theta)(1+\cos 2\psi) + 2\cos^3\alpha\cos^3\theta] \quad (5.6)$$

$$\chi_{zzz,asym} = 2N\beta_{caa}[(\cos\alpha - \cos^3\alpha)\{2\cos\theta - 3(\cos\theta - \cos^3\theta)(1+\cos 2\psi)\} + 2\cos^3\alpha(\cos\theta - \cos^3\theta)] \quad (5.7)$$

where β_{aac}, β_{caa}, β_{ccc} are elements of the hyperpolarizability tensor and N is the number density of the detected molecules. The angle α is a constant of 56°. By detecting and fitting SFG signal in different polarization combinations, ratios of the $\chi^{(2)}$ elements can be calculated and used to determine values of the tilt and twist angles, θ and ψ, respectively. In the above equations, we assumed that both θ and ψ have δ-angle distributions. Also in this study, the twist angle, ψ, was assumed to have free rotation and thus was averaged. For these studies, the value of β_{aac}/β_{ccc} used was 3.4 and the ratio of $\frac{\chi_{yyz,sym}}{\chi_{yzy,asym}}$ for the methyl groups was used.[25]

To calculate the orientation of BDDGE methylene groups, a similar analysis was performed for methylene groups. The non-vanishing components of the second-order nonlinear susceptibility can be written as the following:[22,26,27,28]

$$\chi_{yyz,sym} = \frac{1}{4}N\left(\beta_{aac} + \beta_{bbc} + 2\beta_{ccc}\right) + 2\beta_{ccc}\left\langle\cos\theta\right\rangle + \frac{1}{4}N\left(\beta_{aac} + \beta_{bbc} - 2\beta_{ccc}\right)\left\langle\cos^3\theta\right\rangle \quad (5.8)$$

$$\chi_{yzy,sym} = \frac{-1}{4}N\left(\beta_{aac} + \beta_{bbc} - 2\beta_{ccc}\right)\left(\left\langle\cos\theta\right\rangle - \left\langle\cos^3\theta\right\rangle \approx 0\right. \quad (5.9)$$

$$\chi_{zzz,sym} = \frac{1}{2}N\left(\beta_{aac} + \beta_{bbc}\right)\left\langle\cos\theta\right\rangle - \frac{1}{2}N\left(\beta_{aac} + \beta_{bbc} - 2\beta_{ccc}\right)\left\langle\cos^3\theta\right\rangle \quad (5.10)$$

$$\chi_{yyz,asym} = \frac{-1}{2}N\beta_{caa}\left[\left\langle\cos\theta\right\rangle - \left\langle\cos^3\theta\right\rangle\right] \quad (5.11)$$

$$\chi_{yzy,asym} = \frac{-1}{2}N\beta_{caa}\left\langle\cos^3\theta\right\rangle \quad (5.12)$$

$$\chi_{zzz,asym} = N\beta_{caa}\left(\left\langle\cos\theta\right\rangle - \left\langle\cos^3\theta\right\rangle\right) \quad (5.13)$$

where β_{aac}, β_{bbc}, β_{ccc}, and β_{caa} are elements of the hyperpolarizability tensor and N is the number density of the detected molecules. Here, $\left\langle\cos\theta\right\rangle$ and $\left\langle\cos^3\theta\right\rangle$ denote averages of methylene group tilt angles such that

$$\left\langle\cos^n\theta\right\rangle = \int_0^\pi \cos^n\theta f(\theta)\sin\theta d\theta \quad (5.14)$$

and $f(\theta)$ is a Gaussian distribution function describing the surface methyl angle distribution. The Gaussian distribution can be set from a δ-distribution to a wider Gaussian distribution depending on the surface being studied. In the current study, as the study above of BADGE methyl groups, a δ-distribution was assumed.[22, 29]

Like the methyl group orientation analysis described above, the orientation of methylene groups can be determined by fitting SFG spectra obtained using different polarization combinations of the input and output beams to determine elements of the second-order nonlinear susceptibility. Ratios of the $\chi^{(2)}$ elements can then be used to

determine orientation angle, θ. Here, the ratio $\frac{\chi_{yyz,sym}}{\chi_{yyz,asym}}$ was used with a β_{ccc}/β_{aac} value of 0.14.[28]

The orientation of the phenyl groups of BADGE can also be determined using similar analysis. The phenyl groups of BADGE are para-substituted, and therefore can be thought to have local C_{2v} symmetry. If it is assumed that the BADGE surface is azimuthally isotropic, two angles must be considered: the tilt angle (θ) and the twist angle (ψ). Like the methyl group analysis, we assumed that the twist angle ψ, has free rotation and therefore was averaged.

The components of the second order nonlinear susceptibility, $\chi^{(2)}$ can be written as the following for the A1 and B1 irreducible representations: [26,31,32]

$$\chi_{yyz,A1} = \frac{N_s}{8}[\beta_{aac,A1}\cos\theta\left(3+\cos 2\theta-2\sin^2\theta\cos 2\psi\right) + \beta_{bbc,A1}\cos\theta\left(3+\cos 2\theta+2\sin^2\theta\cos 2\psi\right)+\beta_{ccc,A1}\left(\cos\theta-\cos 3\theta\right)] \quad (5.15)$$

$$\chi_{yzy,A1} = \frac{N_s}{16}[-\beta_{aac,A1}\left(\cos\theta-\cos 3\theta\right)\left(1+\cos 2\psi\right)-\beta_{bbc,A1}\left(\cos\theta-\cos 3\theta\right)\left(1-\cos 2\psi\right) + 2\beta_{ccc,A1}\left(\cos\theta-\cos 3\theta\right)] \quad (5.16)$$

$$\chi_{yyz,B1} = -\frac{N_s}{8}\beta_{aca,B1}\left(\cos\theta-\cos 3\theta\right)\left(1+\cos 2\psi\right) \quad (5.17)$$

$$\chi_{yzy,B1} = \frac{N_s}{8}\beta_{aca,B1}\left[4\cos\theta-\left(\cos\theta-\cos 3\theta\right)\left(1+\cos 2\psi\right)\right] \quad (5.18)$$

The A1 irreducible representation consists of the ν_2 and ν_{20a} phenyl modes while the B1 irreducible representation consists of the ν_{7b} and the ν_{20b} phenyl modes. Using the bond additivity approach, ratios of the non-zero β terms can be determined to be the following for para-substituted phenyl rings: [26,27,32,33]

$$\frac{\beta_{ccc,\nu 2}}{\beta_{aac,\nu 2}} = 0.69\,,\ \frac{\beta_{bbc,\nu 2}}{\beta_{aac,\nu 2}} = 0.04\,,\ \frac{\beta_{aca,\nu 7b}}{\beta_{aac,\nu 2}} = 0.47$$

The only mode observed in SFG spectra of BADGE was the ν_2 mode at 3060 cm^{-1}. For this mode, the appropriate χ ratio was calculated to be the following:

$$\frac{\chi_{yyz,\nu 2}}{\chi_{yzy,\nu 2}} = \frac{25.4\cos\theta - \cos 3\theta - 11.3\cos\theta\sin^2\theta\cos 2\phi}{(\cos\theta - \cos 3\theta)(1 - 2.82\cos 2\phi)}\,. \qquad (5.19)$$

5.2.4 Contact Angle Goniometry Experiments

Static water contact angle goniometry measurements were performed using a CAM 100 Optical Contact Meter (KSV Instruments) contact angle goniometer. Samples of uncured BADGE and uncured BDDGE on fused silica and *d*-PS substrates were studied. Eight measurements were performed for each sample.

5.2.5 Lap Shear Adhesion Testing Experiments

Lap shear adhesion tests were performed using an Instron 5544 Mechanical Testing System. Lap shear tests were performed using ASTM International Standard D3163_01 on cured BADGE before and after moisture exposure and cured BDDGE before moisture exposure. Ten samples of BADGE and BDDGE were tested for each set of adhesion tests.

5.3 Results and Discussion

5.3.1 SFG and Contact Angle Goniometry Studies of Uncured BADGE and BDDGE on Fused Silica and *d*-PS Substrates

As discussed in Section 5.1, epoxies used as underfills in flip-chip devices are deposited into the devices prior to cure, and come into contact with a variety of substrates in the devices. If the epoxies used as underfills deposit differently on different substrates, their surface structures may be altered, affecting how the epoxies adhere to other

materials in flip-chip devices. In this study, thin films of uncured BADGE and BDDGE were deposited on fused silica and *d*-PS substrates. As stated in Section 5.1, *d*-PS was used as a model polymer for polymeric passivation layers used in flip-chip devices.

Figures 5.2 and 5.3 show fitted SFG spectra of uncured BADGE on fused silica and *d*-PS, respectively. Further, Tables 5.1a, 5.1b, 5.2a, and 5.2b show the fitting parameters used. The SFG ssp spectrum of uncured BADGE on fused silica was dominated by symmetric and asymmetric methyl stretches at 2875 cm^{-1} and 2970 cm^{-1}, respectively. There were also symmetric and asymmetric methylene stretches at 2855 cm^{-1} and 2912 cm^{-1}, respectively, a Fermi resonance (FR) at 2940 cm^{-1}, and phenyl C-H stretching at 3060 cm^{-1}. For both cases, the sps spectra were dominated by the asymmetric methyl stretch at 2965 cm^{-1} and weak phenyl signal at 3055 cm^{-1}. On *d*-PS, the uncured BADGE signal was dominated by symmetric methyl signal at 2875 cm^{-1}. Other peaks were the symmetric and asymmetric methylene stretches at 2855 cm^{-1} and 2920 cm^{-1}, respectively, a Fermi Resonance at 2938 cm^{-1} and a phenyl stretch at 3060 cm^{-1}. Also interestingly, signal at 2995 cm^{-1} was observed when the uncured BADGE was deposited on *d*-PS, and attributed to the symmetric stretch of the epoxy ring. This showed that on the surface the epoxy ring stood up when the BADGE was deposited on *d*-PS while it laid down(or was not present on the surface) when deposited on fused silica.

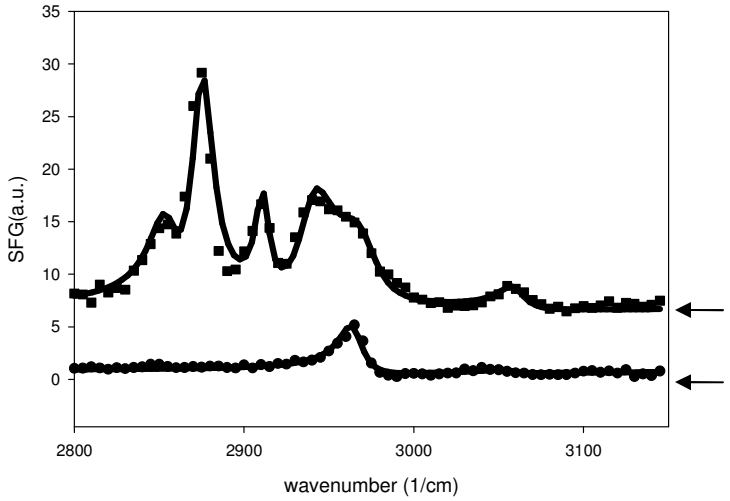

Figure 5.2 SFG spectra of uncured BADGE on fused silica in ssp (squares) and sps (circles). Solid lines are spectral fits. Baselines of spectra are indicated by arrows on right.

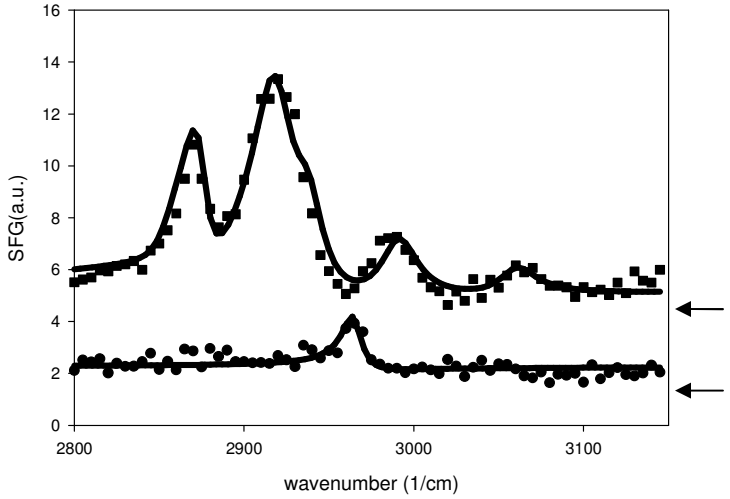

Figure 5.3 SFG spectra of uncured BADGE on *d*-PS in ssp (squares) and sps (circles). Solid lines are spectral fits. Baselines of spectra are indicated by arrows on right.

Frequency	2855	2875	2912	2940	2970	3060
Strength	19.0	33.8	-20.2	46.0	-45.0	13.6
Width	10.2	7.86	5.05	12.0	14.4	9.6
Assignment	CH_2 sym	CH_3 sym	CH_2 asym	FR	CH_3 asym	Phenyl

Table 5.1a Fitting parameters for ssp spectrum of uncured BADGE on fused silica.

Frequency	2965	3055
Strength	17.2	4.27
Width	8.65	9.76
Assignment	CH_3 as	Phenyl

Table 5.1b Fitting parameters used for sps spectrum of uncured BADGE on fused silica.

Frequency	2855	2875	2920	2938	2994	3060
Strength	-8.00	11.7	32.9	13.0	16.5	11.5
Width	15.0	8.33	14.7	11.5	13.2	13.1
Assignment	CH_2 sym	CH_3 sym	CH_2 asym	FR	Epoxy sym	Phenyl

Table 5.2a Fitting parameters used for ssp spectrum of uncured BADGE on *d*-PS.

Frequency	2965
Strength	9.49
Width	7.00
Assignment	CH_3 as

Table 5.2b Fitting parameters used for sps spectrum of uncured BADGE on *d*-PS.

The spectra were fit according to Equation 5.1 and the ratio of $\frac{\chi_{yyz,sym}}{\chi_{yzy,asym}}$ was calculated for surface methyl groups of uncured BADGE on fused silica and *d*-PS. Orientation analysis of the surface methyl groups was performed according to the procedure described in section 5.2.3. Assuming a δ-distribution of angles, it was found that on fused silica, the surface methyl groups of uncured BADGE exhibited a 15^o angle with respect to the surface normal while on *d*-PS, the surface methyl groups of uncured BADGE exhibited a 69^o angle with respect to the surface normal. Therefore, the orientation of the uncured BADGE methyl groups changed significantly with substrate. On the hydrophilic fused silica surface, the methyl groups stood up while on the hydrophobic *d*-PS surface, the methyl groups laid down more. Further, the epoxy groups stood up on the *d*-PS surface while they did not on the fused silica surface.

The ssp SFG spectra of uncured BDDGE on fused silica and of uncured BDDGE on *d*-PS are shown in Figures 5.4 and 5.5, respectively. Also, Table 5.3 and 5.4 show the spectral fitting parameters. When deposited on fused silica, the uncured BDDGE surface ssp spectrum was dominated by peaks at 2855 cm^{-1} and 2915 cm^{-1}, corresponding to the symmetric and asymmetric methylene stretches, respectively. Further, an unassigned peak was observed at 2830 cm^{-1}, a Fermi Resonance was observed at 2935 cm^{-1}, and the symmetric epoxy stretch was observed at 3000 cm^{-1}. This indicated that in addition to the methylene groups, the epoxy groups were also present and ordered at the surface. When deposited on *d*-PS, the ssp spectrum of BDDGE was very similar. The spectrum was dominated by the symmetric and asymmetric methylene stretches at 2855 cm^{-1} and 2915 cm^{-1}, respectively. There was also the unassigned signal at 2830 cm^{-1}, Fermi resonance signal at 2935 cm^{-1} and symmetric epoxy stretching at 3000 cm^{-1}. Therefore, from observing the SFG spectra, it appeared that the BDDGE surface was largely unaffected by substrate.

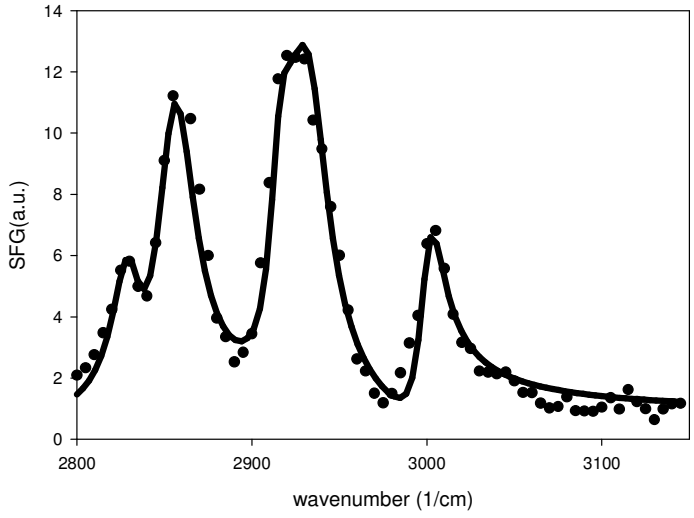

Figure 5.4 SFG spectrum of uncured BDDGE on fused silica in ssp (circles). Solid line is spectral fit.

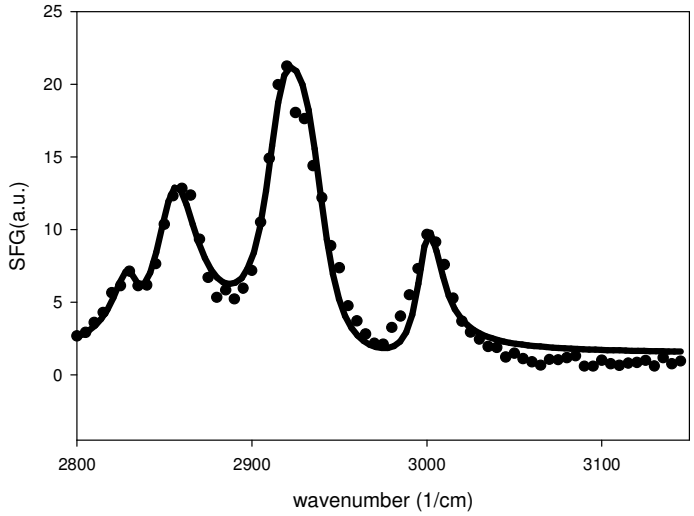

Figure 5.5 SFG spectrum of uncured BDDGE on *d*-PS in ssp (circles). Solid line is spectral fit.

Frequency	2830	2855	2915	2935	3000
Strength	13.8	40.6	-39.1	60.7	15.5
Width	10.0	13.4	7.92	15.0	8.44
Assignment	--	CH_2 sym	CH_2 asym	FR	Epoxy sym

Table 5.3 Fitting parameters used for ssp spectrum of uncured BDDGE on fused silica.

Frequency	2830	2855	2915	2935	3000
Strength	10.2	49.2	-76.5	71.2	22.5
Width	8.65	15.0	13.3	15.0	8.54
Assignment	--	CH_2 sym	CH_2 asym	FR	Epoxy sym

Table 5.4 Fitting parameters used for ssp spectrum of uncured BDDGE on *d*-PS.

The orientation of the surface uncured BDDGE methylene groups on fused silica and *d*-PS was deduced using the fitting parameters and the procedure outlined in section 5.2.3, using the ratio of $\frac{\chi_{yyz,sym}}{\chi_{yyz,asym}}$. On fused silica, assuming a δ-distribution of methylene orientation angles, the surface BDDGE methylene groups was found to have an orientation angle of 29° with respect to the surface normal. Likewise, on *d*-PS, the surface uncured BDDGE methylene groups were also determined to have an orientation

angle of 29^{o} with respect to the surface normal. That is, the orientation of the uncured BDDGE surface methylene groups was unaffected by substrate.

The BADGE surface structures were significantly altered by deposition on the two different substrates, while the BDDGE surface structures were largely unaffected by substrate. Specifically, the BADGE methyl orientation and the BADGE epoxy orientation were different on the different substrates. The BDDGE surface methylene orientation was largely unchanged by substrate, and the epoxy groups were present at the BDDGE surface on both substrates. Perhaps specific interactions between the aromatic rings in BADGE and the surface aromatic groups of *d*-PS caused the BADGE to orient differently when deposited on that substrate, while such interactions did not occur between BDDGE and *d*-PS because there were no aromatic groups in BDDGE to interact with the *d*-PS.

The static water contact angle goniometry measurements for uncured BADGE and BDDGE on fused silica and *d*-PS substrates are reported in Table 5.5. The BADGE water contact angle was different on the fused silica and *d*-PS substrates. This agreed with SFG results showing that interactions between BADGE and *d*-PS may have caused the BADGE to deposit differently on that substrate. Conversely, the water contact angle for BDDGE was not significantly different on the fused silica and *d*-PS substrates, showing that the surface was not altered much by substrate. This was most likely due to the significant surface restructuring observed for uncured BADGE and the lack of significant surface restructuring observed for BDDGE.

	BADGE	BDDGE
Water contact angle with fused silica substrate	$47.8^{o} \pm 11.5$	$30.3^{o} \pm 1.5$
Water contact angle with *d*-PS substrate	$79.0^{o} \pm 5.6$	$21.3^{o} \pm 7.7$

Table 5.5 Static water contact angle goniometry results for uncured BADGE and BDDGE deposited on fused silica and *d*-PS substrates.

To summarize, SFG and contact angle goniometry studies of uncured BADGE and BDDGE on fused silica and *d*-PS substrates showed that the bisphenol-type epoxy deposited differently on the fused silica and *d*-PS substrates. The BDDGE surface structures were not significantly affected by substrate. BADGE molecules contain aromatic groups, which may interact with PS surface phenyl groups more favorably compared to the fused silica surface; therefore BADGE exhibited different surface structures deposited on *d*-PS and fused silica. Specifically, the BADGE surface methyl orientation was affected by substrate. Also, the BADGE epoxy groups stood up when deposited on *d*-PS, while these groups either laid down or were not present on the surface when BADGE was deposited on fused silica. Conversely, BDDGE molecules do not contain aromatic groups and therefore may have similar interactions with *d*-PS and fused silica, so the surface structures were largely unaffected by substrate. Often specific epoxy underfill surface structures are required for adhesion mechanisms to occur, and if the epoxy surface structures are changed because of the substrate, adhesion can be diminished. Therefore, the effect of the various substrates encountered by underfills in flip-chip devices needs to be considered when designing underfill materials.

5.3.2 SFG Studies of Cured Epoxy Surfaces and the Effect of Moisture Exposure on Cured Epoxy Surface Structures

As described in Section 5.1, epoxies used as underfills are cured *in situ* in the flip-chip device. Thus, any surface structural changes that occur during the cure process can impact the adhesion of underfills to the various substrates in flip-chip devices. For example, if the surface structure of an uncured epoxy allows a specific adhesion mechanism to occur, any change in that surface structure after the cure process would diminish the ability of the epoxy to participate in that mechanism. Here, SFG was used to probe the surface structures of BADGE and BDDGE surfaces after they are cured with EDA. Further, the effect of moisture exposure on the surface structures of the two epoxies was investigated. Moisture exposure is known to cause delamination of epoxies. Studying how surface structures of cured epoxies are affected by moisture exposure can help further explain how moisture exposure affects epoxy adhesion.

Figure 5.6 shows SFG spectra of BADGE after it was cured. Tables 5.6a and 5.6b show the fitting parameters used for the ssp and sps SFG spectra. From observing the spectra, it is apparent they were different than those of the uncured BADGE. The ssp spectrum has peaks at 2855 cm^{-1} and 2915 cm^{-1}, corresponding to the symmetric and asymmetric methylene stretches, respectively. Further, there are peaks at 2870 cm^{-1} and 2970 cm^{-1} from the symmetric and asymmetric methyl stretches. There is also Fermi resonance signal at 2940 cm^{-1}, phenyl stretching signal at 3062 cm^{-1}, and symmetric epoxy stretching at 3000 cm^{-1}. The signal at 3000 cm^{-1} indicated that the sample was not completely cured. However, the signal at 3000 cm^{-1} was quite weak and indicated that only a very small amount of uncured epoxy remained. In the sps polarization combination, signal was observed at 2965 cm^{-1}, corresponding to the asymmetric methyl stretch and at 3055 cm^{-1}, corresponding to a phenyl stretch.

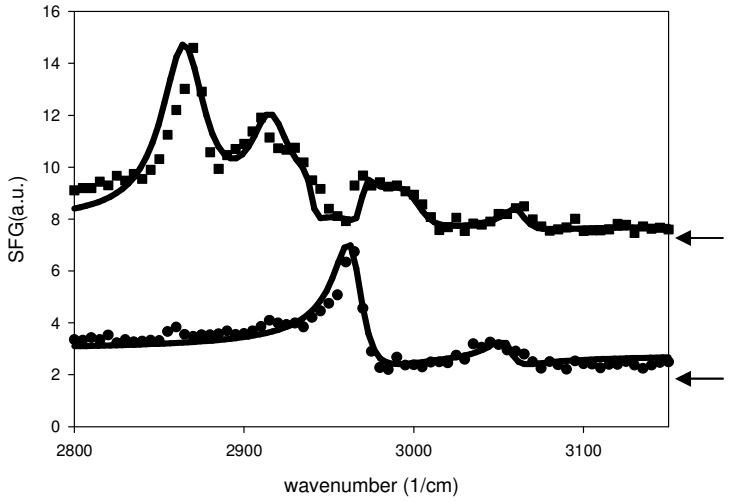

Figure 5.6 SFG spectra of cured BADGE in ssp (squares) and sps (circles). Solid lines are spectral fits. Baselines of spectra are indicated by arrows on right.

Frequency	2855	2870	2915	2940	2970	3000	3062
Strength	1.78	41.5	-34.6	3.11	-3.27	11.9	5.78
Width	15.0	15.0	14.5	4.52	4.24	13.7	7.64
Assignment	CH_2 sym	CH_3 sym	CH_2 asym	FR	CH_3 asym	Epoxy sym	Phenyl

Table 5.6a Fitting parameters used for ssp spectrum of cured BADGE.

Frequency	2965	3055
Strength	18.8	4.86
Width	10.0	6.66
Assignment	CH_3 as	Phenyl

Table 5.6b Fitting parameters used for sps spectrum of cured BADGE.

The SFG spectra were fit according to equation 5.1, and orientation analysis of the surface methyl groups was performed using the procedure described in section 5.2.3. The ratio of $\frac{\chi_{yyz,sym}}{\chi_{yzy,asym}}$ was calculated and the angle of the methyl groups with respect to the surface normal was calculated, assuming a δ-distribution of methyl angles. It was calculated that the cured BADGE surface methyl groups were at a 31^o angle with respect

to the surface normal. Interestingly, this orientation was different than that of the uncured BADGE methyl groups on either fused silica or *d*-PS, indicating that the surface methyl groups reoriented during the cure process.

Figure 5.7 shows SFG spectra of cured BADGE after moisture exposure, and Tables 5.7a and 5.7b show the fitting parameters used for the ssp and sps spectra. After moisture exposure, the ssp spectrum contained peaks at 2869 cm^{-1} and 2965 cm^{-1}, corresponding to the symmetric and asymmetric methyl stretches, respectively. Further, peaks were observed at 2912 cm^{-1}, from the asymmetric methylene stretch, 2940 cm^{-1} from a Fermi resonance, 3000 cm^{-1} from the epoxy symmetric stretch, and 3060 cm^{-1} from phenyl stretching. Interestingly, after moisture exposure, the phenyl signal was much stronger than it was before moisture exposure. Therefore, moisture exposure caused the phenyl groups to reorient such that they were standing up more. A similar phenomenon was observed using SFG for a phenolic resin. In this study, it was believed that water formed hydrogen bonds with the oxygen atoms near the aromatic rings, dragging the aromatic rings toward the surface normal.[30] This surface restructuring could diminish adhesion if the structure after moisture exposure was not favorable for adhesion mechanisms. The sps spectrum was dominated by signal at 2965 cm^{-1} from the methyl asymmetric stretch and weaker signal at 3055 cm^{-1} from a phenyl stretch.

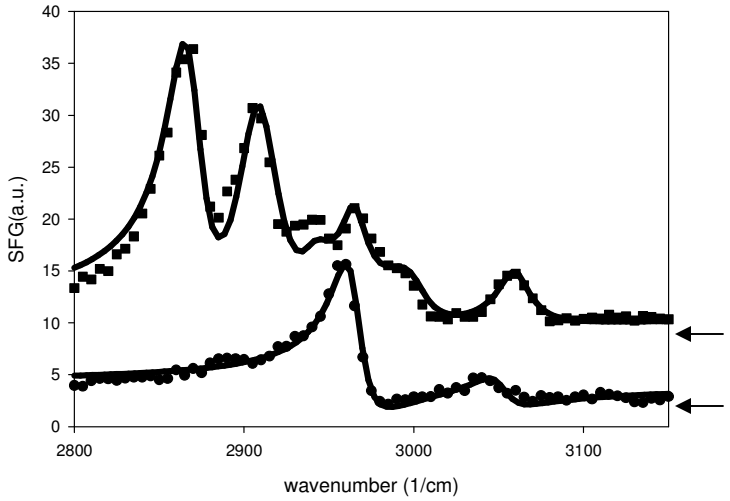

Figure 5.7 SFG spectra of cured BADGE after moisture exposure in ssp (squares) and sps (circles). Solid lines are spectral fits. Baselines of spectra are indicated by arrows on right.

Frequency	2869	2912	2940	2965	3000	3060
Strength	46.7	61.8	16.0	-39.3	26.4	24.3
Width	12.4	15.0	12.0	9.28	15.0	11.9
Assignment	CH_3 sym	CH_2 asym	FR	CH_3 asym	Epoxy sym	Phenyl

Table 5.7a Fitting parameters used for ssp spectrum of cured BADGE after moisture exposure.

Frequency	2965	3055
Strength	30.6	10.8
Width	10.5	12.0
Assignment	CH_3 as	Phenyl

Table 5.7b Fitting parameters used for sps spectrum of cured BADGE after moisture exposure.

The spectra were fit according to equation 5.1, and the ratio of $\frac{\chi_{yyz,sym}}{\chi_{yzy,asym}}$ for the surface methyl groups was calculated after moisture exposure. When orientation analysis was performed, assuming a δ-distribution of surface methyl orientation, the surface methyl groups were found to be at a 47^o angle with respect to the surface normal. This

showed that the surface methyl groups laid down more after being exposed to moisture. This change in surface orientation could affect adhesion properties after moisture exposure. The ratio of $\frac{\chi_{yyz,\nu_2}}{\chi_{yzy,\nu_2}}$ for the phenyl ν_2 stretches were also calculated using the fitting parameters from the cured BADGE and from the cured BADGE after moisture exposure. The ratio for cured BADGE before moisture exposure was 1.04 while the ratio for cured BADGE after moisture exposure was 2.27. We attempted to perform the phenyl orientation analysis described in section 5.2.3. However, the ratios from the experimental results were out of the range of the calculated orientation. This indicates that twist angle is not random and cannot be averaged. The one measurement obtained with SFG is not enough for the accurate determination of the twist angle and tile angle at the same time, and thus we cannot provide a detailed, quantitative description of the phenyl group orientation here.

The SFG spectrum of cured BDDGE is shown in Figure 5.8, and its fitting parameters are shown in Table 5.8. The cured BDDGE ssp spectrum was dominated by symmetric and asymmetric methylene stretching at 2855 cm^{-1} and 2915 cm^{-1}. There was also unassigned signal at 2830 cm^{-1} and Fermi resonance signal at 2935 cm^{-1}. Of note, the peak at 3000 cm^{-1} was absent after cure, indicating that the BDDGE surface was largely cured.

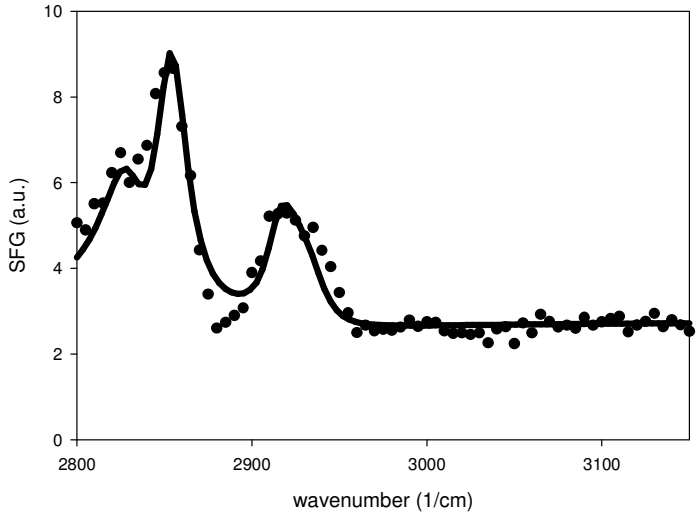

Figure 5.8 SFG spectrum of cured BDDGE in ssp (circles). Solid line is spectral fit.

Frequency	2830	2855	2915	2935
Strength	16.92	24.51	-22.93	20.42
Width	15	11.04	10.62	15
Assignment	--	CH_2 sym	CH_2 asym	FR

Table 5.8 Fitting parameters used for ssp spectrum of cured BDDGE.

The spectra were fit according to equation 5.1, and orientation analysis was performed by calculating the ratio of $\frac{\chi_{yyz,sym}}{\chi_{yyz,asym}}$ for the surface methylene groups and using this ratio to determine the angle of the methylene groups with respect to the surface normal, assuming a δ-distribution. Here, the orientation angle of the methylene groups was calculated to be 28.^{o}. This was nearly identical to the methylene orientation calculated for uncured BDDGE, showing that the BDDGE methylene structure did not change significantly after the system was cured.

Lastly, the cured BDDGE thin films were exposed to moisture, and this spectrum and its fit is shown in Figure 5.9. The fit parameters are seen in Table 5.9. After moisture exposure, the cured BDDGE surface was still dominated by symmetric and asymmetric

methyl stretches at 2855 cm^{-1} and 2915 cm^{-1}, respectively, as well as an unassigned peak at 2830 cm^{-1}.

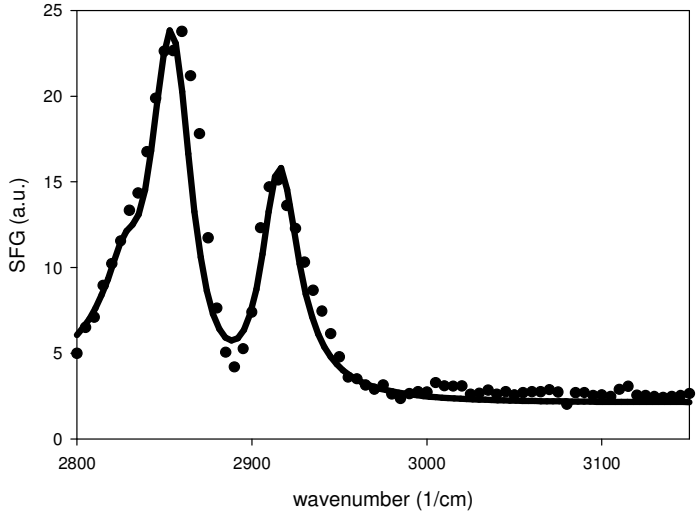

Figure 5.9 SFG spectrum of cured BDDGE after moisture exposure in ssp (circles). Solid line is spectral fit.

Frequency	2830	2855	2915
Strength	7.83	73.3	-54.6
Width	10.8	15.0	13.0
Assignment	--	CH_2 sym	CH_2 asym

Table 5.9 Fitting parameters used for ssp spectrum of cured BDDGE after moisture exposure.

Spectral fitting and orientation analysis of the BDDGE methylene groups revealed that after moisture exposure, the BDDGE methylene groups exhibited a 28^o angle with respect to the surface normal. This orientation angle is nearly the same as the cured and uncured BDDGE. Therefore, BDDGE methylene orientation was largely unaffected by curing and by moisture exposure.

The studies of cured BADGE and BDDGE showed that the surface structures of epoxies can change with cure. The orientation of the BADGE surface methyl groups

changed with cure. The spectra of the cured BDDGE surface showed evidence of the curing reaction occurring at the surface, because the epoxy ring signal disappeared. However, the orientation of the BDDGE methylene groups did not change significantly with cure. These studies demonstrated that SFG can be used to monitor surface cure reactions and cure-induced structural changes that may affect the adhesion of underfills in flip-chip devices.

Further, these studies demonstrated the effect of moisture exposure on cured epoxy surfaces. Understanding how moisture affects epoxy surfaces is of great importance because moisture exposure can cause adhesion failure. While the BDDGE surface structure did not significantly change after moisture exposure, the BADGE surface did restructure, in that the methyl orientation changed and the phenyl groups reordered towards the surface normal. The restructuring of the BADGE surface with moisture exposure could affect how it could participate in adhesion mechanisms and needs to be considered when formulating underfills.

5.3.3 SFG and Lap Shear Adhesion Testing Studies of the Buried Interfaces Between *d*-PS and Cured Epoxies and the Effect of Moisture Exposure on the Buried Interfaces Between *d*-PS and Cured Epoxies

While the studies in Sections 5.3.1 and 5.3.2 were important in developing a fundamental understanding of the surface structures of BADGE and BDDGE, they were not sufficient to understand the adhesion of epoxies used as underfills in flip-chip devices. Interfacial mechanisms between adhesive and adherend largely define adhesion, so the buried interfacial structures between the two materials need to be understood. These

buried interfacial structures can be different from the adhesive surface structures due to interactions with the adherend.

In this section, studies of the buried interfacial structures between *d*-PS thin films and thick cured BADGE or BDDGE films were investigated with SFG. Before that research, SFG studies were conducted of the buried interfaces between *d*-PS thin films and thick uncured BADGE or BDDGE films. However, no SFG signal was observed for any of these buried interfaces (not shown). It was concluded that the buried interfaces between *d*-PS and uncured BADGE and BDDGE were disordered. That is, the uncured BADGE and BDDGE adopted random interfacial structures.

The effect of moisture on the *d*-PS/cured BADGE and *d*-PS/cured BDDGE interfaces was also investigated. SFG spectra of the buried interfaces were obtained after moisture exposure to determine if and how moisture affects any ordered buried interfacial structures at the *d*-PS/cured epoxy interface. Any moisture-induced changes in buried interfacial structure may help to further explain why moisture causes epoxy underfill delaminanation in flip-chip devices.

Lastly, lap shear adhesion testing was performed on PS/cured epoxy interfaces to determine how moisture exposure affected the adhesion strength between PS and the epoxies. Adhesion strength, as measured by the adhesion strength in MPa for lap-shear adhesion, was correlated to buried interfacial structure of the epoxies.

Figure 5.10 shows SFG spectra in the ssp polarization combination of the *d*-PS/cured BADGE buried interface before and after moisture exposure. In Figure 5.10, in the spectrum with closed circles, weak signal between 2910 and 2940 cm^{-1} can be attributed to methylene signal from the *d*-PS/cured BADGE buried interface. Unlike the

uncured BADGE, the cured BADGE appeared to have some orientational order at the buried *d*-PS interface. However, the signal decreased after the *d*-PS/cured BADGE buried interface was exposed to moisture. Due to moisture absorption, the buried interface became deformed and the interfacial orientational order of the BADGE was lost. This was most likely due to moisture-induced swelling of the epoxy.

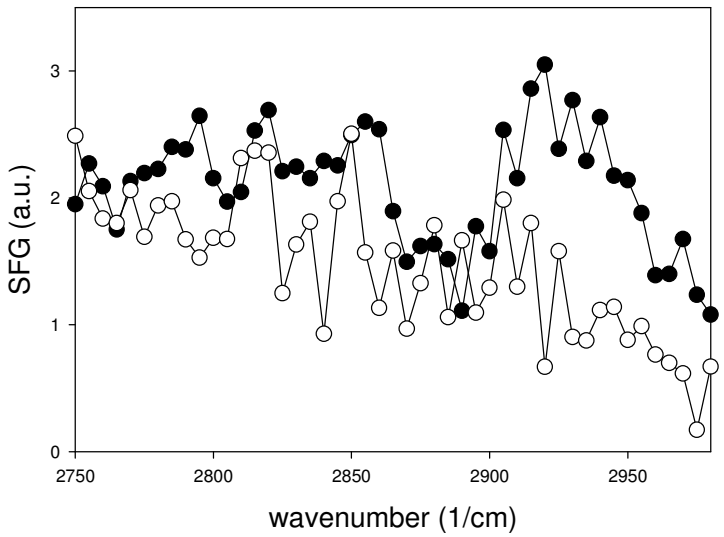

Figure 5.10 SFG spectra (ssp) of *d*-PS/cured BADGE buried interface before moisture exposure (closed circles) and after moisture exposure (open circles).

Figure 5.11 shows ssp SFG spectra of the *d*-PS/cured BDDGE buried interface before and after moisture exposure. Prior to moisture exposure, signal at 2850 cm^{-1} was attributed to the methylene symmetric stretch of the BDDGE at the buried interface. While the uncured BDDGE did not order at the *d*-PS buried interface, after the cure process, the cured BDDGE did exhibit some interfacial ordering, showing interfacial structural changes during the cure process. This interfacial ordering may contribute to adhesion. Further, after the *d*-PS/cured BDDGE buried interface was exposed to moisture, the symmetric methylene signal decreased significantly. Like the *d*-PS/cured

BADGE interface, moisture exposure caused the buried interface to become disordered, most likely because swelling deformed the epoxy.

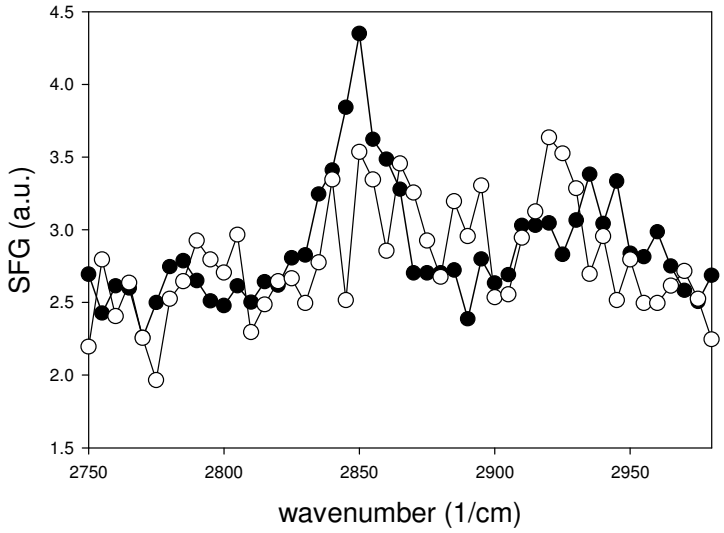

Figure 5.11. SFG spectra (ssp) of *d*-PS/cured BDDGE buried interface before moisture exposure (black circles) and after moisture exposure (open circles).

The lap-shear adhesion testing results are shown in Table 5.10. After cure, both the BADGE and BDDGE showed adhesion to PS, as measured by the adhesion strength in MPa for lap-shear adhesion. The adhesion correlated to the more ordered buried interfacial structures. It is possible that the buried interfacial orientational ordering of the epoxies promoted stronger adhesion. After moisture exposure, the adhesion decreased for both epoxies. The BDDGE adhesion strength decreased to negligible amounts while the BADGE adhesion strength decreased significantly as well. This correlated to the loss of buried interfacial ordering of the epoxies seen after moisture exposure.

	BADGE /PS Interfaces	BDDGE /PS Interfaces
Cured	4.47 MPa ± 0.45	3.08 MPa ± 0.57
Cured after water exposure	3.45 MPa ± 0.53	n/a

Table 5.10 Lap shear adhesion testing results from the *d*-PS/BADGE and *d*-PS/BDDGE interfaces. Note n/a refers to an interface with negligible adhesion.

To summarize, buried interfaces between *d*-PS and the epoxies were probed with SFG. It was found that the uncured epoxies formed disordered interfaces with *d*-PS and therefore did not yield SFG signal. However, SFG spectra of the cured samples including both BADGE and BDDGE showed evidence of the epoxy methylene groups ordering at the buried interface. The formation of ordered buried interfaces was correlated to improved adhesion via lap shear tests. Additionally, moisture exposure was shown to decrease the order of the buried *d*-PS/cured epoxy interfaces, and this was correlated to decreased lap shear adhesion.

5.4 Conclusions

Developing an understanding of the adhesion of underfills in flip-chip devices is critical for designing improved underfill formulations to maximize flip-chip device performance. In these studies, SFG was used to study the surface structures of uncured and cured epoxies used as underfills, as well as the buried interfaces between a model polymer and the underfill epoxies. It was found that an uncured bisphenol-type epoxy deposited differently on fused silica and polymeric substrates while an aliphatic-type epoxy did not. When epoxy-based underfills are deposited into flip-chip devices prior to cure, the underfill material comes into contact with a variety of substrates, and needs to be accounted for when designing underfill formulations.

Further, it was shown that the epoxy surface structures changed after they were cured. This has important implications for underfill design. Underfills are cured *in situ* in flip-chip devices. If specific surface structures are needed for the epoxy underfill to participate in specific adhesion mechanisms, any change in epoxy underfill surface structure during cure would affect adhesion, and needs to be understood. The effect of moisture exposure on epoxy surfaces was also investigated, and it was found that moisture caused surface reorientation of bisphenol-type epoxies but not aliphatic-type epoxies. Because moisture is known to cause delamination of epoxy underfills in flip-chip devices, it was important to determine how moisture exposure affected epoxy surface structure.

Lastly, the studies were expanded to buried interfaces between *d*-PS and the epoxies both before and after moisture exposure to better understand the structures at adhesive interfaces. It was shown that buried interfaces between *d*-PS and uncured epoxies were disordered. However, the buried interfaces between *d*-PS and cured epoxies did exhibit BADGE and BDDGE methylene ordering, and these interfaces adhered. Interfacial molecular ordering of the epoxy methylene backbones may be necessary for an adhesion mechanism to occur. Further, after moisture exposure, the interfacial epoxy ordering decreased, and adhesion strength diminished, most likely due to swelling-induced epoxy deformation.

This work explored surface and buried interfacial structures of epoxies used as underfills in flip-chip technology. It was shown that surface and buried interfacial structures could be correlated to adhesion strength, which could aid in the design of optimized underfills for flip-chip devices.

5.5 References

1. Bae, J-W.; Kim, W.; Park, S-W.; Ha, C-S.; Lee, J-K. *J. Appl. Polym. Sci.* **2002**, *83*, 2617-2624.

2. Ernst, L.J.; van't Hoff, C.; Yang, D.G.; Kiasat, M.S.; Zhang, G.Q.; Bressers, H.J.L.; den Boer, A.W.J.; Janssen, J. *J. Electronic Packaging.* **2002**, *124*, 97-105.

3. Ferguson, T.P.; Qu, J. *IEEE Trans.* **2006**, *29*, 105-111.

4. Luo, S.; Wong, C.P. *IEEE Trans.* **2005**, *28,* 88-94.

5. Lee, W.S.; Han, I.Y.; Yu, J.; Kim, S.J.; Byun, K.Y. *Thermochimica Acta*. **2007**, *455*, 148-155.

6. Yacobi, B.G.; Martin, S.; Davis, K.; Hudson, A.; Hubert, M. *J. Applied Phys.* **2002**, *91*, 6227-6262.

7. Arvanitopoulos, C.D.; Koenig, J.L. *Applied Spectroscopy.* **1996**, *50*, 11-18.

8. Gonzalez-Benito. *J. Colloid Interf. Sci.* **2003**, *267*, 326-332.

9. Brahatheeswaran, C.; Gupta, V.B. *Polymer*. **1993**, *34*, 289-294.

10. Dufresne, A.; Lacabanne, C. *Polymer*. **1995**, *36*, 4417-4424.

11. Lange, J. ; Toll, S. ; Manson, J-A. *Polymer.* **1997**, *38*, 809-815.

12. Ardebili, H. ; Wong, E.H. ; Pecht, M. *IEEE Trans.* **2003**, *26*, 206-214.

13. Bain, C.D. *J. Chem. Soc. Faraday Trans.* **1995**, *91*, 1218-1296.

14. Buck, M.; Himmelhaus, M. *J. Vac. Sci. Technol. A.* **2001**, *19*, 2717-2736.

15. Lambert, A.G.; Davies, P.B.; Neivandt, D. *J. Appl. Spectrosc. Rev.* **2005**, *40*, 103-145.

16. Shen, Y.R. *The Principles of Nonlinear Optics*; Wiley: New York, 1984.

17. Shen, Y.R. *Nature*, **1989**, *337*, 519-525.

18. Loch, C.L.; Ahn, D.; Chen, Z. *J. Phys. Chem. B.* **2006**, *110*, 914-918.

19. Chen, C.; Wang, J.; Loch, C.L.; Ahn, D.; Chen, Z. *J. Am. Chem. Soc.* **2004**, *126*, 1174-1179.

20. Wang, J.; Woodcock, S.E.; Buck, S.M.; Chen, C.; Chen, Z. *J. Am. Chem. Soc.* **2001,** *308*, 9470-9471.

22. Wang, J.; Chen, C.; Buck, S.M.; Chen, Z. *J. Phys. Chem. B.* **2001**, *105*, 12118-12125.

23. Loch, C.L.; Ahn, D.; Chen, C.; Chen, Z. *J. Adhes.* **2005**, *81*, 319-345.

24. Chen, C.; Wang, J.; Chen, Z. *Langmuir*. **2004**, *20*, 10186-10193.

25. Kataoka, S.; Cremer, P.S. *J. Am. Chem. Soc.* **2006**, *128*, 5516-5522.

26. Hirose, C.; Akamatsu, N.; Damen, K. *Appl. Spectrosc.* **1992**, *46*, 1051-1072.

27. Duffy, D.; Davies, P.; Bain, C. *J. Phys. Chem.* **1995**, *99*, 15241-15246.

28. Lu, R.; Gan, W.; Wu, B.H.; Chen, H. ; Wang, H.F. *J. Phys. Chem. B.* **2004**, *108*, 7297-7306.

29. Chen, C.; Wang, J.; Woodcock, S.; Chen, Z. *Langmuir*. **2002**, *18*, 1302-1309.

30. Lu, X.; Han, J.; Shephard, N.; Rhodes, S.; Martin, A.; Li, D.; Xue, G.; Chen, Z. *J. Phys. Chem. B.* **2009**, *113*, 12944-12951.

31. Chen, C.Y.; Wang, J.; Even, M.A.; Chen, Z. *Macromolecules*. **2002**, *35*, 8093-8097.

32. Hirose, C.; Akamatsu, N.; Domen, K. *J. Chem. Phys*. **1992**, *96*, 997-1004.

33. Hirose, C.; Yamamoto, H.; Akamatsu, N.; Domen, K. *J. Phys. Chem.* **1993**, *97*, 10064-10069

CHAPTER 6

CONCLUSIONS

With the increasing use of polymers in various industrial applications, there is a great need for the development of polymer adhesives that can robustly adhere to other polymeric substrates for applications in the electronics, automotive, construction and aviation fields. To design better adhesives, it is necessary to understand the molecular-level mechanisms of adhesion in these systems. Probing polymer adhesive surfaces and buried interfaces between polymer adhesives and common substrates would allow one to deduce adhesion mechanisms or prerequisite physical conditions necessary for adhesion. This knowledge could aid in the development of better polymer adhesives for specific applications.

Many surface analytical techniques such as XPS, ATR-FTIR and Raman spectroscopies have provided information about the surface structures of polymer adhesives, such as silicone elastomers and epoxy resins, and these studies have informed development of these adhesives. However, none of these techniques can provide detailed molecular-level information about these surfaces *in situ*, nor can they probe the buried interfaces formed by adhesive bonds. In the studies presented in previous chapters, the nonlinear optical technique SFG has been used to study polymer adhesive surfaces and buried interfaces *in situ*. SFG studies have provided detailed molecular-level information

about the surface structure of polymer adhesives, as well as the ordering of polymer adhesive chemical groups at the buried interfaces between polymer adhesives and common polymeric substrates. Prior SFG studies have deduced the ordering and absolute orientation of silane adhesion promoting molecules at polymer interfaces, have detected the presence of hydrogen bonds between polymers and silane adhesion promoting molecules, and have detected the diffusion of silane adhesion promoting molecules through polymer films. All of this work demonstrated that SFG is an effective tool to detect the interfacial conditions required for adhesion mechanisms to occur, and that SFG can study adhesion mechanisms.

The presented studies use SFG to explore polymer adhesive surfaces and the buried interfaces between polymer adhesives and polymeric substrates. Chapters 2 and 3 focus on the buried interfacial structures of silane adhesion promoters used to enhance the adhesion of silicone elastomers to polymers such as PET. Silane adhesion promoters are often mixed into silicone elastomers to enhance their adhesion to a variety of substrates. The use of adhesion promoters removes the need for silicone surface oxidative treatments to enhance adhesion in many industrial applications. While the effectiveness of silane adhesion promoters is known, molecular-level mechanisms of adhesion promotion and the physical structures required for adhesion promotion are poorly understood. In Chapter 2, the interfacial structures of a known silane adhesion promoting mixture of γ-GPS and MVS were compared to those of other silanes and silane/MVS mixtures not used as adhesion promoters at the d_4-PET/liquid silane (or silane/MVS mixture) interface, the d_4-PET/uncured silicone interface and the d_4-PET/cured silicone elastomer interface. The buried interfacial structures of silanes at the

polymer/cured silicone elastomer interface were correlated to adhesion strength. SFG spectral analysis showed that ordering of the silane methoxy groups at the polymer interface may be required for adhesion promotion to occur, because only the γ-GPS in the γ-GPS/MVS mixture ordered at all the interfaces studied, and only the γ-GPS/MVS mixture enhanced adhesion. Also, silane structures of the d_4-PET/liquid silane (or silane/MVS mixture) interface could not be directly correlated to the structures of the d_4-PET/silicone elastomer interface, showing that interactions with the silicone elastomer must also influence silane adhesion promoter ordering.

The work in Chapter 3 explored interactions between silicone elastomer and the silane adhesion promoting mixture of γ-GPS and MVS as well as the other silanes not used as adhesion promoters to determine how the silicone affected silane structure. It was found that while the methoxy groups of all the neat silanes ordered at the silicone surface, only the γ-GPS maintained its interfacial orientational order when mixed with MVS. MVS is a necessary part of any adhesion promoter for silicone. Therefore, any necessary silane interfacial structures must be maintained when mixed with MVS. Only the γ-GPS in the γ-GPS/MVS silane adhesion promoting mixture maintained interfacial ordering after being mixed with MVS. This was further evidence that the ordering of silane methoxy groups at buried polymer interfaces must be a necessary prerequisite condition for adhesion promotion mechanisms to occur.

In the future, it would be advantageous to continue studies of the silane adhesion promoting mixture of γ-GPS and MVS to further determine its adhesion promotion mechanism. Preliminary studies have shown that the effectiveness of this adhesion promoter is cure temperature-dependent, indicating that a temperature-dependent

adhesion promotion mechanism such as chemical reaction or interdiffusion may be occurring. Determining what this mechanism is would be an important step in understanding the action of adhesion promoters. This may be accomplished by SFG studies of simpler model systems or by other techniques such as chromatography to look for reaction byproducts.

While the use of adhesion promoters is advantageous in many applications, there are some applications in which the use of oxidative surface treatments are used to enhance the adhesion of silicone elastomer to polymeric substrates. One common application is the fabrication of microfluidics devices, in which pieces of silicone are sealed together by the use of oxidative surface treatments. However, the effects of such surface treatments are temporary because of hydrophobic recovery. It is known that extracting low molecular weight oligomers and other additives from silicone prior to surface oxidative treatments can slow hydrophobic, but the reason for this was not well understood. In Chapter 4, the effect of removing extractable materials on silicone surface structure was investigated to determine how this may impact the effectiveness of oxidative surface treatments. From SFG analysis, it was found that the density of crosslinked silicone elastomer on the sample surface increased and that the surface methyl groups reoriented as extractable materials were removed. These changes in surface structure after solvent extractions may slow hydrophobic recover. These studies have important implications for the fabrication of microfluidics devices in which oxidative surface treatments are used to enhance the adhesion of silicone elastomer.

Lastly, the study of polymer adhesives was expanded from silicone elastomers to epoxy resins in Chapter 5. Epoxies are used as underfill adhesives in flip-chip

semiconductor devices. The success or failure of a flip-chip device is often tied to the adhesion of the underfill to the multiple substrates it encounters. One common cause of underfill adhesion failure is moisture exposure because moisture causes swelling of the epoxy. In the presented work, the surface structures of two different types of epoxies were elucidated with SFG, and the effect of substrate, cure and moisture exposure on surface structures were explored. It was found that the bisphenol-type epoxy surface structure was more greatly affected by these factors than the aliphatic-type epoxy surface. Underfills are largely made of bisphenol-type epoxies, so such changes in surface structure could significantly affect flip-chip devices. These factors need to be accounted for when designing epoxy formulations for underfill applications because the underfills are cured *in situ* in flip-chip devices. Also, the effect of moisture exposure on epoxy structure may help explain why moisture causes underfill delamination. Further, buried interfaces between a model polymer and the epoxies before and after moisture exposure were studied with SFG, and correlated to lap-shear adhesion strength. Cured epoxies were found to create ordered buried interfaces with *d*-PS while uncured epoxies formed disordered interfaces. After moisture exposure, interfacial ordering was lost. This was correlated to a loss of lap shear adhesion strength, indicating that the formation of ordered buried interfaces may be necessary for adhesion in these systems.

In the future, more studies of epoxy underfill interfaces should be performed. While *d*-PS was used as a model polymer substrate for these initial studies, it would be ideal to study buried interfaces with polymers used as passivation layers in semiconductor devices, such as polyimides. Perhaps SFG of such buried interfaces could deduce adhesion mechanisms for this system. For example, the buried interfaces could

be monitored for evidence of chemical reaction or diffusion, and the effect of moisture exposure on these mechanisms could be explored. Additionally, different cure conditions such as temperature and crosslink density, could be systematically explored to determine optimal conditions for improving adhesion strength and minimizing the effect of moisture exposure.

This work demonstrates that SFG is a powerful tool for studying polymer adhesion mechanisms and the surface and interfacial structures required for adhesion mechanisms to occur. The studies revealed how buried interfacial structures of silane adhesion promoting molecules can be correlated to adhesion strength. Further, SFG was used to determine how surface molecular structures of silicone elastomer may influence the effectiveness of oxidative surface treatments used to enhance silicone adhesion to polymeric substrates. Lastly, SFG was used to study a different class of polymer adhesives, epoxies, which are used as underfill adhesives in semiconductor devices. The effect of moisture, a common cause of adhesion failure, on surface and buried interfacial structures was determined and correlated to adhesion strength. Continued *in situ* studies of polymer adhesive surfaces and polymer/adhesive interfaces using SFG may lead to the development of better adhesives and adhesion promoters for a variety of important industrial applications.